

Classical vs. Quantum Decoherence

— DISSERTATION —

zur Erlangung des akademischen Grades
Doctor rerum naturalium
(Dr. rer. nat.)

vorgelegt

der Fakultät Mathematik und
Naturwissenschaften
der Technischen Universität Dresden

von

Julius Helm

geboren am 17.06.1980 in Stuttgart

Eingereicht am 25. Oktober 2011

Synopsis

Based on the superposition principle, any two states of a quantum system may be coherently superposed to yield a novel state. Such a simple construction is at the heart of genuinely quantum phenomena such as interference of massive particles or quantum entanglement. Yet, these superpositions are susceptible to environmental influences, eventually leading to a complete disappearance of the system's quantum character. In principle, two distinct mechanisms responsible for this process of *decoherence* may be identified. In a *classical decoherence* setting, on the one hand, stochastic fluctuations of classical, ambient fields are the relevant source. This approach leads to a formulation in terms of stochastic Hamiltonians; the dynamics is *unitary, yet stochastic*. In a *quantum decoherence* scenario, on the other hand, the system is described in the language of *open quantum systems*. Here, the environmental degrees of freedom are to be treated quantum mechanically, too. The loss of coherence is then a direct consequence of growing correlations between system and environment.

The purpose of the present thesis is to clarify the distinction between classical and quantum decoherence. It is known that there exist decoherence processes that are not reconcilable with the classical approach. We deem it desirable to have a simple, feasible model at hand of which it is known that it cannot be understood in terms of fluctuating fields. Indeed, we find such an example of *true quantum decoherence*. The calculation of the norm distance to the convex set of classical dynamics allows for a quantitative assessment of the results. In order to incorporate genuine irreversibility, we extend the original toy model by an additional bath. Here, the fragility of the true quantum nature of the dynamics under increasing coupling strength is evident. The geometric character of our findings offers remarkable insights into the geometry of the set of non-classical decoherence maps. We give a very intuitive geometrical measure—a volume—for the *quantumness* of dynamics. This enables us to identify the decoherence process of maximum quantumness, that is, having maximal distance to the convex set of dynamics consistent with the stochastic, classical approach. In addition, we observe a distinct correlation between the *decoherence potential* of a given dynamics and its achievable quantumness. In a last step, we study the notion of quantum decoherence in the context of a bipartite system which couples locally to the subsystems' respective environments. A simple argument shows that in the case of a separable environment the resulting dynamics is of classical nature. Based on a realistic experiment, we analyze the impact of entanglement between the local environments on the nature of the dynamics. Interestingly, despite the variety of entangled environmental states scrutinized, no single instance of true quantum decoherence is encountered. In part, the identification of the classical nature relies on numerical schemes. However, for a large class of dynamics, we are able to exclude analytically the true quantum nature.

Contents

1	Introduction	1
2	State of the Art	7
2.1	Entangled States	8
2.1.1	Mixed-State Entanglement	9
2.1.2	Entanglement with Continuous Variables	11
2.2	Decoherence	14
2.2.1	Quantum Decoherence	15
2.2.2	Classical Decoherence	16
2.2.3	A Comment on the Terminology	21
2.2.4	Pure Decoherence: Phase Damping	22
2.3	Quantum Channels	23
2.3.1	Random Unitary (RU) Channels	25
2.3.2	Phase-Damping Channels	26
2.3.3	Norm of Complete Boundedness	27
2.4	Channel-State Duality—The Jamiolkowski Isomorphism	28
2.5	Birkhoff’s Theorem	29
2.6	Positive Operator-Valued Measure (POVM)	31
2.6.1	Informationally Complete (IC)-POVM	32
2.6.2	Symmetric Informationally Complete (SIC)-POVM	32
3	Classical vs. Quantum Decoherence	35
3.1	Birkhoff’s Theorem—The Quantum Analogue	35
3.2	Physical Model of Quantum Decoherence	39
3.2.1	Generalization to Arbitrary Dimension	43
3.3	A Measure of Quantumness—The Birkhoff Defect	44
3.3.1	The Calculation Scheme	45
3.3.2	Birkhoff Defect: Results	46
3.4	Adding Irreversibility	46
4	A Geometric Measure of Quantumness	53
4.1	Bloch Volume as a Measure of Quantumness	54
4.1.1	Direct Calculation of the Bloch Volume	55
4.1.2	The Channel with Maximum Bloch Volume	58
4.1.3	SIC-POVMs and Quantum Decoherence	58
4.2	Characterization of Two-Qubit Phase Damping	60
4.2.1	Purity of a Phase-Damping Channel	61

Contents

4.2.2	Mixed Channels of Maximum Quantumness (MCMQ)	63
4.3	Quantumness of Assistance	64
4.4	Comparison of Bloch Volume and Quantumness of Assistance	68
4.4.1	Quantum Channels With Constant Bloch Volume	69
4.5	Characterization in the Quantumness-Purity-Plane	71
5	Quantum Decoherence via Entangled Local Reservoirs?	75
5.1	Experimental Setup	76
5.1.1	Resonant Coupling	77
5.1.2	Conditional Quantum Phase Gate	78
5.2	Two Modes Sharing a Single Photon	79
5.3	Two Modes in a Gaussian Entangled State	81
5.3.1	Direct Assessment of the RU Character	82
5.4	Entangled State With Negative Wigner Function	84
6	Conclusion and Outlook	87
A	Technical Toolkit	93
A.1	Convex Roof Construction	93
A.2	The Cholesky Factorization	93
A.3	Bloch Representation for N-level Systems	94
A.4	Identifying a FSOV Using the Bloch representation	95
A.5	Calculation of the cb-Norm	96
A.5.1	Specifics for Diagonal Maps of Full Rank	98
A.6	Volume Spanned by a FSOV	98
A.7	Phase-Damping of a Single Qubit: Deformation of the Bloch Sphere	99
B	Calculation of the Bloch Volume	101
B.1	The Caley-Menger Determinant	101
B.2	Bloch Volume of a Phase-Damping Channel	102
B.3	Bloch Volume of a SIC-POVM	104
C	Calculations in the Wigner Representation	107
C.1	The Two-Mode Entangled Channel	107
C.2	Wigner Function of Two Modes Sharing 1,2, and 3 Photons	110
	Bibliography	115

1 Introduction

A thorough introduction to quantum theory cannot go without the discussion of a double slit experiment involving massive particles. It works best to exemplify the seemingly paradoxical wave-like interpretation of massive objects first introduced by de Broglie in 1924 (see references in [1]). In the experiment, a beam of neutrons, for example, is aimed at a screen with two parallel slits. At a certain distance behind, a second screen is placed, allowing for the detection of the transmitted neutrons with spatial resolution. According to classical mechanics, the expected distribution pattern of the neutrons is simply the sum of the patterns of the individual slits. The experiment, however, reveals a quite different outcome (Fig. 1.1).

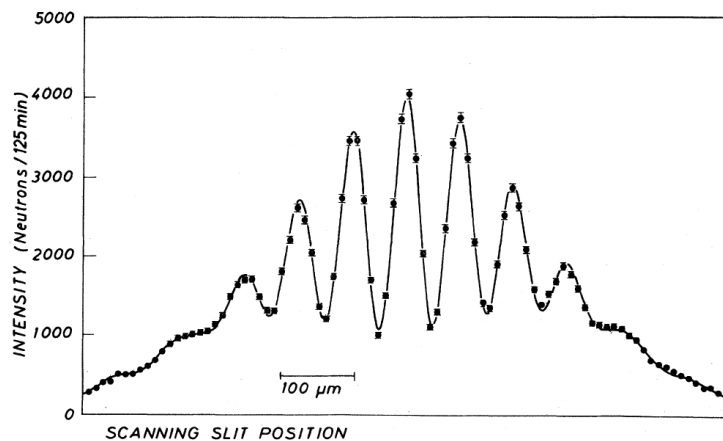


Figure 1.1: Experimentally obtained interference pattern of neutrons diffracted by a double slit. The points represent data taken in the actual experiment, while the solid curve displays the theoretical, quantum mechanical prediction (Picture taken from [2]).

In order to explain the intensity pattern of the incident beam on the second screen, one has to account for interferences between the partial waves travelling through either one of the slits. For larger particles, the manifold interactions with their surroundings become less and less controllable. With increasing interaction, the actual path of an individual particle becomes ever more defined. As a result, the wavelike description of the propagation has to be abandoned in favor of a classical, trajectory-based interpretation. This is part of the reason why the observation of quantum interference becomes increasingly difficult with growing

1 Introduction

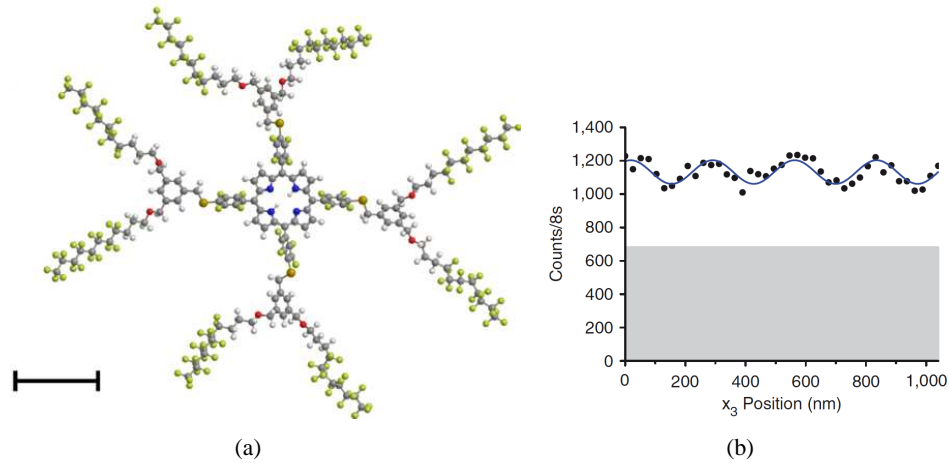


Figure 1.2: (a) In recent experiments, interference effects with large organic molecules are studied [3]. Depicted here is a schematic image of TPPF152 with a total number of 430 atoms, adding up to a mass of 5310 AMU (atomic mass units). The bar in the lower left corner corresponds to 10 Å. (b) The recorded diffraction pattern (black dots) is in line with the theoretical model (solid line) involving quantum interference. Note, that in this experiment a grating instead of a double slit is used (Pictures taken from [3]).

object size (see Fig. 1.2).

Mathematically, the ability of a quantum system to interfere is described by its coherences, stemming from a coherent superposition of distinct states. Processes leading to a decrease of the coherences, thereby destroying the interference potential, are usually subsumed under the name *decoherence*. Not only is decoherence responsible for the absence of wave interference of massive particles, it may also be seen as the main reason for the emergence of classicality on a human scale [4, 5, 6]. In general, damping (population transfer) is to be distinguished from decoherence (the loss of phase relations in a certain basis). While damping necessarily implies decoherence, the converse need not be true for suitable interactions. In many instances, e.g., the coherences of a quantum system decay with a rate much larger than the rate at which energy is transferred to the environment. In terms of the time scale defined by this larger rate, the coherences are then typically lost long before the system relaxes into a stationary state [7]. Such dynamics are typically referred to as *pure decoherence* or *phase damping* (also known as *dephasing*).

Yet, even on a microscopic scale, the effect of decoherence may often not be neglected. This is especially true for attempts to exploit the vast potential forecast to applied quantum information processing, where the information to be processed is encoded in coherent superpositions of states. The potential applications range from the actual realization of a quantum

computer, to quantum cryptography protocols, the teleportation of quantum states, or quantum dense coding [8, 9]. The exponential increase of Hilbert space dimension with growing system size leads to a tremendous superiority of certain quantum algorithms over conventional, classical schemes. However, the processing, storage, and transmission of quantum information require very high experimental accuracy. The ability to avoid or correct potential errors is of great significance for their success. It is thus indisputable that sound knowledge of the relevant decoherence mechanisms is needed.

At this point, a very important question has to be asked: namely, what is the origin of decoherence? What sort of microscopic models have to be used in order to account for the loss of coherences? May the phenomenon be described in the framework of quantum mechanics—that is, from within the theory itself? Or does one need some additional input to the quantum mechanical description? Put more boldly, is the emergence of classicality a pure quantum effect?

It may not come as a surprise that the question evades an easy answer. It is of course true that decoherence may be introduced based on the situation where both the system of interest and its environment are treated quantum mechanically [5]. As an immediate aftermath of almost any interaction, system and environment build up correlations which induce a loss of the coherences of the system. Often, yet not necessarily, these correlations are of quantum nature [10]; system and environment are then said to be *entangled*. This understanding of decoherence stemming from the coupling to a quantum environment represents the standard textbook approach. For obvious reasons, we will refer to this scenario as *quantum decoherence*.

However, decoherence may also be introduced without invoking a quantum environment at all. In this case, the ways to theoretically approach the system of interest and its surroundings differ substantially. While the system is described in the language of quantum mechanics, there is no need to quantize the ambient degrees of freedom. Rather, the environment may be treated as classical input into the system's quantum description. Its influence is incorporated as a classical parameter in the system Hamiltonian. As a prototypical example, consider a single spin exposed to an electromagnetic field. In the case of a strong field, the influence of the spin on the field may be weak enough to disregard. Stochastic fluctuations (spatial or temporal, e.g.) of the ambient field are then a source of decoherence of the system. The time evolution may thus be described in terms of a stochastic Hamiltonian. We refer to this notion of decoherence as *classical decoherence*.

Classical decoherence scenarios have played an essential role in the modelling of decoherence in a controlled fashion, both in theory and in experiment (see [11] and references in [6]). They have also been identified as *the* relevant decoherence mechanism in ion trap quan-

1 Introduction

tum computers where fluctuations are present both in the magnetic field of the trap and in the frequency of the laser addressing the individual ions [12, 13]. Also, the very often employed model of Markovian dephasing [14, 15, 16], which is described in terms of a Lindblad master equation, belongs to the classical regime since any self-adjoint Lindblad operator may be identified with a white noise term in a suitable Hamiltonian.

Yet, the question may not be side-stepped: How generic is this classical approach to decoherence? May any loss of coherence be explained in this fashion? Due to their unitary yet stochastic character the classical decoherence processes are often denoted *random unitary* (RU). It is known that for quantum systems of small dimension—namely, dimension 2 and 3—any phase-damping process may be explained in terms of RU dynamics. For higher dimension, however, this ceases to be true [17, 18]. So far, there is no known simple criterion able to decide whether a given dynamics is of RU type. In fact, despite the notable attention the issue has received lately [19, 20, 21, 22, 23], very little is known about the nature of *true* quantum decoherence, that is, decoherence that may not be explained in terms of a classically described environment.

This question is also relevant in the context of environment-assisted error correction, where the actual correction procedure is conditional on classical information obtained from a measurement on the environment. Such a correction scheme is successful if and only if the error may *in principle* be described in terms of RU dynamics [19]. More recently, processes of this kind have also been applied to quantum networks [24, 25, 26], where the authors study the asymptotic dynamics under repeated application of RU channels and find an attractor space of reasonably low dimensions.

In the present thesis we discuss possible ways to distinguish true quantum decoherence from RU dynamics. The analysis is based on the language of quantum channels, which may be regarded as one of the most general approaches to quantum dynamics. We deem it desirable to have a simple, explicit example of quantum decoherence at hand of which it is known that it cannot be expressed using stochastic Hamiltonians. Based on this physically feasible model, we analyse different measures of *quantumness*, which give an estimate of how non-classical a certain decoherence process is. Our findings allow us to introduce a new, geometrically motivated measure of quantumness. Due to its simple and intuitive character we are thus enabled to characterize the set of true quantum phase-damping channels, leading to identification of the channel of maximum distance to the convex set of RU dynamics.

Structure of the Thesis

The thesis is structured as follows. In Chapter 2 we begin with a summary of the basic theoretical concepts used. We formally introduce the notion of entanglement and give accounts

of how it can be measured. The differentiation of decoherence into *classical* and *quantum* is discussed in detail. Also, some examples for both notions are shown. For the dynamical description of quantum systems we choose the language of quantum channels, allowing for a very general formulation of time evolution. Further concepts include the Jamiolkowski isomorphism and certain classes of generalized measures which will play a significant role in the characterization of decoherence.

In Chapter 3 we lay the formal groundwork for the discrimination of classical and quantum decoherence. In its pure form, it is based on extremality with respect to the convex set of quantum channels. We present a toy model for which we show that it cannot be understood in terms of a classical decoherence process. The resulting channels are analyzed with respect to their quantumness, i.e., the norm distance to the convex set of channels representing classical decoherence. The toy model is then extended in order to incorporate true irreversibility, which makes the decoherence scenario more realistic. Again, the quantumness of the resulting dynamics is studied and compared to the original, reversible scenario.

In Chapter 4 we introduce an intuitive, geometric measure for the quantumness of dynamics. It is based on a simple volume related to a representation of the corresponding channel using vectors in real space. The geometric character of the newly introduced measure permits us to characterize the set of phase-damping channels on two-qubit systems with respect to their quantumness. In order to validate our findings, we compare it to yet another measure of quantumness which is based on the channel-state duality introduced by Jamiolkowski [27]. Using the toy model presented in Chapter 3, we compare the different methods of quantification.

In Chapter 5 we study whether entanglement between local reservoirs may effect the category (classical or quantum) to which a channel belongs. The discussion is based on an existing experimental setup. On the basis of a model which couples the two elements of a bipartite system to their respective local environments, different initial configurations of the environmental state are analysed.

Finally, in Chapter 6 we summarize and discuss future perspectives.

2 State of the Art

The present chapter discusses the basic theoretical concepts needed for the thesis at hand. In most applications of quantum information processing, entanglement is the core ingredient responsible for the superior efficiency as compared to conventional classical schemes. Based on this central significance, the chapter commences with a brief introduction into entanglement theory. Starting with the rather tractable pure state scenario, we hint at difficulties arising in the context of mixed quantum states. Here, we discuss two different ways of interpreting the amount of entanglement contained in a given state. In addition, we briefly discuss entanglement in systems described by continuous variables. As a relevant antagonist to entanglement, decoherence is presented thereafter. We refine the distinction between classical and quantum decoherence—a distinction that plays a central role in the present thesis. In order to shed some more light on the different approaches, we explore several examples.

The language of quantum channels offers a remarkably effective way to describe dynamics of quantum systems in a very general manner. Indeed, no assumptions about the underlying processes have to be made; rather, the approach is suitable for situations where little to nothing is known about the microscopic mechanisms involved. Note, however, that the approach is limited due to its fundamental assumption of no initial correlations between the system of interest and its environment. As an example of the quantum channel formalism we discuss the class of random unitary (RU) channels, whose elements are stochastic mixtures of unitary dynamics. These RU channels will be ideally suited to formally describe the notion of classical decoherence.

The Jamiolkowski isomorphism, introducing an intriguing duality between the dynamics (quantum channels) and states of quantum systems, has proven a useful concept in several contexts. It also plays a role in the present thesis, and will be included in this chapter. For completeness, we also briefly discuss the “classical” form of the Birkhoff theorem (see [17], e.g.). The significance becomes clearer only after being translated into its quantum version in Chapter 3. The present chapter concludes with a brief discussion of positive operator-valued measures (POVMs), which are a general way to describe measurements in quantum mechanics. In particular, the class of *symmetric informationally complete* POVMs will play a role in the subsequent discourse.

2.1 Entangled States

The idea of *entanglement* goes back to the early days of quantum theory. In fact, it was Schrödinger himself who was the first to speak of the seemingly paradoxical situation that “the best possible knowledge of the whole does not necessarily include the best knowledge of all its parts¹” [28] (translation after [29]). Mathematically, pure-state entanglement follows from the tensor product structure of Hilbert space describing multipartite systems together with the superposition principle. Consider, e.g., a bipartite quantum system consisting of two parts \mathcal{A} and \mathcal{B} , which is described in terms of the product of the individual Hilbert spaces, $\mathcal{H} = \mathcal{H}_{\mathcal{A}} \otimes \mathcal{H}_{\mathcal{B}}$. A pure state is called *separable* if it can be written as a product of subsystem states, that is

$$|\Psi\rangle = |\mu\rangle \otimes |\nu\rangle, \quad |\mu\rangle \in \mathcal{H}_{\mathcal{A}}, |\nu\rangle \in \mathcal{H}_{\mathcal{B}}. \quad (2.1)$$

As an immediate consequence one may note that a measurement performed on one subsystem has no direct influence on the state of the other. In contrast, for an entangled pure state one cannot find a similar representation. By means of local (i.e., acting solely on either subsystem) unitary transformations, it is however possible to write the state as

$$|\Psi\rangle = \sum_{i=1}^N \sqrt{\lambda_i} |e_i\rangle \otimes |f_i\rangle, \quad \lambda_i > 0, N \leq \min\{N_1, N_2\}, \quad (2.2)$$

where appropriate bases $\{|e_i\rangle\}_{i=1}^{N_1}$ of $\mathcal{H}_{\mathcal{A}}$ and $\{|f_j\rangle\}_{j=1}^{N_2}$ of $\mathcal{H}_{\mathcal{B}}$ are to be found [30]. This is subject matter of the so-called *Schmidt decomposition* [30]. The *Schmidt coefficients* λ_i are often combined in the *Schmidt vector* $\vec{\lambda}$. N is usually called the *Schmidt rank* of the state; for $N = \min\{N_1, N_2\}$ and $\lambda_i = 1/\sqrt{N}$ the state is said to be maximally entangled.

Entropy of Entanglement

Pure state entanglement can be detected rather easily. Based on the observation by Schrödinger, namely that knowledge about a composite state does not necessarily improve knowledge about its compounds, one may define a measure of entanglement: the less is known about the subsystem, the more entangled the full state. The *entropy of entanglement* is a way to formally conceive this approach [31]. For the pure state $|\Psi\rangle \in \mathcal{H}_{\mathcal{A}} \otimes \mathcal{H}_{\mathcal{B}}$, it estimates the amount of entanglement in terms of the von Neumann entropy of the reduced

¹That is, the parameters describing the individual parts may be indeterminate, while the global state is fully known.

states

$$E(\Psi) = S(\rho_A) = S(\rho_B), \quad (2.3)$$

where $S(\rho) = -\text{tr} \rho \log_2 \rho$. The reduced states are obtained by tracing out the degrees of freedom of either subsystem, e.g., $\rho_A = \text{tr}_{\mathcal{H}_B} |\Psi\rangle\langle\Psi| = \sum_i \langle f_i | \Psi\rangle\langle\Psi | f_i\rangle$, where $\{|f_i\rangle\}$ denotes an arbitrary basis of \mathcal{H}_B . In terms of the Schmidt coefficients this simply reduces to [30]

$$E(\Psi) = - \sum_{i=1}^N \lambda_i \log_2 \lambda_i. \quad (2.4)$$

In this form it is obvious that the entanglement entropy of a compound is symmetric with respect to its constituents. The quantity E ranges from zero for a product state to $\log_2 N$ for a maximally entangled state.

2.1.1 Mixed-State Entanglement

For a physical system in a mixed state it turns out to be much more difficult to detect entanglement [32]. Here, separability is not synonymous to the state being in product form (cf. Eq. (2.1)); rather, one has to distinguish between *quantum correlations* (i.e., entanglement) and *classical correlations*. A mixed state is called separable (or classically correlated) if states σ_i on \mathcal{H}_A and τ_i on \mathcal{H}_B exist with [33]

$$\rho = \sum_i p_i \sigma_i \otimes \tau_i, \quad p_i > 0, \sum_i p_i = 1. \quad (2.5)$$

In general, mixed state entanglement can be detected with the help of positive maps [34]. A linear map Λ is called positive, if it maps positive operators on positive ones, that is if

$$\Lambda(\rho) \geq 0 \quad \text{for all } \rho \geq 0. \quad (2.6)$$

The identification of an entangled state relies on the fact that a trivial extension of such a positive map, $\Lambda \otimes \mathbb{1}_n$, where $\mathbb{1}_n$ is the identity operator in dimension n , need not be positive any more.

In our bipartite situation we may thus define a map $\Lambda \otimes \mathbb{1}$, with Λ a positive map on \mathcal{H}_A and the identity on \mathcal{H}_B . When applied to a separable state,

$$(\Lambda \otimes \mathbb{1})\rho = \sum_i p_i \Lambda(\sigma_i) \otimes \tau_i, \quad (2.7)$$

2 State of the Art

the result is still a positive operator. In case of an entangled state, however, the final state need not be positive any more. By means of an appropriate positive map Λ , any entangled state may be identified in this vein [34]. It is, however, not obvious a priori how to construct such an *entanglement witness*. The transposition T embodies a prominent example of such a map, first used in the context of entanglement theory by Peres [35]. It is easily verified that the transposition is positive. Consider, however, the case of a bipartite quantum system, $\mathcal{H} = \mathcal{H}_A \otimes \mathcal{H}_B$. Applying T to either one of the subsystems while leaving the other unaltered defines the *partial transposition* $T \otimes \mathbb{1}$ (or $\mathbb{1} \otimes T$), which is not a positive map anymore. Let us consider a system of two qubits, for example, which is in the entangled state $|\psi\rangle = (|00\rangle + |11\rangle)/\sqrt{2}$. Applying the map $T \otimes \mathbb{1}$ to this state yields

$$|\psi\rangle\langle\psi| = \frac{1}{2} \begin{pmatrix} 1 & 0 & 0 & 1 \\ 0 & 0 & 0 & 0 \\ 0 & 0 & 0 & 0 \\ 1 & 0 & 0 & 1 \end{pmatrix} \xrightarrow{T \otimes \mathbb{1}} \frac{1}{2} \begin{pmatrix} 1 & 0 & 0 & 0 \\ 0 & 0 & 1 & 0 \\ 0 & 1 & 0 & 0 \\ 0 & 0 & 0 & 1 \end{pmatrix}, \quad (2.8)$$

which has a negative eigenvalue. The partial transposition is thus able to identify the state as being entangled. For systems of dimension 2×2 and 2×3 it was shown, moreover, that negativity under the map $T \otimes \mathbb{1}$ is not only a sufficient but also a necessary criterion for a state to be non-separable [35].

Entanglement of Formation

In the attempt to evaluate mixed state entanglement the subsystem's entropy alone does not suffice. Moreover, it is even hopeless to completely characterize mixed state entanglement with a single parameter. This is due to the fact that both classical and quantum correlations are encountered [14]. The *entanglement of formation* is one way to give a physically meaningful definition of an entanglement measure [31]. It looks for the minimum amount of pure state entanglement that is needed in order to reconstruct the mixed state. It requires a minimization over all possible decompositions into pure states:

$$E_F(\rho) := \min_{\{p_i, |\psi_i\rangle\}} \left\{ \sum_i p_i E(\psi_i) : \sum_i p_i |\psi_i\rangle\langle\psi_i| = \rho \right\} \quad (2.9)$$

This is the so-called *convex roof construction* of an entanglement measure. In general, the task of finding the decomposition optimal in the sense of Eq. (2.9) requires a multidimensional optimization procedure. One possible way to computationally approach this problem is outlined in App. A.1.

Entanglement of Assistance

The *entanglement of assistance* may be motivated in a scenario where three parties (\mathcal{A} , \mathcal{B} , and \mathcal{C}) share multiple copies of a pure state, $|\Psi\rangle$ [36, 37]. One of the three, the so-called “helper” \mathcal{C} , tries to assist by performing measurements in order to maximize the entanglement shared by the other two parties. Any classical information it obtains from the measurements it is allowed to transmit. The task is thus to identify the potentially available entanglement “hidden” in the state $\rho_{\mathcal{A}\mathcal{B}} = \text{tr}_{\mathcal{C}}(|\Psi\rangle\langle\Psi|)$.

Maybe surprisingly, the hereby defined quantity is an attribute of the reduced state $\rho_{\mathcal{A}\mathcal{B}}$ alone. It may be evaluated via [37]

$$E_A(\rho_{\mathcal{A}\mathcal{B}}) := \max_{\{p_i, |\psi_i\rangle\}} \left\{ \sum_i p_i E(\psi_i) : \sum_i p_i |\psi_i\rangle\langle\psi_i| = \rho_{\mathcal{A}\mathcal{B}} \right\}. \quad (2.10)$$

Note that the entanglement of assistance, E_A , is in a sense dual to the entanglement of formation: replacing the max in Eq. (2.10) with min yields Eq. (2.9).

Several bounds to the entanglement of assistance have been identified, including the *entropic bound* [37, 38]. It is given by the minimum of the partial entropies seen by the parties \mathcal{A} and \mathcal{B} ,

$$E_A(\rho_{\mathcal{A}\mathcal{B}}) \leq \min \left\{ S(\rho_{\mathcal{A}}), S(\rho_{\mathcal{B}}) \right\}, \quad (2.11)$$

where $\rho_{\mathcal{A}}$ and $\rho_{\mathcal{B}}$ denote the states obtained as the partial trace of $\rho_{\mathcal{A}\mathcal{B}}$ over subsystem \mathcal{B} and \mathcal{A} , respectively.

2.1.2 Entanglement with Continuous Variables

A prototypical example of a quantum system described in terms of continuous variables is a bosonic field mode, described by an infinite dimensional Hilbert space. The canonical coordinates of position and momentum² are [39]

$$\hat{q} = \frac{1}{\sqrt{2}}(\hat{a} + \hat{a}^\dagger), \quad \hat{p} = \frac{1}{i\sqrt{2}}(\hat{a} - \hat{a}^\dagger), \quad (2.12)$$

²Note that in the present section we use the common mode of discrimination between quantum operators and classical variables: the former are equipped with a *hat*.

2 State of the Art

where \hat{a}, \hat{a}^\dagger are the bosonic annihilation and creation operators, respectively. Such a quantum system with state $\hat{\rho}$ is uniquely determined by its characteristic function [40]

$$\chi(\eta) = \text{tr} \left[\hat{\rho} e^{\eta \hat{a}^\dagger - \eta^* \hat{a}} \right], \quad (2.13a)$$

where $\eta \in \mathbb{C}$. Besides this symmetrically ordered function one may also define characteristic functions that are normally and antinormally ordered,

$$\chi_N(\eta) = \text{tr} \left[\hat{\rho} e^{\eta \hat{a}^\dagger} e^{\eta^* \hat{a}} \right] = \chi(\eta) e^{1/2|\eta|^2}, \quad (2.13b)$$

$$\chi_A(\eta) = \text{tr} \left[\hat{\rho} e^{\eta^* \hat{a}} e^{\eta \hat{a}^\dagger} \right] = \chi(\eta) e^{-1/2|\eta|^2}. \quad (2.13c)$$

Performing a two-dimensional Fourier transform on these characteristic functions the corresponding phase space functions are obtained [40],

$$f(q, p) = f(z, z^*) = \frac{1}{\pi^2} \int d^2\eta \chi(\eta) e^{z\eta^* - z^*\eta}, \quad (2.14)$$

where the phase-space coordinates are defined via $q = (z + z^*)/\sqrt{2}, p = (z - z^*)/\sqrt{2}i$. In case of symmetric ordering $f(q, p)$ is the well-known Wigner function. Commonly, the following identifications for the characteristic functions with symmetric, normal, and anti-normal ordering are used

$$\chi \rightarrow \text{Wigner function: } f(q, p) =: W(q, p), \quad (2.15a)$$

$$\chi_N \rightarrow \text{P function: } f(q, p) =: P(q, p), \quad (2.15b)$$

$$\chi_A \rightarrow \text{Q function: } f(q, p) =: Q(q, p). \quad (2.15c)$$

In the following we will consider the Wigner representation only.

On basis of the Wigner function of a quantum state $\hat{\rho}$ the expectation values of any operator \hat{A} may be computed performing the integral

$$\begin{aligned} \langle \hat{A} \rangle &= \text{tr} [\hat{\rho} \hat{A}] \\ &= \int dq dp A^{(W)}(q, p) W(q, p), \end{aligned} \quad (2.16)$$

where the appropriate phase-space representation of the operator is given by

$$A^{(W)}(q, p) = \int dq' \langle q + \frac{q'}{2} | \hat{A}(\hat{q}, \hat{p}) | q - \frac{q'}{2} \rangle e^{-i/\hbar q' p}, \quad (2.17)$$

the so-called *Weyl-Wigner correspondence* [41].

Gaussian States

As the name already indicates, Gaussian states stand out due to the fact that the characteristic function is Gaussian. For a state of N modes with phase-space coordinates $\vec{\xi} = (q_1, p_1, q_2, p_2, \dots, q_N, p_N) \in \mathbb{R}^{2N}$ the characteristic function may be expressed as [42]

$$\chi(\eta) = \exp \left\{ -\frac{1}{2} \eta M \eta^T \right\}. \quad (2.18)$$

where M is the real and symmetric correlation matrix comprised of the second moments [43]

$$M_{ij} = \text{tr} \left[\hat{\rho} (\Delta \hat{\xi}_i \Delta \hat{\xi}_j + \Delta \hat{\xi}_j \Delta \hat{\xi}_i) / 2 \right] = \int d^{2N} \xi f(\vec{\xi}) \xi_i \xi_j. \quad (2.19)$$

The canonical commutation relations

$$[\hat{\xi}_i, \hat{\xi}_j] = \frac{i}{2} \Lambda_{ij}, \quad \text{with } \Lambda = \bigoplus_{n=1}^N \begin{pmatrix} 0 & 1 \\ -1 & 0 \end{pmatrix}, \quad (2.20)$$

lead to the additional constraint for the matrix M [43]

$$M - \frac{i}{4} \Lambda \geq 0. \quad (2.21)$$

A prototypical example for an entangled continuous-variable state of two modes a and b (with appropriate annihilation operators \hat{a} and \hat{b} , respectively) is the pure two-mode squeezed state $|\Psi_{a,b}\rangle = \exp\{-r(\hat{a}\hat{b} - \hat{a}^\dagger\hat{b}^\dagger)\}|0_a 0_b\rangle$ [44]. Depending on the amount of squeezing, measured by the squeezing parameter r , its correlation matrix equates to [43]

$$M = \begin{pmatrix} \cosh(2r) & 0 & \sinh(2r) & 0 \\ 0 & \cosh(2r) & 0 & -\sinh(2r) \\ \sinh(2r) & 0 & \cosh(2r) & 0 \\ 0 & -\sinh(2r) & 0 & \cosh(2r) \end{pmatrix}. \quad (2.22)$$

Performing the Fourier transform on the characteristic function yields the Wigner function of the entangled state,

$$W(q_a, p_a, q_b, p_b) = \frac{4}{\pi^2} \exp \left\{ -e^{-2r} [(q_a + q_b)^2 + (p_a - p_b)^2] - e^{2r} [(q_a - q_b)^2 + (p_a + p_b)^2] \right\}. \quad (2.23)$$

As in the finite dimensional case, a possible physical interpretation of entanglement in the

two-mode squeezed state relies on the reduced state with one mode traced out. At a given energy, the reduced state (mode b traced out) is given by

$$\begin{aligned} W_{\text{red}}(q_a, p_a) &= \int dq_b \int dp_b W(q_a, p_a, q_b, p_b) \\ &= \frac{2}{\pi(1 + 2 \sinh^2(r))} \exp \left\{ - \left(\frac{2(q_a^2 + p_a^2)}{1 + 2 \sinh^2(r)} \right) \right\}. \end{aligned} \quad (2.24)$$

It corresponds to the thermal state of mode a . With growing squeezing parameter r the uncertainties in both position and momentum increase. The entanglement of the total state may be given in terms of the von Neumann entropy,

$$E(\hat{\rho}) = \cosh^2(r) \log_2(\cosh^2(r)) - \sinh^2(r) \log_2(\sinh^2(r)). \quad (2.25)$$

It thus depends on the squeezing parameter only. The same is true for the mean number of photons in the mode, which is given by $\bar{n} = \sinh^2 r$ [43].

2.2 Decoherence

The superposition principle states that *any* two states $|\psi_1\rangle, |\psi_2\rangle$ of a quantum system may be superposed, yielding the new state³ $|\Psi\rangle = \frac{1}{\sqrt{2}}(|\psi_1\rangle + |\psi_2\rangle)$: “the system can be in two different states at the same time”. Environmental influences may however cause the *coherences* $|\psi_1\rangle\langle\psi_2|, |\psi_2\rangle\langle\psi_1|$ to decay, thereby eradicating the associated potential for interference. Processes of this kind may be subsumed under the term *decoherence* [5].

For many experimental purposes, decoherence is an unwanted and disturbing effect, destroying the vast potential of quantum systems. Entanglement, for example, has been shown to be fragile under decoherence. It may be lost long before the coherences are washed out [45]. Attempts to make use of this non-classical feature as a resource, like quantum computation [46], quantum-enhanced measurements [47], quantum cryptography [48], or the teleportation of states [49], heavily rely on techniques to fight or avoid decoherence. Quantum error-correction attempts to create codes which are fault-tolerant by construction, similar to redundancy-based classical techniques [8]. In addition, syndrome measurements may be used to identify which type of error has occurred, giving the chance to undo it. As yet another Ansatz, the theory of decoherence-free subspaces rests on the identification of relevant symmetries in the global physical description [50]. These symmetries may be used to single out sets of states that are unaffected by the dynamics.

³For simplicity we consider the case of an equal superposition. In general, states of the form $c_1|\psi_1\rangle + c_2|\psi_2\rangle$ with complex numbers c_1, c_2 and $|c_1|^2 + |c_2|^2 = 1$ are allowed.

In another context, on the other hand, decoherence is a welcome concept in order to explain the emergence of classicality as experienced in everyday life [4, 5, 6]. It is a fruitful concept to account for the non-existence of macroscopic superpositions of states. Furthermore, some ideas about how to exploit decoherence in the context of quantum computation have been introduced recently. By engineering local environments accordingly, the effects of decoherence may be used to steer a quantum system towards a desired state [51].

In the following Sections 2.2.1 and 2.2.2, we discuss the notions of quantum and classical decoherence in detail. At first, the general microscopic mechanisms involved are introduced. In addition, we discuss several examples elucidating the different approaches.

2.2.1 Quantum Decoherence

The standard textbook approach to the theory of decoherence is based on the language of *open quantum systems*, which treats the effects of an uncontrollable environment on the quantum evolution of the system [52]. Here, the system of interest is merely seen as a subsystem of a larger quantum system including the relevant environmental degrees of freedom. The dynamics of the total (closed) state is then given in terms of a unitary transformation U . Initially, system and environment are assumed to be in a product state, $\rho \otimes \sigma_E$. In the process of “averaging over all unobserved degrees of freedom”[6], the final state of the system is eventually obtained by tracing out the environment:

$$\rho' = \text{tr}_E [U(\rho \otimes \sigma_E)U^\dagger]. \quad (2.26)$$

Clearly, time evolution of the system alone, $\rho \mapsto \rho'$, is in general non-unitary. Decoherence is then a direct consequence of growing correlations between system and environment [4, 6, 53]. Typically, these correlations are of quantum nature and the interaction leads to entanglement between system and environment. However, this may not occur. Depending on the interaction and the respective initial states, the system’s coherences may decay considerably while the total state is still separable [10, 54].

Quantum Decoherence in an Idealized Measurement

The notion of quantum decoherence plays a vital role in the dynamical description of the *collapse of the wave function*. The collapse is necessary for the emergence of a classical outcome in an idealized version of a measurement apparatus, also known as *the measurement problem* [4, 5, 6, 53]. Consider the system of interest to be in the state $|n\rangle$. Ideally, one wishes

2 State of the Art

a measurement apparatus initially in $|A_0\rangle$ to interact with the system according to

$$|n\rangle |A_0\rangle \longmapsto |n\rangle |A_n\rangle. \quad (2.27)$$

The state $|A_n\rangle$ is then called a *pointer state*, since it corresponds to a specific pointer position on the measurement apparatus indicating the outcome “system in state n ”. Since the apparatus shall be assumed to be macroscopic, it strongly interacts with its environment E . The results of the measurement are thus rapidly transferred to the environment [4]. For the joint state of system, apparatus plus environment, this implies

$$|n\rangle |A_0\rangle |E_0\rangle \longmapsto |n\rangle |A_n\rangle |E_n\rangle. \quad (2.28)$$

Decoherence enters the situation when the system of interest is initially described by a coherent superposition of quantum states, that is, $\sum_n c_n |n\rangle$. From Eq. (2.27) and linearity of time evolution we know that the compound state evolves according to

$$|\Psi_0\rangle = \left(\sum_n c_n |n\rangle \right) |A_0\rangle |E_0\rangle \longmapsto |\Psi_t\rangle = \sum_n c_n |n\rangle |A_n\rangle |E_n\rangle. \quad (2.29)$$

The key idea is that the pointer states $|A_n\rangle$ are sufficiently robust, so that they are not affected much by the interaction with the environment. These *preferred states* are singled out in a process called *environment induced superselection* [5]. As an important effect the environmental states quickly become mutually orthogonal, that is, $\langle E_m | E_n \rangle \approx \delta_{mn}$. Since we are interested in the state of system and apparatus, only, we may discard all information about the environment by performing the trace

$$\mathrm{tr}_E \left[|\Psi_t\rangle \langle \Psi_t| \right] = \sum_n |c_n|^2 |n\rangle \langle n| \otimes |A_n\rangle \langle A_n|. \quad (2.30)$$

The resulting state is now given in terms of a classical mixture of the different measurement outcomes n , with correct probabilities according to standard measurement theory [55].

2.2.2 Classical Decoherence

As another possible source of decoherence, one may identify temporal or spatial fluctuations of ambient classical fields (also called “random external fields” [56]). This effect plays a role in situations where, in effect, an ensemble average is measured. For each individual representative of the ensemble the time evolution is given in terms of a Hamiltonian and hence unitary; the dynamics are thus—at least in principle—reversible. Formally this may

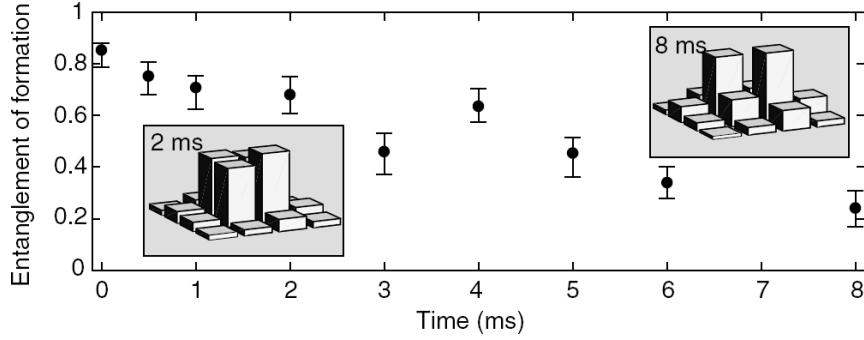


Figure 2.1: Decoherence in experiment: The plot shows the decay of the entanglement of formation in a two-qubit system. The two insets depict the magnitude of the density matrix elements at times $t = 2\text{ms}$ and $t = 8\text{ms}$, respectively (Picture taken from [58]).

be written as

$$\rho(t) = \left\langle\left\langle U_{\xi}(t)\rho U_{\xi}^{\dagger}(t) \right\rangle\right\rangle_{\Xi}, \quad (2.31)$$

where $\langle\langle \cdot \rangle\rangle$ defines an ensemble average over different parameter values ξ of a certain space of events Ξ . For any $\xi \in \Xi$, U_{ξ} is a unitary operator. We will denote dynamics of this sort as *random unitary (RU)*: the time evolution is unitary, yet stochastic.

To contrast this notion to the *quantum* version of decoherence, where the relevant environmental degrees of freedom have to be treated quantum mechanically (see Sec. 2.2.1), we choose the term *classical* decoherence. In the following sections we discuss two scenarios exemplifying this idea.

Decoherence in an Ion Trap Quantum Computer

Experiments in Innsbruck study the implementation of quantum algorithms based on an architecture using trapped ions as logical qubits. Their system consists of a string of $^{40}\text{Ca}^+$ ions confined in a linear Paul trap. Metastable hyperfine states of the ions are used as the qubit basis $\{|0\rangle, |1\rangle\}$ [57]. A preparation of entangled states of up to 14 qubits has been successfully demonstrated [13]. Yet, the system is not immune to environmental influences. Using the example of $|\Psi\rangle = \frac{1}{\sqrt{2}}(|01\rangle + |10\rangle)$ (a Bell state) as initial state, Fig. 2.1 shows that decoherence also precipitates a decay of entanglement. The insets allow for an observation of the state's density matrix elements. Taking a closer look at the qualitative nature of the coherence decay, one observes a Gaussian rather than an exponential behaviour (cf. Fig. 2.2(a)). Note that an exponential decay would conform well to a model based on a Markovian master equation, often used as a standard approach to decoherence [14].

2 State of the Art

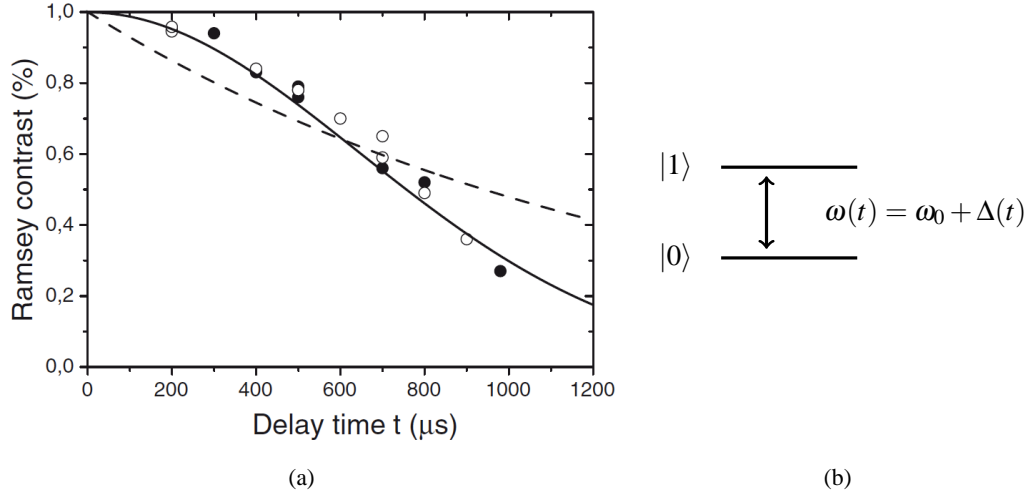


Figure 2.2: (a) Coherence decay of a single qubit. Rather than an exponential curve, which would be expected on basis of a Markovian model, a Gaussian curve proves appropriate to fit the experimental data. Solid (open) circles: active magnetic field compensation turned off (on) (Picture taken from [59]). (b) Schematic illustration of the relevant qubit levels $|0\rangle$ and $|1\rangle$. The level separation $\omega(t)$ depends on a stochastic parameter $\Delta(t)$.

It turns out that the relevant decoherence mechanism may be understood on basis of temporal fluctuations of the ambient magnetic field. Consider a single qubit, where the relevant states $|0\rangle$ and $|1\rangle$ have a field-dependent energy separation of $\omega(t)$ (cf. Fig. 2.2(b)). Random fluctuations have been included in the description by introduction of the stochastic parameter $\Delta(t)$, describing the aberration of the magnetic field from its mean ω_0 . The Hamiltonian describing the qubit is given by $H = \omega(t)/2 \sigma_z$, leading to the unitary time evolution

$$U_\omega(t) = e^{-\frac{i}{2}\Omega(t)\sigma_z}, \quad \Omega(t) = \int_0^t d\tau \omega(\tau). \quad (2.32)$$

The initial state shall be described by the 2×2 density matrix ρ_0 . Averaging over the many realizations performed in an experiment leads to the time-evolved state

$$\begin{aligned} \rho(t) &= \langle\langle U_\omega(t)\rho_0 U_\omega^\dagger(t) \rangle\rangle \\ &= \begin{pmatrix} \rho_{11} & \langle\langle e^{-i\Omega(t)} \rangle\rangle \rho_{12} \\ \langle\langle e^{i\Omega(t)} \rangle\rangle \rho_{21} & \rho_{22} \end{pmatrix}. \end{aligned} \quad (2.33)$$

A careful examination identified the power line as the relevant source of fluctuations [59].

Assuming the noise to be Gaussian one finds [60]

$$\langle\langle e^{\pm i\Omega(t)} \rangle\rangle = e^{\pm i\langle\Omega(t)\rangle} e^{-\frac{1}{2}\sigma^2(t)}, \quad (2.34)$$

where $\langle\langle\Omega(t)\rangle\rangle$ is simply given by $\omega_0 t$. Comparing the relevant time-scales one can furthermore assume the noise to be perfectly auto-correlated for the duration of a single measurement. The variance $\sigma^2(t)$ is thus given by [61]

$$\begin{aligned} \sigma^2(t) &= \int_0^t \int_0^t d\tau d\tau' \langle\langle (\omega(\tau) - \langle\omega(\tau)\rangle) (\omega(\tau') - \langle\omega(\tau')\rangle) \rangle\rangle \\ &= \int_0^t \int_0^t d\tau d\tau' \Gamma(\tau - \tau') = \int_0^t \int_0^t d\tau d\tau' \sigma_0^2 = \sigma_0^2 t^2. \end{aligned} \quad (2.35)$$

In the evaluation of Eq. (2.35) the additional assumption has been made that the stochastic process $\omega(t)$ is stationary. With these results at hand we arrive at

$$\rho(t) = \begin{pmatrix} \rho_{11} & e^{-\frac{1}{2}\sigma_0^2 t^2} e^{-i\omega_0 t} \rho_{12} \\ e^{-\frac{1}{2}\sigma_0^2 t^2} e^{i\omega_0 t} \rho_{21} & \rho_{22} \end{pmatrix}, \quad (2.36)$$

reproducing the Gaussian decay of coherences observed in the experiment.

The decoherence mechanism based on stochastically fluctuating fields was again affirmed in recent experiments, where the coherence decay was studied with respect to the number N of qubits involved. The observed scaling factor of N^2 is in perfect agreement with predictions based on global fluctuations of the ambient field [13].

Spin Echo—Reversing Decoherence in an Ensemble of Spins

Maybe the most prominent example of a classical decoherence mechanism was studied by Erwin Hahn in experiments based on *nuclear magnetic resonance* (NMR) in 1950 [62]. The involved mechanism became known as the *Spin Echo* technique. In a prototypical NMR experiment, the object of interest is a cloud of randomly distributed molecules immersed in a liquid. When brought into a homogeneous and static magnetic field, $\vec{B} = (0, 0, B_z)$, the magnetic moments of the nuclear spins become aligned. Consider, for instance, a molecule with nuclear spin $1/2$. Here, the corresponding magnetic moment may be oriented either parallel or anti-parallel to the field axis z (spin up and spin down, respectively). Due to the spin quantization, the respective moments may not, however, be perfectly aligned with the field, forcing them to precess around the z -axis with frequencies differing by the Larmor

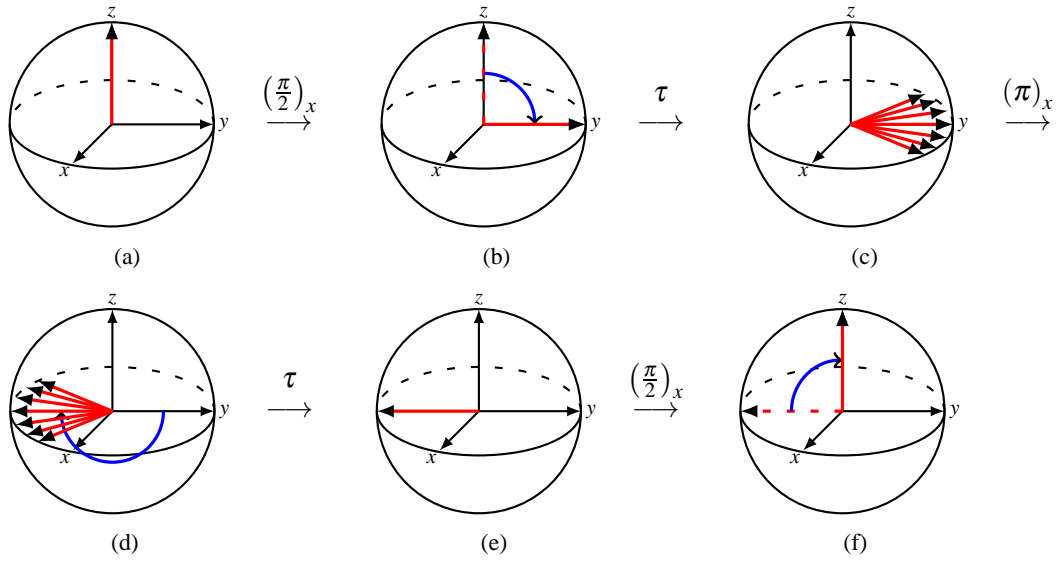


Figure 2.3: (a) All spins are initially prepared parallel to the z -axis. (b) A first $(\frac{\pi}{2})_x$ -pulse rotates the Bloch vectors into the x - y -plane. (c) The spins are left to evolve freely over a duration τ . The spatial variation of the magnetic field induces relative phase shifts between the individual spins: the Bloch vectors disperse along the equator. (d) A second pulse, now $(\pi)_x$, flips the spins about the x -axis. (e) In a second interval of free precession with the same duration τ as before, the spins are allowed to realign. (f) A final $(\frac{\pi}{2})_x$ -pulse moves the spins back to their initial position.

frequency ω_0 . The size of ω_0 depends linearly on the magnetic field, and the so-called gyromagnetic ratio of the nucleus. A transition between the different orientations may now be stimulated using additional pulses in resonance with the Larmor frequency [63].

There are, however, several mechanisms leading to a relaxation of the ensemble towards the equilibrium state. The *longitudinal (spin-lattice) relaxation* is responsible for the equilibration of the spin populations parallel and antiparallel to the static magnetic field, usually described with the time constant T_1 . The *transverse (spin-spin) relaxation* describes the coherence decay. Careful examination of this process allows the identification of at least two relevant sources [63]. Firstly, homogeneous broadening, which is due to fluctuating microscopic magnetic fields and quantified by the time constant T_2 . Secondly, the spatial variation of the macroscopic field over the volume of the sample leads to an inhomogeneous broadening, quantified by the time constant T_2^* . It is this second source of decoherence that may be reversed in experiment.

The basic idea is best understood in terms of the Bloch representation of the spin states (Fig. 2.3, see also App. A.3). Initially, all spins shall be prepared in the spin up state, aligned

parallel to the z -axis. The first pulse $(\frac{\pi}{2})_x$ rotates the spins around the x -axis about an angle of $\pi/2$, moving them into the x - y -plane. The spatial variation of the stationary magnetic field makes the single spins precess at different speeds, leading to a relative phase difference depending on the duration τ ; the individual Bloch vectors spread out across the equator. Now, a π -pulse is applied, rotating the spins once more around the x -axis, now about an angle of 180° . A subsequent free evolution of duration τ prompts the spins to refocus, so that an additional $(\frac{\pi}{2})_x$ -pulse re-establishes the initial state.

2.2.3 A Comment on the Terminology

Throughout the thesis we use the prefixes *classical* and *quantum* in order to specify the microscopic processes leading to a loss of coherences. It is, however, often argued that the term decoherence should be reserved for what we refer to as *quantum* decoherence. It is then “a distinctly quantum mechanical effect with no classical analog” [6] which is based on growing correlations between the system and its environment. Classical decoherence, on the other hand, is seen merely as a “fake” process with seemingly alike results.

This distinction is justified in two ways. First, it is argued that the ensemble-based, classical decoherence may *in principle* be corrected based on sensitive measurements on the environment. That is because the dynamics of each individual element of the ensemble is unitary and hence reversible. Note, however, that the prospect of correction is not only present in the classical case. In this context we should reference the result by Gregoratti and Werner [19] (see also Sec. 2.3.1). In their paper they show that quantum decoherence, too, may be perfectly reversed—provided the dynamics is of RU type. In the context of corrigibility, rather than the dispute whether the decoherence is classical or quantum, the question *RU or not RU* is important.

The second argument stresses that no information whatsoever is transferred from system to environment; a process which is believed to be vital for the quantum-to-classical transition [6]. In this context it is also often claimed that decoherence relies on growing entanglement between the system of interest and its surrounding degrees of freedom. This may, in fact, be true if the system starts out in a pure state. It is, however, possible that the system decoheres completely before becoming entangled with its environment [10, 54].

In addition, for an experimenter, classical and quantum decoherence may often not be distinguishable. What term should he then use in a phenomenological description, without any knowledge about the actual mechanisms involved? From his point of view it may seem somewhat pedantic to reserve the name decoherence for processes involving quantum entanglement. Rather, we suggest to use the term in the context the meaning of the word itself implies: de-coherence, that is, the *loss of coherence*. Additional detailing may then be

achieved using the expressions *classical* and *quantum*. In this context, the thesis provides an enhanced understanding of the differences of the two mechanisms.

2.2.4 Pure Decoherence: Phase Damping

In some decoherence scenarios it is possible to identify a basis $\{|n\rangle\}$ of states that are dynamically robust. Transitions between these *preferred states* might, for example, occur on a much longer time-scale than the decay of coherences [7]. The success of the Spin Echo technique (Sec. 2.2.2) relies on this differentiation of time scales: a complete reversal of the spin-spin relaxation described by the time constant T_2^* is only possible if $T_2^* \ll T_2, T_1$ [63]. Such a case of long-lasting populations and relatively fragile coherences is usually termed *pure decoherence* or *phase damping* (also known as *dephasing*). Accordingly, the basis of preferred states is denoted *phase-damping basis*.

In a quantum model of decoherence (cf. Eq. (2.26)), the phase-damping dynamics may be described in terms of an overlap of relative states of the environment (where relative denotes relative to the phase-damping basis). The robustness of the preferred states allows for a representation of the joint time evolution of system and environment in controlled-unitary form [64],

$$U = \sum_n |n\rangle\langle n| \otimes \tilde{U}_n, \quad (2.37)$$

where now the unitary operators $\tilde{U}_n = \langle n|U|n\rangle$ act on the environment only. Assuming the environment is initially described by $|\psi_0\rangle$, the time evolution of the system's state ρ is given by

$$\begin{aligned} \rho'_{mn} &= \langle m|\text{tr}_E [U(\rho \otimes |\psi_0\rangle\langle\psi_0|)U^\dagger] |n\rangle \\ &= \langle\psi_0|\tilde{U}_n^\dagger\tilde{U}_m|\psi_0\rangle \rho_{mn} \\ &=: \langle\psi_n|\psi_m\rangle \rho_{mn}, \end{aligned} \quad (2.38)$$

where we denote the relative states with $|\psi_n\rangle = \tilde{U}_n|\psi_0\rangle$.

In a classical decoherence scenario, the unitaries entering the ensemble average in Eq. (2.31) are diagonal matrices of the form $U_\xi = \text{diagonal}(e^{i\xi_1}, e^{i\xi_2}, \dots, e^{i\xi_N})$, such that the density operator evolves according to

$$\rho'_{mn} = \left\langle\left\langle e^{i(\xi_m - \xi_n)} \right\rangle\right\rangle \cdot \rho_{mn}. \quad (2.39)$$

2.3 Quantum Channels

The present section is an introduction to the language of *quantum channels*. It enables a description of discrete time evolution of quantum systems in a very general way—no consideration of the underlying physical processes has to be made. It is thus an adequate tool for the description of both classical and quantum decoherence. The quantum channel simply acts as a map, mapping an arbitrary initial state ρ to its dedicated final state ρ' . For this reason it may thus be called a “black-box” approach; the physical processes involved are regarded as second rate. The definition of a quantum channel rests on the following [30]:

Definition 2.1 (Quantum Channel)

A *quantum channel* is a linear map $\mathcal{E} : \rho \mapsto \rho'$ mapping the set of density operators onto itself. That is, for any density operator ρ one finds

- (i) $\rho' = (\rho')^\dagger$ (*Hermiticity*),
- (ii) $\text{tr}[\rho'] = 1$ (*trace preservation*),
- (iii) $\rho \geq 0$ (*positivity*).

Furthermore, the map is required to be *completely positive*, that is,

- (iv) $\mathcal{E}(\rho \otimes \mathbb{1}_n) \geq 0$ (*complete positivity (CP)*),

where $\mathbb{1}_n$ is the identity in arbitrary dimension $n \in \mathbb{N}$.

In addition, a quantum channel is said to be *unital* if it leaves the completely mixed state $\mathbb{1}_N/N$ invariant or, equivalently,

$$\mathcal{E}(\mathbb{1}_N) = \mathbb{1}_N. \quad (2.40)$$

Note that in the definition of quantum channels, ρ and ρ' do not necessarily have to be assigned to the same Hilbert space. For the sake of simplicity, we will however assume here and in the following treatment that this is indeed so. In a given basis, the set of operators acting on a N -dimensional Hilbert space may be represented with \mathcal{M}_N , the set of $N \times N$ complex matrices. A quantum channel is then described as a map $\mathcal{E} : \mathcal{M}_N \rightarrow \mathcal{M}_N$.

Complete Positivity

The definition of quantum channels introduces the notion of complete positivity, equivalent to positivity of the map under arbitrary trivial extensions $\mathcal{E} \otimes \mathbb{1}_n$. The physical motivation of this constraint rests on the idea that the quantum system under scrutiny may initially be entangled with a second system (e.g. its environment). A quantum channel changing only

2 State of the Art

the state of the system is described by $\mathcal{E} \otimes \mathbb{1}_E$, with $\mathbb{1}_E$ the identity on the environment. Complete positivity is then able to ensure that the compound map is still positive. Recall that we have previously discussed an example of a positive yet not completely positive map: the transposition T . This feature was in fact used in Sec. 2.1.1 in order to detect entanglement in a bipartite state.

Kraus Representation

It was shown by Kraus [65] that a quantum channel may always be written in terms of an operator sum,

$$\rho' = \sum_i K_i \rho K_i^\dagger, \quad (2.41)$$

with so-called *Kraus operators* K_i . For the map to be trace-preserving one finds $\sum_i K_i^\dagger K_i = \mathbb{1}_N$. If the channel is unital, the Kraus operators additionally obey $\sum_i K_i K_i^\dagger = \mathbb{1}_N$. Note that the Kraus representation is not unique. The matrices K_i may however be taken linearly independent, fixing the number of terms in Eq. (2.41). The number of Kraus operators needed in this minimal representation is called the *Kraus rank* (often also simply *rank*) of the channel \mathcal{E} . Two different representations $\{K_i\}_{i=1}^s$ and $\{\tilde{K}_i\}_{i=1}^s$ are related by an isometry,

$$\tilde{K}_i = \sum_{j=1}^s V_{ij} K_j, \quad (2.42)$$

with $V : \mathbb{C}^s \rightarrow \mathbb{C}^s, V^\dagger V = \mathbb{1}_s$. In the case that both representations are linearly independent, the matrix V is unitary [17].

Quite surprisingly, despite the rather axiomatic approach taken in Def. 2.1, the concept of quantum channels is intimately connected to the standard unitary propagation scheme in quantum mechanics: it may be attributed to the dynamics of an open quantum system. Following the so-called *Stinespring dilation theorem*, one may arrive at the general form of a quantum channel by successive exertion of the following steps:

- (i) Dilation of Hilbert space with an auxiliary system:

$$\rho \mapsto \rho \otimes \sigma_{\text{aux}}, \quad (2.43)$$

- (ii) Unitary propagation within the enlarged state space:

$$\rho \otimes \sigma_{\text{aux}} \mapsto U (\rho \otimes \sigma_{\text{aux}}) U^\dagger, \quad (2.44)$$

(iii) Tracing out the auxiliary system:

$$\mathrm{tr}_{\mathrm{aux}} [U (\rho \otimes \sigma_{\mathrm{aux}}) U^\dagger] =: \rho'. \quad (2.45)$$

It turns out that the dimension of the additional quantum system σ_{aux} in step (i) has to be no greater than the squared Hilbert space dimension of the system of interest [8]. Note that in step (i) it is commonly assumed that the total state of the system of interest and the auxiliary part are factorizable (i.e., $\rho \otimes \sigma_{\mathrm{aux}}$). This way, the resulting channel $\rho \mapsto \rho'$ is guaranteed to be completely positive [66]. Only recently, necessary and sufficient conditions for complete positivity based on *quantum discord* have been identified. Similar to the concept of entanglement, the quantum discord estimates the non-classical character of correlations shared in bipartite systems [67, 68]. Note, however, that while vanishing discord ensures the state to be separable, non-zero discord does not necessarily involve entanglement. It was shown that the reduced dynamics is completely positive if and only if the initial state has zero discord [69].

The linearity in Def. 2.1 allows for a representation of a quantum channel in terms of a linear superoperator $\Phi^\mathcal{E}$: in a given basis of the state space, $\{|n\rangle\}$, we may define [30]

$$\rho'_{mn} = \sum_{rs} \Phi_{mn,rs}^\mathcal{E} \rho_{rs}, \quad (2.46)$$

where

$$\rho_{mn} = \langle m | \rho | n \rangle \quad \text{and} \quad \Phi_{mn,rs}^\mathcal{E} = \langle m | \mathcal{E}(|r\rangle\langle s|) | n \rangle. \quad (2.47)$$

2.3.1 Random Unitary (RU) Channels

RU channels represent a quite special class of channels: the dynamics is unitary, yet stochastic. This situation is resembling the one encountered in Sec. 2.2.2 describing classical decoherence, where the uncertainty concerning the ambient classical field leads to a description based on a stochastic Hamiltonian. After taking the ensemble average one arrives at a stochastic, unitary time evolution. Such an RU channel may be written in the following form

$$\rho' = \sum_i p_i U_i \rho U_i^\dagger, \quad (2.48)$$

with probabilities p_i and unitary U_i . Comparing Eq. (2.48) to the Kraus representation, Eq. (2.41), reveals that the Kraus operators may be chosen to be $K_i = \sqrt{p_i} U_i$: they are proportional to a unitary matrix.

These RU channels are quite convenient due to their analytical amenability and have been studied in different contexts. The authors of [24, 25, 26], e.g., study the asymptotic dynamics under repeated application of RU channels and find an attractor space of relative low dimension. We ourselves have studied the entanglement evolution of two qubits under RU dynamics [70], where we successfully arrived at analytical expressions.

Corrigibility of RU Channels

Perhaps the most important result connected to RU channels is that they are the only type of dynamics that may be fully undone [19]. Note that in this context the dynamics is due to interaction with a *quantum* environment, as is the case for the notion of quantum decoherence, Sec. 2.2.1. The correction scheme is based on suitable measurements on the quantum environment of the system of interest. The authors show that, provided that the environment's initial state is pure, to any Kraus representation with operators K_i (resulting from a global time evolution U) there exist observables M_i on the environment such that

$$K_i \rho K_i^\dagger = \text{tr}_E \left\{ U \left(\rho \otimes |\psi_0\rangle\langle\psi_0| \right) U^\dagger \left(\mathbb{1} \otimes M_i \right) \right\}. \quad (2.49)$$

As before, ρ denotes the quantum state of the system, $|\psi_0\rangle$ is the pure initial state of the environment. The unitary matrix U describes the joint time evolution.

The idea of the correction scheme may now be sketched as follows. Upon measuring the proper set of observables, such that the corresponding Kraus representation is RU, the correction is possible by simply applying the inverse of the respective unitary transformation (see also [71]). Note that in order to reverse the dynamics full knowledge about the global Hamiltonian dynamics (described by U) is needed.

2.3.2 Phase-Damping Channels

A phase-damping process stands out due to the existence of a basis of robust states: the phase-damping basis (see Sec. 2.2.4). As a consequence, in this basis a *phase-damping channel* D may be written as a diagonal map

$$\rho' = \sum_{m,n} D_{mn} \rho_{mn} |m\rangle\langle n|. \quad (2.50)$$

with a non-negative matrix⁴ D . For convenience we may also write $\rho' = D \star \rho$ where \star is the so-called *Hadamard product*, that is, the entry-wise product of matrices of the same size

⁴Note that with a slight abuse of notation we denote the channel and its matrix representation with the same symbol D .

[72]. For the entries of the matrix D in one finds $|D_{mn}| \leq 1$, where the robustness of the phase-damping basis implies $D_{nn} = 1$.

The non-negativity of D implies the existence of (generally non-unique) matrices A with $D = AA^\dagger$ [73]. On basis of such a square root A , it is possible to introduce the concept of *dynamical vectors*: a set of complex, normalized vectors describing the phase-damping dynamics. Identifying the n -th row of A with the vector $|a_n\rangle$ it is straightforward to see that

$$D_{mn} = (AA^\dagger)_{mn} = \langle a_n | a_m \rangle. \quad (2.51)$$

As an example, a phase-damping channel of dimension 4, i.e., acting on a 4-dimensional quantum system, may be written as

$$D = \begin{pmatrix} 1 & \langle a_2 | a_1 \rangle & \langle a_3 | a_1 \rangle & \langle a_4 | a_1 \rangle \\ \langle a_1 | a_2 \rangle & 1 & \langle a_3 | a_2 \rangle & \langle a_4 | a_2 \rangle \\ \langle a_1 | a_3 \rangle & \langle a_2 | a_3 \rangle & 1 & \langle a_4 | a_3 \rangle \\ \langle a_1 | a_4 \rangle & \langle a_2 | a_4 \rangle & \langle a_3 | a_4 \rangle & 1 \end{pmatrix}. \quad (2.52)$$

The Cholesky factorization (App. A.2) introduces a means of obtaining a square root A in lower triangular form. Furthermore, it allows the identification of dynamical vectors of minimal dimension, being equal to the Kraus rank r of the channel D .

Note that an example of these dynamical vectors was already encountered in Sec. 2.2.4. There, the dynamical vectors are the relative states of the environment obtained in a quantum model of decoherence. In a classical decoherence scenario no such physical interpretation seems possible. Based on the dynamical vectors obtained, e.g., from the Cholesky factorization, it is however possible to construct a *minimal quantum model*, that is, a model in the language of open quantum systems. Minimal refers to the smallest viable dimension of the environment. Note that the first row of the matrix A is given by $(1, 0, 0, \dots)$. Taking this state as the initial state of the environment, the required unitary operators \tilde{U}_n of Eq. (2.37) may simply be obtained using the actual dynamical vectors $|a_n\rangle$ as the first column, while the only constraint for the remaining columns is to preserve unitarity.

2.3.3 Norm of Complete Boundedness

The same reasoning that is applied in the physical justification of complete positivity of a quantum channel is true when introducing a norm on quantum channels. The system the channel is acting on may again be seen as being only part of a larger compound. A meaningful definition (i.e., meaningful in a physical sense) of a norm thus has to take this additional complexity into account.

Definition 2.2 (Norm of Complete Boundedness)

A linear map Λ is called *completely bounded* if the supremum of the operator norm over all trivial extensions, $\sup_n \|\Lambda \otimes \mathbb{1}_n\|$, is finite. Then,

$$\|\Lambda\|_{\text{cb}} = \sup_n \|\Lambda \otimes \mathbb{1}_n\| \quad (2.53)$$

is called the *norm of complete boundedness (cb-norm)* [74].

In order to give an example for a map whose trivial extension differs in norm from the original map we may again rely on the transposition. On basis of the induced operator norm $\|\Lambda\| = \sup\{\|\Lambda(X)\| \mid X \in \mathcal{M}_d, \|X\| = 1\}$ it is obvious that the transposition has norm 1: the norm of a matrix does not change by transposing it. If we again look at the example used in Sec. 2.1.1, this time, however, in reversed order, we know that

$$\begin{pmatrix} 1 & 0 & 0 & 0 \\ 0 & 0 & 1 & 0 \\ 0 & 1 & 0 & 0 \\ 0 & 0 & 0 & 1 \end{pmatrix} \xrightarrow{T \otimes \mathbb{1}_2} \begin{pmatrix} 1 & 0 & 0 & 1 \\ 0 & 0 & 0 & 0 \\ 0 & 0 & 0 & 0 \\ 1 & 0 & 0 & 1 \end{pmatrix}. \quad (2.54)$$

From

$$\left\| \begin{pmatrix} 1 & 0 & 0 & 0 \\ 0 & 0 & 1 & 0 \\ 0 & 1 & 0 & 0 \\ 0 & 0 & 0 & 1 \end{pmatrix} \right\| = 1 \quad \text{and} \quad \left\| \begin{pmatrix} 1 & 0 & 0 & 1 \\ 0 & 0 & 0 & 0 \\ 0 & 0 & 0 & 0 \\ 1 & 0 & 0 & 1 \end{pmatrix} \right\| = 2 \quad (2.55)$$

it follows immediately that $\|T \otimes \mathbb{1}_2\| \geq 2$. In the case of a completely positive, completely bounded map \mathcal{E} one finds [74]

$$\|\mathcal{E}\|_{\text{cb}} = \|\mathcal{E}(\mathbb{1})\|. \quad (2.56)$$

Note that for a unital channel this immediately implies $\|\mathcal{E}\|_{\text{cb}} = 1$.

2.4 Channel-State Duality—The Jamiolkowski Isomorphism

A very intriguing concept in quantum information theory is the channel-state duality introduced by Jamiolkowski in 1972 [27]. To any given quantum channel $\mathcal{E} : \mathcal{M}_N \rightarrow \mathcal{M}_N$, the

Jamiolkowski isomorphism introduces the so-called *Jamiolkowski state* $\rho^\mathcal{E}$ on \mathcal{M}_{N^2} via

$$\begin{aligned}\rho^\mathcal{E} &= (\mathcal{E} \otimes \mathbb{1}) \frac{1}{d} \sum_{m,n=1}^N |mm\rangle\langle nn| \\ &= \frac{1}{N} \sum_{m,n=1}^N \mathcal{E}(|m\rangle\langle n|) \otimes |m\rangle\langle n|.\end{aligned}\quad (2.57)$$

The channel is thus applied to one half of the pure bipartite maximally entangled state $\sum_{n=1}^N |nn\rangle / \sqrt{N}$. Consequently, compared to the initial quantum channel, the state $\rho^\mathcal{E}$ is defined on a Hilbert space of squared dimension, N^2 .

It is of course evident that the Jamiolkowski state does not contain any more information than the channel itself: its matrix representation may be obtained from the superoperator representation, Eq. (2.46), by a simple reshuffling of matrix elements [30]. Using the common definitions

$$\rho_{mn,rs}^\mathcal{E} = \langle m| \otimes \langle n| \rho^\mathcal{E} |r\rangle \otimes |s\rangle \quad \text{and} \quad \Phi_{mn,rs}^\mathcal{E} = \langle m| \mathcal{E}(|r\rangle\langle s|) |n\rangle, \quad (2.58)$$

one finds that

$$\rho_{mn,rs}^\mathcal{E} = \Phi_{mr,ns}^\mathcal{E}. \quad (2.59)$$

Conceptually, however, the Jamiolkowski isomorphism has been widely used in simplifying proofs [75] or pointing out novel properties [76]. One striking feature of the duality is that complete positivity of the map \mathcal{E} is tantamount to positivity of the related state $\rho^\mathcal{E}$. Furthermore, the Kraus rank of a channel is equal to the rank (i.e., the number of non-zero eigenvalues) of the corresponding Jamiolkowski state [77].

2.5 Birkhoff's Theorem

A magic square consists of N^2 numbers, arranged in an array of $N \times N$ entries, such that the sum of each column, row, or diagonal gives the same value. If, in addition, the entries contain all integer numbers from 1 to N^2 , the magic square is called *normal*. People have been fascinated by such objects for many centuries. In fact, a prominent example is the *Lo shu* square (cf Fig. 2.4), dating back to a mythical story told in ancient China [78]. The name stands for ‘‘Lo River writing’’, and the story tells of the mythical King Yu who supposedly saw the numbers written on the carapace of a sacred turtle.

An object very similar to the magic square is given by *doubly stochastic matrices*. A

2	7	6
9	5	1
4	3	8

Figure 2.4: The *Lo shu* square, a normal, magic square known since ancient China. The values of each row, column, and diagonal sum up to 15.

matrix $A = (a_{mn}) \in \mathbb{R}^{N \times N}$, $a_{mn} \geq 0$, is called doubly stochastic if the elements of each row and column sum to one, i.e.,

$$\sum_{m=1}^d a_{mn} = \sum_{n=1}^d a_{mn} = 1. \quad (2.60)$$

Each row may thus be thought of as a discrete probability distribution on a sample space containing d elements [72]. Perhaps the simplest examples of doubly stochastic matrices are given by the *permutation matrices*, square matrices which have exactly one entry, 1, in each row and each column, and 0 elsewhere. A theorem by Garrett Birkhoff [79] identifies these permutation matrices as the extreme points of the convex hull of doubly stochastic matrices.

Theorem 1. (*Birkhoff*) *A matrix $A \in \mathbb{R}^{N \times N}$ is doubly stochastic if and only if it is a convex combination of permutation matrices, i.e., for some $K < \infty$ there are permutation matrices $P_1, \dots, P_K \in \mathbb{R}^{N \times N}$ and probabilities⁵ a_1, \dots, a_K such that $A = \sum_{i=1}^K a_i P_i$.*

Since there are exactly $N!$ distinct permutation matrices in $\mathbb{R}^{N \times N}$, the set of doubly stochastic matrices is a convex set with $N!$ vertices, the so-called *Birkhoff polytope*. It is contained within a $(N^2 - 2N + 1)$ -dimensional subspace of the space of all real $N \times N$ matrices [72, 80]. Note that a permutation matrix may easily be inverted via the transposition, that is,

$$PP^T = \mathbb{1}. \quad (2.61)$$

The inverse of a permutation matrix is another permutation matrix, and hence also doubly stochastic. In general, however, the inverse of a matrix with (2.60) may no longer be doubly stochastic.

⁵With *probabilities* we denote a set of positive, real numbers that sum to one.

2.6 Positive Operator-Valued Measure (POVM)

Probably the most familiar approach to measurements in quantum mechanics goes via *projective* measurements. The basic elements are operators $\Pi(\mu_i) := |\mu_i\rangle\langle\mu_i|$, describing the projection onto mutually orthogonal states $|\mu_i\rangle$. A projective measurement is described by an *observable* M , having spectral decomposition [8]

$$M = \sum_{i=1}^N \lambda_i \Pi(e_i). \quad (2.62)$$

The λ_i are the eigenvalues of the observable, corresponding to the possible outcomes of the measurement. If the quantum system under scrutiny is described by the state $|\psi\rangle$, the probability of getting result λ_i is $P(\lambda_i) = \langle\psi|\Pi(e_i)|\psi\rangle$. The post-measurement state of an outcome λ_i is given by

$$\frac{\Pi(e_i)|\psi\rangle}{\sqrt{\langle\psi|\Pi(e_i)|\psi\rangle}}. \quad (2.63)$$

The attempt to generalize the above concept of orthogonal projective measurement in quantum mechanics leads to the idea of *positive operator-valued measure* (POVM) [8]. A POVM consists of positive operators $\{E_i\}_{i=1}^d$ with

$$\sum_{i=1}^d E_i = \mathbb{1}. \quad (2.64)$$

Note that here the elements E_i are not required to be mutually orthogonal. Given the state $|\psi\rangle$, the probability of outcome i is given by $P(i) = \langle\psi|E_i|\psi\rangle$.

A very illustrative example of such a POVM may be given in terms of coherent states [30]. A coherent state $|\alpha\rangle$ is defined as eigenstate of the annihilation operator, that is, $\hat{a}|\alpha\rangle = \alpha|\alpha\rangle$ ($\alpha \in \mathbb{C}$). In terms of the Fock basis it may be expressed as $|\alpha\rangle = \exp\{-|\alpha|^2/2\} \sum_n \alpha^n |n\rangle / \sqrt{n!}$ [40]. The POVM is then given by the resolution of the identity

$$\int \frac{d^2\alpha}{\pi} |\alpha\rangle\langle\alpha| = \mathbb{1}, \quad (2.65)$$

where the additional normalization factor $1/\pi$ is present due to over-completeness of the coherent states.

2.6.1 Informationally Complete (IC)-POVM

The concept of *informationally complete* (IC)-POVMs is relevant in the context of state discrimination [81]. With a quantum system at hand, it is a natural question to ask how many measurements are required in an attempt to learn the full state of the system. Consider, e.g., a quantum system with a state space of dimension N . It is quite straightforward to see that a general mixed state will be specified by $N^2 - 1$ real parameters (recall that a density operator is Hermitian and of trace 1). In an attempt to learn the full density matrix representation one thus has to be able to perform measurements revealing all possible information about the system. A POVM meeting this requirement is thus called *informationally complete*.

As introduced in Sec. 2.6, a POVM in an N -dimensional Hilbert space consists of operators E_i with $\sum_i E_i = \mathbb{1}_N$. In order to be informationally complete, the operators E_i have to form a (possibly over-complete) operator basis on the Hilbert space. Clearly, thus, a minimum of N^2 elements E_i are required.

2.6.2 Symmetric Informationally Complete (SIC)-POVM

A *symmetric informationally complete* (SIC)-POVM is a set of N^2 operators $E_i = \Pi_i/N$, where the Π_i are rank-one projectors, $\Pi_i = |\mu_i\rangle\langle\mu_i|$ on $\mathcal{H} = \mathbb{C}^N$, satisfying [82]

$$\text{tr}[\Pi_i\Pi_j] = |\langle\mu_i|\mu_j\rangle|^2 = \frac{1}{N+1}, \quad i \neq j. \quad (2.66)$$

The elements of the SIC-POVM are thus subnormalized projectors that are in a sense symmetrically placed in Hilbert space. It is worth a remark that the requirement in Eq. (2.66) is already sufficient to guarantee completeness, i.e. $\sum_i E_i = \mathbb{1}_N$, as well as informational completeness of the E_i [82]. Despite the very simple definition, little is known about the form or even the existence of SIC-POVMs in arbitrary dimension. What is known is that they exist for $N = 2, 3, 4, 5$ and 8. In addition, numerical evidence suggests existence up to dimension 45 [82].

As an example, consider the simplest case of the two-dimensional Hilbert space \mathbb{C}^2 . This example will also allow for some geometric intuition. We are thus interested in a SIC-POVM on the Hilbert space of a single qubit. Here, the projectors Π_i can be rewritten using the Bloch representation (App. A.3)

$$\Pi_i = \frac{1}{2}(\mathbb{1} + \vec{b}_i \cdot \vec{\sigma}), \quad (2.67)$$

where $\vec{b}_i \in \mathbb{R}^3$, $|\vec{b}_i| = 1$, and $\vec{\sigma} = (\sigma_x, \sigma_y, \sigma_z)$, the vector of Pauli spin matrices. The defining

property, Eq. (2.66), now reads

$$\begin{aligned}
 \text{tr}[\Pi_i \Pi_j] &= \frac{1}{4} \text{tr} \left[(\mathbb{1} + \vec{b}_i \cdot \vec{\sigma}) (\mathbb{1} + \vec{b}_j \cdot \vec{\sigma}) \right] \\
 &= \frac{1}{2} (1 + \vec{b}_i \cdot \vec{b}_j) \\
 &= 1/3, \quad i \neq j.
 \end{aligned} \tag{2.68}$$

Hence, the inner product of the Bloch vectors is given by

$$\vec{b}_i \cdot \vec{b}_j = -\frac{1}{3}, \quad i \neq j. \tag{2.69}$$

The angle $\alpha = \arccos(-\frac{1}{3})$ is also known as the *tetrahedral angle*, i.e., the angle between the four vectors spanning a regular tetrahedron. In Bloch representation we can thus conclude that the vectors corresponding to a SIC-POVM are symmetrically placed inside the Bloch sphere, such that they span a regular tetrahedron.

As a last point, it is worth noting that the tensor power of a SIC-POVM is no longer a SIC-POVM. In order to see this, consider the tensor products $|\tilde{\mu}_{ij}\rangle := |\mu_i\rangle \otimes |\mu_j\rangle$ ($i, j = 1, \dots, N^2$), where the projectors $\Pi_i = |\mu_i\rangle\langle\mu_i|$ on \mathcal{H} obey (2.66). For these new projectors $\tilde{\Pi}_{ij} := |\tilde{\mu}_{ij}\rangle\langle\tilde{\mu}_{ij}|$ on $\mathcal{H} \otimes \mathcal{H}$ one finds

$$\begin{aligned}
 \text{tr}[\tilde{\Pi}_{ij} \tilde{\Pi}_{kl}] &= |\langle\tilde{\mu}_{ij} | \tilde{\mu}_{kl}\rangle|^2 = |\langle\mu_i | \mu_k\rangle \langle\mu_j | \mu_l\rangle|^2 \\
 &= \begin{cases} 1 & i = k \text{ and } j = l, \\ \frac{1}{N+1} & \text{either } i = k \text{ or } j = l, \\ \frac{1}{(N+1)^2} & i \neq k \text{ and } j \neq l. \end{cases}
 \end{aligned} \tag{2.70}$$

Clearly, these new projectors do not form a SIC-POVM.

3 Classical vs. Quantum Decoherence

In the introduction of decoherence theory, Sec. 2.2, we discuss the fundamental principles of classical and quantum decoherence and show some illustrative examples. Nothing is said, however, about ways to discriminate between the two, let alone whether such a discrimination is possible at all. These questions call for the more formal approach taken in the present chapter: the quantum analogue of Birkhoff's theorem, which is discussed in Sec. 3.1. It is based on the quantum channel formalism and studies the relationship between unital and RU dynamics. Not only does it help in refining the distinction, it also introduces a method of discrimination which is based on a channel's extremality with respect to the convex set of quantum channels.

In order to arrive at a more physically motivated interpretation of the rather mathematical results, we successfully construct a feasible toy model shedding some more light on the notion of true quantum decoherence. The corresponding channels are studied with respect to their quantumness in terms of the *Birkhoff defect*, which is defined as the norm distance to the convex set of channels describing classical decoherence processes. Despite its computational complexity, the Birkhoff defect enables us to reliably distinguish *true quantum* from RU dynamics. In order to reflect the irreversible nature usually associated with the phenomenon of decoherence, we extend the toy model accordingly by introducing an additional bath. We study how the quantumness depends on the strength of the coupling to the bath. It turns out that the quantum nature of the dynamics is quite vulnerable to the disturbance by the additional environment. This fragility leads to a complete disappearance of the quantumness for sufficiently strong coupling.

3.1 Birkhoff's Theorem—The Quantum Analogue

In quantum mechanics, one can formulate an analogue to Birkhoff's theorem (Sec. 2.5) in terms of complex matrices [17]. For this, two modifications are to be undertaken:

- (I) First, doubly stochastic matrices turn into *unital channels* (*doubly stochastic completely positive maps*). Recall that a channel $\mathcal{E} : \mathcal{M}_N \rightarrow \mathcal{M}_N$ is called unital if it leaves

3 Classical vs. Quantum Decoherence

the completely mixed state invariant, that is

$$\mathcal{E}(\mathbb{1}_N) = \mathbb{1}_N. \quad (3.1)$$

In terms of the Kraus representation, Eq. (2.41), this is equivalent to $\sum_i K_i K_i^\dagger = \mathbb{1}_N$.

(II) Second, the (invertible) unitary maps take the role of the (invertible) permutation matrices.

The quantum analogue of Birkhoff's theorem is thus concerned with the question of whether or not a given unital channel may be written as a convex sum of unitary transformations (i.e., a RU channel, see Sec. 2.3.1). In physical terms, the question is directly related to the discrimination of classical and quantum decoherence: we have seen that our notion of classical decoherence was equivalent to a formal description in terms of a RU channel (cf. Secs. 2.2.2 and 2.3.1). Note that—without emphasizing the fact—we have already encountered two examples of unital channels in Chap. 2. Clearly, a RU channel belongs to the set of unital channels, for we have

$$\sum_i p_i U_i U_i^\dagger = \sum_i p_i \mathbb{1}_N = \mathbb{1}_N. \quad (3.2)$$

Trivially, furthermore, a phase-damping channel is unital: in the phase-damping basis, the completely mixed state is nothing but an equal (incoherent) mixture of the basis elements—the robust states—and hence unaffected by definition. In the spirit of Birkhoff's theorem we may thus ask if phase-damping dynamics is always consistent with a description based on the RU approach.

In 1993 Landau and Streater were able to show that, in opposition to the classical case, the quantum analogue of Birkhoff's theorem fails to be true: there exist unital channels which may not be written as a convex sum of unitary transformations. The identification makes use of a channel's extremality with respect to the set of unital quantum channels, based on the following theorem by Choi [17].

Theorem 2. (*Extremality in the set of channels*) *A channel $\mathcal{E} : \mathcal{M}_N \rightarrow \mathcal{M}_N$ is extremal with respect to the set of quantum channels if and only if it may be written in terms of a Kraus representation $\{K_i\}_{i=1}^r$, where*

$$\left\{ K_i^\dagger K_j \right\}_{i,j=1}^r \quad (3.3)$$

is a linearly independent set of matrices.

Landau and Streater show that the condition of unitality has to be incorporated in the following way [17]:

Theorem 3. (*Extremality in the set of unital channels*) A quantum channel $\mathcal{E} : \mathcal{M}_N \rightarrow \mathcal{M}_N$ is extreme in the set of unital channels if and only if it admits a Kraus representation $\{K_i\}_{i=1}^r$ with

$$\sum_i K_i K_i^\dagger = \mathbb{1}_N, \quad \text{and} \quad \left\{ K_i^\dagger K_j \oplus K_j K_i^\dagger \right\}_{i,j=1}^r \quad (3.4)$$

is a linearly independent set of matrices. (Note that with \oplus we denote the direct sum of linear spaces. For matrices $K, L \in \mathcal{M}_N$ we have $K \oplus L \in \mathcal{M}_{2N}$.)

How can this result now be utilized in order to answer our question? What are the implications on extremality of phase-damping channels? We have already seen that any set of Kraus operators representing a phase-damping channel D is diagonal. Hence, all matrices in the representation trivially commute mutually. It is thus easy to see that the condition of linear independence of the direct sum in Eq. (3.4) is equivalent to linear independence in (3.3). For diagonal maps, extremality in the set of unital channels therefore implies the usually weaker condition of extremality with respect to all quantum channels.

From these considerations it is clear that for a phase-damping channel to be extremal it has to meet $r^2 \leq N$. This implies the following [17]¹

- Single qubit or qutrit ($N < 4$)

The extremal channels in the set of unital channels are precisely the unitary ($r = 1$) transformations (Fig. 3.1(a)). Any phase-damping channel thus allows for a RU representation. Indeed, in case of a single qubit for example an arbitrary phase damping channel

$$\rho' = e^{-i\phi_0 \sigma_z} (p\rho + (1-p)\sigma_z \rho \sigma_z) e^{i\phi_0 \sigma_z} \quad (3.5)$$

may obviously be obtained from $U_\phi = e^{-i\phi \sigma_z}$ with a random variable ϕ with mean value $\langle\langle \phi \rangle\rangle =: \phi_0$ and $\langle\langle \cos^2(\phi - \phi_0) \rangle\rangle =: p$ (Here we assume $\langle\langle \cos(\phi - \phi_0) \sin(\phi - \phi_0) \rangle\rangle = \langle\langle \sin(2(\phi - \phi_0))/2 \rangle\rangle = 0$).

¹Note that the results by Landau and Streater were also found independently in [83] and [18].

3 Classical vs. Quantum Decoherence

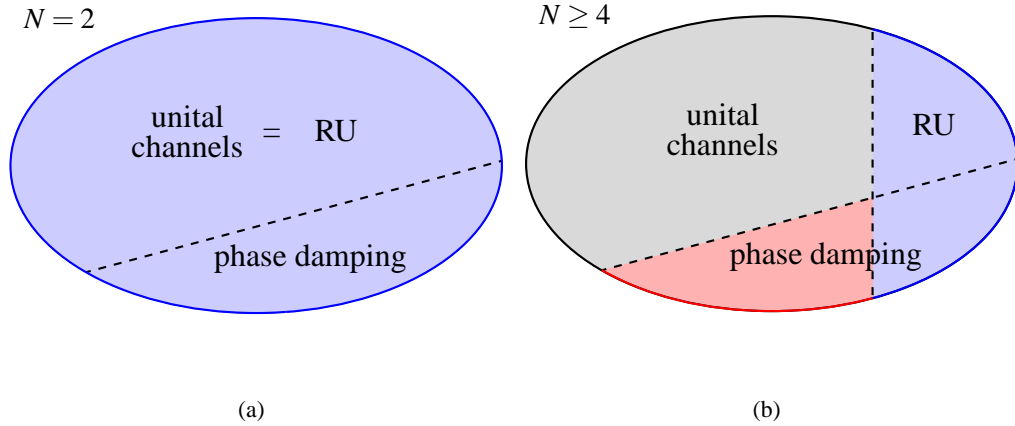


Figure 3.1: (a) In the case of a single qubit ($N = 2$), the unital channels are the convex hull of unitary channels. Any unital channel acting on the state space of a single qubit can thus be represented in terms of a RU channel. (b) For Hilbert space dimension $N \geq 4$ there exist non-unitary extremal channels in the set of unital channels which are thus not of RU type.

- Two or more qubits ($N \geq 4$)

Based on the extremality criterion it is possible for non-unitary ($r > 1$), extremal phase-damping channels to exist. In the following we give several examples. It is thus evident that there are channels that may not be described in terms of RU dynamics (Fig. 3.1(b)).

Recall that a given phase-damping channel $D : \mathcal{M}_N \rightarrow \mathcal{M}_N$ may be described in terms of complex, normalized vectors $\{|a_1\rangle, \dots, |a_N\rangle\} \subset \mathbb{C}^r$, with r being the rank of D . Linear independence of the corresponding Kraus operators is equivalent to a quality of the vectors called “full set of vectors” (FSOV) [17], which is attained if, for a complex matrix $M \in \mathcal{M}_r$, $\langle a_n | M | a_n \rangle = 0 \forall n$ implies $M = 0$. In other words, the projectors $|a_n\rangle\langle a_n|$ have to form a (possibly over-complete) operator basis of \mathcal{M}_r (recall that the projectors are thus said to form an IC-POVM as defined in Sec. 2.6.1).

Based on the formal criterion of extremality it is rather straightforward to come up with examples of a FSOV in any dimension. In the following list we give examples of FSOV for

$r = 2, 3$, and 4 which represent extremal maps in dimension $N = 4, 9$ and 16, respectively:

$$\begin{aligned} & \begin{pmatrix} 1 \\ 0 \end{pmatrix} \begin{pmatrix} 1 \\ 1 \end{pmatrix} \begin{pmatrix} 1 \\ i \end{pmatrix} \begin{pmatrix} 0 \\ 1 \end{pmatrix}, \\ & \begin{pmatrix} 1 \\ 0 \\ 0 \end{pmatrix} \begin{pmatrix} 1 \\ 1 \\ 0 \end{pmatrix} \begin{pmatrix} 1 \\ i \\ 0 \end{pmatrix} \begin{pmatrix} 1 \\ 0 \\ 1 \end{pmatrix} \begin{pmatrix} 1 \\ 0 \\ i \end{pmatrix} \begin{pmatrix} 0 \\ 1 \\ 0 \end{pmatrix} \begin{pmatrix} 0 \\ 1 \\ 1 \end{pmatrix} \begin{pmatrix} 0 \\ 1 \\ i \end{pmatrix} \begin{pmatrix} 0 \\ 0 \\ 1 \end{pmatrix}, \\ & \begin{pmatrix} 1 \\ 0 \\ 0 \\ 0 \end{pmatrix} \begin{pmatrix} 1 \\ 1 \\ 0 \\ 0 \end{pmatrix} \begin{pmatrix} 1 \\ i \\ 0 \\ 0 \end{pmatrix} \begin{pmatrix} 1 \\ 0 \\ 0 \\ 1 \end{pmatrix} \begin{pmatrix} 1 \\ 0 \\ 0 \\ i \end{pmatrix} \begin{pmatrix} 0 \\ 1 \\ 1 \\ 0 \end{pmatrix} \begin{pmatrix} 0 \\ 1 \\ i \\ 0 \end{pmatrix} \begin{pmatrix} 0 \\ 1 \\ 1 \\ 1 \end{pmatrix} \begin{pmatrix} 0 \\ 1 \\ 1 \\ 0 \end{pmatrix} \begin{pmatrix} 0 \\ 0 \\ 1 \\ 1 \end{pmatrix} \begin{pmatrix} 0 \\ 0 \\ 1 \\ i \end{pmatrix} \begin{pmatrix} 0 \\ 0 \\ 1 \\ 1 \end{pmatrix} \begin{pmatrix} 0 \\ 0 \\ 1 \\ i \end{pmatrix} \begin{pmatrix} 0 \\ 0 \\ 1 \\ 1 \end{pmatrix}. \end{aligned}$$

The list may easily be continued to arbitrary dimension.

3.2 Physical Model of Quantum Decoherence

Mathematically, the construction of an extremal and hence true quantum decoherence channel is rather straightforward (Eq. (3.6)). We are, however, also interested in a more physical interpretation of the previous results. In order to allow for some intuitive insight we deem it interesting to have a physically feasible model at hand. We start with the simplest case: a system of two qubits. Note that in case of a two-qubit channel extremality implies $r \leq 2$. For $r = 1$ this is just unitary dynamics, so that $r = 2$ gives the only possibility of an extremal, non-unitary phase damping channel, implying the relative environmental vectors $|a_n\rangle$ to be two-level states (i.e., qubits). In the quest to construct a physical model of quantum decoherence we therefore consider a toy model of a system of two qubits \mathcal{A} and \mathcal{B} , interacting with an “environment” consisting of just a single qubit \mathcal{R} (cf. Fig. 3.2).

The global three-qubit time evolution shall be described by a Hamiltonian

$$H = H_S + H_J + H_{\mathcal{R}}, \quad (3.6)$$

where the interaction of system and reservoir is described by H_J , while their respective free evolution is governed by H_S and $H_{\mathcal{R}}$. The desired phase-damping nature of the dynamics implies all operators acting on the system to be diagonal. We may thus set

$$H_J = \kappa_A \sigma_z^A \otimes \sigma_z^{\mathcal{R}} + \kappa_B \sigma_z^B \otimes \sigma_z^{\mathcal{R}}, \quad (3.7)$$

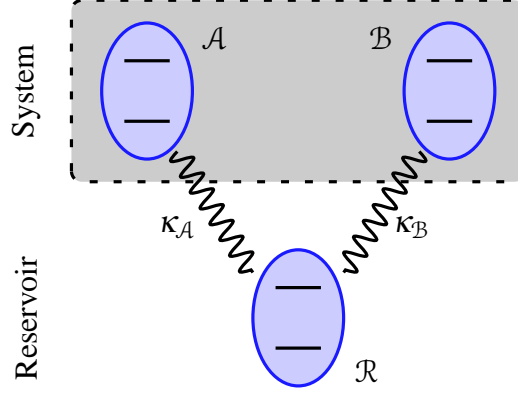


Figure 3.2: In the attempt to construct a physically feasible toy model of a quantum phase-damping channel, a system of two qubits \mathcal{A} and \mathcal{B} is coupled to a simple environment consisting of a single qubit \mathcal{R} .

while free evolution of the reservoir is given by

$$H_{\mathcal{R}} = \vec{\Gamma} \cdot \vec{\sigma}^{\mathcal{R}}. \quad (3.8)$$

(Note that couplings in the form of H_J are present in the context of NMR experiments, where they are used to describe the internuclear dipole-dipole interaction with transverse coupling neglected [84]. In addition, they play a vital role in experiments on ion-trap quantum computers [12].) For simplicity, the system's free Hamiltonian ($H_S = (\Omega_A/2)\sigma_z^A + (\Omega_B/2)\sigma_z^B$) is neglected in the following consideration. For any given time t and assuming the usual product initial state, $\rho \otimes \sigma$, these dynamics lead to a phase-damping channel

$$\rho' = \text{tr}_{\mathcal{R}} [e^{-iHt} (\rho \otimes \sigma) e^{iHt}]. \quad (3.9)$$

The diagonal character of the coupling allows for the diagonalization of the total Hamiltonian with respect to the phase-damping basis of the system,

$$H = \sum_{n=1}^4 |n\rangle\langle n| \otimes \tilde{H}_{\mathcal{R}}^{(n)}. \quad (3.10)$$

The relative Hamiltonians $\tilde{H}_{\mathcal{R}}^{(n)}$ are now responsible for the relative dynamics of the single qubit representing the environment. With the environmental qubit initially in state $|\psi_0\rangle$ we thus arrive at the relative states of the reservoir, $|\psi_n\rangle := \exp\{-i\tilde{H}_{\mathcal{R}}^{(n)}t\}|\psi_0\rangle$. The dynamics of the two-qubit system is then fully determined by these dynamical vectors. As discussed in Sec. 2.3.2, time evolution of the individual elements of the system's density matrix is

3.2 Physical Model of Quantum Decoherence

given in terms of overlaps of these states, that is, $\rho'_{mn} = \langle \psi_n | \psi_m \rangle \rho_{mn}$. In order to identify extremality of the channel, we have to assess whether the relative states $|\psi_n\rangle$ form a FSOV. Using the Bloch representation for these states, $|\psi_n\rangle \mapsto \vec{b}_n$, where the \vec{b}_n denote the so-called Bloch vectors (cf. App. A.4), we arrive at the following equivalence

$$\begin{array}{l} \text{The relative states } |\psi_n\rangle \text{ with } n = 1, \dots, 4 \\ \text{form a FSOV} \end{array} \iff \Sigma := \begin{vmatrix} 1 & 1 & 1 & 1 \\ \vec{b}_1 & \vec{b}_2 & \vec{b}_3 & \vec{b}_4 \end{vmatrix} \neq 0. \quad (3.11)$$

The FSOV condition is thus equivalent to the determinant Σ being non-zero.

Each of the relative environmental Hamiltonians $\tilde{H}_R^{(n)}$ (Eq. (3.7)) describes time evolution of a two-state system. Being a Hermitian matrix, it may thus be rewritten using the Pauli spin matrices, $\tilde{H}_R^{(n)} = \frac{\theta_n}{2}(\vec{v}_n \cdot \vec{\sigma})$, so that

$$|\psi_n\rangle = e^{-i\frac{\theta_n}{2}(\vec{v}_n \cdot \vec{\sigma})t} |\psi_0\rangle. \quad (3.12)$$

It is now obvious that the Hamiltonians define rotations of the initial state of the environment of

$$\begin{aligned} \theta_1 &= \sqrt{\Gamma_x^2 + \Gamma_y^2 + (\Gamma_z + \kappa_A + \kappa_B)^2}, & \theta_2 &= \sqrt{\Gamma_x^2 + \Gamma_y^2 + (\Gamma_z + \kappa_A - \kappa_B)^2}, \\ \theta_3 &= \sqrt{\Gamma_x^2 + \Gamma_y^2 + (\Gamma_z - \kappa_A + \kappa_B)^2}, & \theta_4 &= \sqrt{\Gamma_x^2 + \Gamma_y^2 + (\Gamma_z - \kappa_A - \kappa_B)^2}, \end{aligned} \quad (3.13)$$

about the axes given by the normalized vectors

$$\begin{aligned} \vec{v}_1 &= \frac{1}{\theta_1} \begin{pmatrix} \Gamma_x \\ \Gamma_y \\ \Gamma_z + \kappa_A + \kappa_B \end{pmatrix}, & \vec{v}_2 &= \frac{1}{\theta_2} \begin{pmatrix} \Gamma_x \\ \Gamma_y \\ \Gamma_z + \kappa_A - \kappa_B \end{pmatrix}, \\ \vec{v}_3 &= \frac{1}{\theta_3} \begin{pmatrix} \Gamma_x \\ \Gamma_y \\ \Gamma_z - \kappa_A + \kappa_B \end{pmatrix}, & \vec{v}_4 &= \frac{1}{\theta_4} \begin{pmatrix} \Gamma_x \\ \Gamma_y \\ \Gamma_z - \kappa_A - \kappa_B \end{pmatrix}. \end{aligned} \quad (3.14)$$

We may then use the simple relation

$$e^{\pm i\frac{\theta_n}{2}(\vec{v}_n \cdot \vec{\sigma})t} = \cos\left(\frac{\theta_n}{2}t\right) \mathbb{1} \pm i \sin\left(\frac{\theta_n}{2}t\right) (\vec{v}_n \cdot \vec{\sigma}) \quad (3.15)$$

to arrive at the relative states at time t . For the Bloch vectors this results in the following

3 Classical vs. Quantum Decoherence

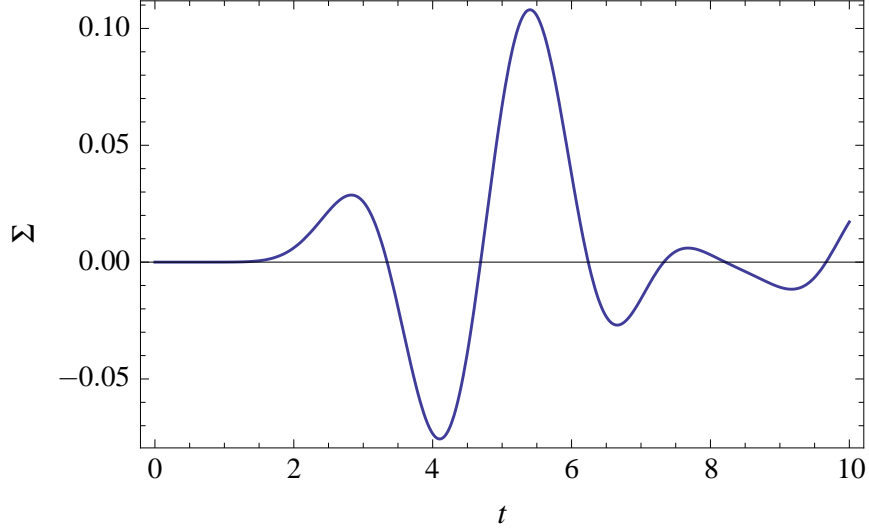


Figure 3.3: Plot of the determinant Σ defined in Eq. (3.11) for the set of parameters [$\kappa_A = 0.4$; $\kappa_B = 1.2$; $\vec{\Gamma} = (0.4, 0, 1.0)$]. For any fixed time t the discrete time evolution according to the Hamiltonian H may be interpreted as a channel. At times t with non-zero determinant the corresponding channel represents an instance of quantum decoherence.

time-dependence:

$$\vec{b}_n(t) = \vec{v}_n (\vec{v}_n \cdot \vec{b}_0) + \cos(\theta_n t) (\vec{v}_n \times \vec{b}_0) \times \vec{v}_n + \sin(\theta_n t) (\vec{v}_n \times \vec{b}_0), \quad (3.16)$$

where \vec{b}_0 represents the initial state $|\psi_0\rangle$.

We let the initial state of the environment start at the north pole of the Bloch sphere, that is, $\vec{b}_0 = (0, 0, 1)$. We find that extremality requires the parameters of our model to meet essentially three conditions

- (i) asymmetric coupling: $0 \neq \kappa_A \neq \kappa_B \neq 0$,
- (ii) $\Gamma_x \neq 0$ or $\Gamma_y \neq 0$, and
- (iii) $\Gamma_z \neq 0$.

In Fig. 3.3 we show the determinant from Eq. (3.11) against time t for a set of parameters with all three conditions met. Clearly, the corresponding phase-damping channels are extremal and hence non-RU at almost any time t . We have thus successfully defined channels describing dynamics of genuine quantum nature. To our knowledge this is the first physically feasible model of quantum decoherence.

3.2.1 Generalization to Arbitrary Dimension

We have seen that extremality of a phase-damping channel is possible only if the square of the rank r of the channel is smaller than or equal to the Hilbert space dimension, i.e., $r^2 \leq N$. Using the model of an extremal phase-damping channel on a Hilbert space of dimension 4 from the last section there are two possible ways to arrive at extremal channels in higher dimension.

- (I) Let D be an extremal channel of rank r and dimension N . The Cholesky factorization (App. A.2) may be used to obtain a set of vectors $|a_n\rangle \in \mathbb{C}^r, n = 1, \dots, N$, such that $D_{mn} = \langle a_n | a_m \rangle$. Augmenting the set of vectors with M arbitrary, normalized vectors $|\tilde{a}_k\rangle \in \mathbb{C}^r$ we arrive at a channel which is still of rank r , but now has dimension $N + M$. Since the FSOV condition is not affected by this procedure the channel is still extremal.
- (II) An extremal channel of higher rank may be constructed in the same spirit as the 4-dimensional prototype of Sec. 3.2. For a rank r extremal channel, the qubits of our original toy model have to be replaced by r -state systems (Fig. 3.4). Accordingly, the channel has dimension $N = r^2$.

In analogy to the two-qubit model, the Hamiltonian may be set to be

$$H = H_S + H_J + H_{\mathcal{R}} \quad (3.17)$$

with

$$H_J = \sum_{i,j} \left(\kappa_{ij}^A \sigma_i^A \otimes \sigma_j^{\mathcal{R}} + \kappa_{ij}^B \sigma_i^B \otimes \sigma_j^{\mathcal{R}} \right). \quad (3.18)$$

Here, the σ_i denote a set of traceless generators of the $SU(r)$. In order to invoke a phase-damping channel on the system, we have to require H_S , as well as all operators σ_i^A, σ_i^B , to be diagonal. As in the two-qubit model, a diagonalization of the total Hamiltonian with respect to the phase-damping basis of system S leads to relative states $|\psi_n\rangle$ of the reservoir. Extremality is again guaranteed for channels where the relative states $\{|\psi_1\rangle, \dots, |\psi_{r^2}\rangle\} \subset \mathbb{C}^r$ of the reservoir form a FSOV. This may again be checked utilizing the Bloch representation, now for the r -level system of qudit \mathcal{R} (see App. A.4)

$$\begin{array}{l} \text{The relative states } |\psi_n\rangle \text{ with} \\ n = 1, \dots, r^2 \text{ form a FSOV} \end{array} \iff \begin{vmatrix} 2/r & 2/r & \cdots & 2/r \\ \vec{b}_1 & \vec{b}_2 & \cdots & \vec{b}_{r^2} \end{vmatrix} \neq 0. \quad (3.19)$$

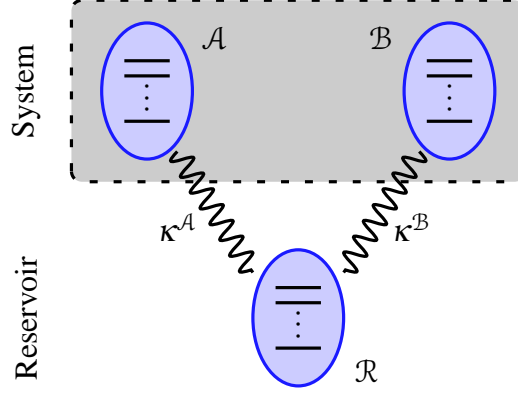


Figure 3.4: An extremal phase-damping channel of arbitrary rank r may be obtained using r -state systems instead of qubits. Accordingly, the system's Hilbert space is of dimension $N = r^2$.

Note that (I) implies that all extremal channels with $r^2 < N$ directly relate to an extremal channel with $r^2 = \tilde{N}$ for some $\tilde{N} < N$. This is the case because, of the N Bloch vectors, only \tilde{N} can possibly yield a non-zero determinant (3.19). It is thus clear that the interesting cases are channels with $N = r^2$ ($N = 4, 9, 16, \dots$).

3.3 A Measure of Quantumness—The Birkhoff Defect

Up to now, the identification of non-classical decoherence dynamics relies on the extremal character of the corresponding channels. The FSOV criterion, and the constructive test using the Bloch representation, allow for the construction of a simple toy model exemplifying the notion of quantum decoherence. Nothing can be said, however, if the channel is not extremal. In the present section, we want to overcome this limitation using a distance measure, this way also engaging in a more quantitative discussion. Based on our model of quantum decoherence, we ask how *quantum* the corresponding channel is. This quantumness may be defined in terms of the *Birkhoff defect*, denoted by d_B [85]. It is defined as the norm-distance of a given channel to the set of RU channels, thus involving the norm of a difference between two quantum channels. Such a difference is, of course, still a linear map, though not necessarily completely positive.

As in the original proposal, we may define the Birkhoff defect of a quantum channel $\mathcal{E} : \mathcal{M}_N \rightarrow \mathcal{M}_N$ in terms of the cb-norm distance

$$d_B(\mathcal{E}) = \inf \|\mathcal{E} - \mathcal{E}_{\text{RU}}\|_{cb}, \quad (3.20)$$

where the infimum is taken over all RU channels \mathcal{E}_{RU} .

3.3.1 The Calculation Scheme

The numerical evaluation of the Birkhoff defect involves two independent minimization procedures: (1) Minimization over all RU channels \mathcal{E}_{RU} , and (2) Minimization with respect to equivalent generalized Kraus representations of the channel difference $\mathcal{E} - \mathcal{E}_{\text{RU}}$ (see App. A.5). In step (1), the set of diagonal RU channels has to be parameterized. For this it is important to note that the number of unitary transformations needed to express a given RU channel depends on the channel's rank: in the case of rank r , the number of unitaries necessary is known not to exceed r^2 [77]. For a system of two qubits we may thus conclude that the set of diagonal RU channels is fully parameterized in terms of angles φ_n^i defining matrices

$$U_i = \text{diagonal}(e^{i\varphi_1^i}, e^{i\varphi_2^i}, e^{i\varphi_3^i}, e^{i\varphi_4^i}), \quad (3.21)$$

and probabilities $p_i, \sum_i p_i = 1$ with $i = 1, \dots, 16$. Note that in the operator sum the diagonal matrices U_i may be brought into the equivalent form

$$U_i = \text{diagonal}(1, e^{i(\varphi_2^i - \varphi_1^i)}, e^{i(\varphi_3^i - \varphi_1^i)}, e^{i(\varphi_4^i - \varphi_1^i)}), \quad (3.22)$$

leaving a total number of 63 free parameters in step (1) (48 angles and 15 probabilities). Step (2) requires minimization over the set of 4×4 positive matrices $S \in \mathcal{M}_4$, including a total number of 19 free parameters (a diagonal matrix of the 4 positive eigenvalues and 15 parameters involved in the subsequent unitary rotation [86]).

The global minimization is thus a complex, high-dimensional optimization procedure. In order to apply the numerical minimization we use the following algorithm:

(1) Initialization

In order to select the point where additional minimization starts, five different sets of probabilities p_i and random positive matrices $S \in \mathcal{M}_4$ are drawn. With these values fixed, minimization with respect to the angles φ_n^i is performed. The best out of the five is then selected for further minimization.

(2) Alternating Minimization

The cb-norm distance is optimized with respect to (one at a time)

- the positive matrices $S \in \mathcal{M}_4$,
- the probabilities p_i , and

3 Classical vs. Quantum Decoherence

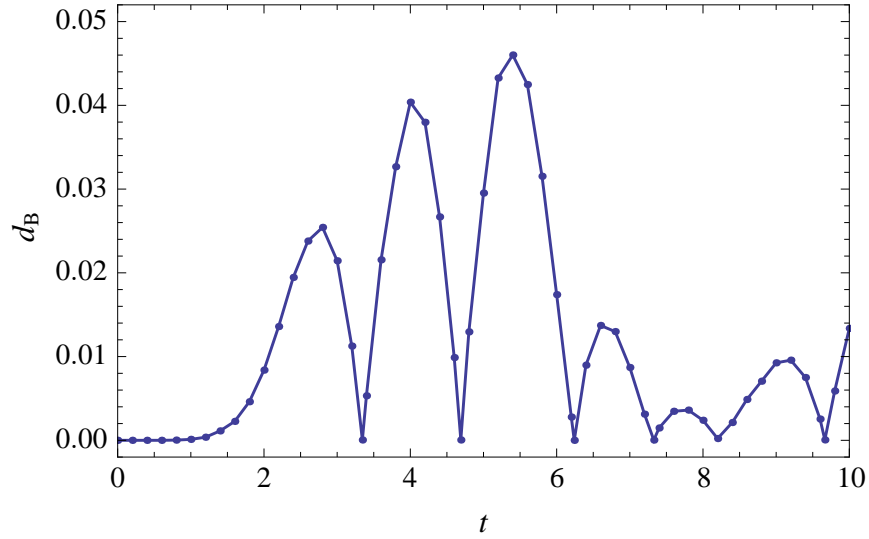


Figure 3.5: Birkhoff defect d_B against time t for the dynamics resulting from the two-qubit toy model. The results allow for a quantitative estimation of quantumness of the corresponding channels.

– the angles φ_k^i ,

whereas the other respective variable sets are left constant. These steps are repeated until no improvement is observed for two complete cycles.

3.3.2 Birkhoff Defect: Results

We evaluate the Birkhoff defect for the channels defined in our toy model with the same parameters as before, i.e., $[\kappa_A = 0.4; \kappa_B = 1.2; \vec{\Gamma} = (0.4, 0, 1.0)]$. The results are shown in Fig. 3.5. The quality of the results is quite satisfactory. For times where the determinant in Eq. (3.11) vanishes—giving a channel of RU type—we equally find the Birkhoff defect to be zero, $d_B = 0$. Plus, it shows a rather smooth time-dependence, there are no considerable fluctuations which could indicate an instability of the numerics.

Quite interestingly, we observe that the Birkhoff defect initially stays close to zero for a long time. Only after $t \approx 1$ a quantumness of appreciable size is assessed. Then, however, it stays well above zero for almost all times.

3.4 Adding Irreversibility

The physical model of quantum decoherence introduced in Sec. 3.2 was achieved via coupling of the quantum system to a single environmental qubit. The reservoir is thus trivially

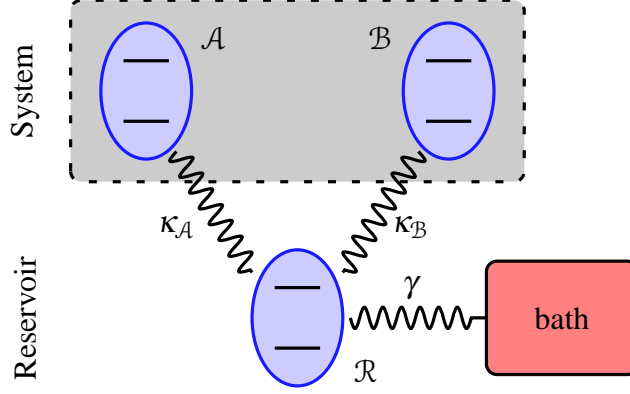


Figure 3.6: In order to arrive at a more realistic decoherence scenario the original toy model is extended by an additional bath. For a coupling between reservoir qubit and bath with $\gamma \neq 0$ the system's decoherence is irreversible.

finite-dimensional, making the dynamics fully reversible and furthermore periodic. Note that these are features one would clearly refute in the context of “real” decoherence: rather than periodic revivals of the coherences, a complete loss of the system's quantum nature would be expected. In order to suppress these coherence revivals, we introduce an additional bath, leading to a deterioration of the correlations shared between system and reservoir. To this end, the reservoir qubit is coupled to some extra degrees of freedom driven by a Markovian master equation. In addition to the time evolution governed by the three-qubit Hamiltonian H , the von Neumann equation is extended by a so-called Lindblad operator \mathcal{L} [87]:

$$\dot{\rho} = -i[H, \rho] + \mathcal{L}(\rho). \quad (3.23)$$

Since \mathcal{L} acts on the reservoir qubit alone and since the Hamiltonian is block-diagonal in the phase-damping basis, that is,

$$H = \begin{pmatrix} \tilde{H}_{\mathcal{R}}^{(1)} & & & 0 \\ & \tilde{H}_{\mathcal{R}}^{(2)} & & \\ & & \tilde{H}_{\mathcal{R}}^{(3)} & \\ 0 & & & \tilde{H}_{\mathcal{R}}^{(4)} \end{pmatrix}, \quad (3.24)$$

we may rewrite Eq. (3.23) according to

$$\dot{\tilde{\rho}}_{mn} = -i\tilde{H}_{\mathcal{R}}^{(m)}\tilde{\rho}_{mn} + i\tilde{\rho}_{mn}\tilde{H}_{\mathcal{R}}^{(n)} + \mathcal{L}(\tilde{\rho}_{mn}). \quad (3.25)$$

3 Classical vs. Quantum Decoherence

Here, we used $\rho = \sum_{m,n} \tilde{\rho}_{mn} |m\rangle\langle n|$ with $\tilde{\rho}_{mn} = \langle m|\rho|n\rangle$, with $\{|n\rangle\}_{n=1}^4$ denoting the phase-damping basis of the system's Hilbert space $\mathcal{H}_S = \mathcal{H}_A \otimes \mathcal{H}_B$.

For the coupling of the reservoir qubit to the heat bath we consider two distinct processes: (I) relaxation into a heat bath of zero temperature, and (II) phase damping. In terms of the Pauli matrices σ_x, σ_y and σ_z and the ladder operators $\sigma_{\pm} := 1/2(\sigma_x \pm i\sigma_y)$, the corresponding Lindblad operators read [87]

$$\begin{aligned} \mathcal{L}^{(I)}(\tilde{\rho}_{mn}) &= \frac{\gamma}{2}(\bar{n}+1) \left\{ 2\sigma_-^{\mathcal{R}} \tilde{\rho}_{mn} \sigma_+^{\mathcal{R}} - \sigma_+^{\mathcal{R}} \sigma_-^{\mathcal{R}} \tilde{\rho}_{mn} - \tilde{\rho}_{mn} \sigma_+^{\mathcal{R}} \sigma_-^{\mathcal{R}} \right\} \\ &\quad + \frac{\gamma}{2}\bar{n} \left\{ 2\sigma_+^{\mathcal{R}} \tilde{\rho}_{mn} \sigma_-^{\mathcal{R}} - \sigma_-^{\mathcal{R}} \sigma_+^{\mathcal{R}} \tilde{\rho}_{mn} - \tilde{\rho}_{mn} \sigma_-^{\mathcal{R}} \sigma_+^{\mathcal{R}} \right\}. \end{aligned} \quad (3.26)$$

and

$$\mathcal{L}^{(II)}(\tilde{\rho}_{mn}) = \frac{\gamma}{2} \left\{ \sigma_z^{\mathcal{R}} \tilde{\rho}_{mn} \sigma_z^{\mathcal{R}} - \tilde{\rho}_{mn} \right\}, \quad (3.27)$$

respectively. In both cases, the parameter γ denotes the strength of the coupling between reservoir qubit and the newly introduced bath (see also Fig. 3.6).

The set of differential equations for the $\tilde{\rho}_{mn}$ is now solved numerically. As a measure for the mixedness of a quantum state, the *purity* of the system \mathcal{S} is well suited for measuring the irreversibility of the dynamics. For a quantum system in state ρ , the purity P is defined as the trace of the squared density matrix

$$P(\rho) = \text{tr}[\rho^2]. \quad (3.28)$$

The maximally possible value is equal to 1, which is attained if and only if the system is in a pure state (that is, ρ is a projector, $\rho^2 = \rho$). In dimension N it is, furthermore, bound from below by $1/N$, corresponding to the completely mixed state $\mathbb{1}_N/N$.

In the case of the original toy model, the dynamics are of periodic nature by construction. This periodicity may be observed in long-term periodic revivals of the purity (see Fig. 3.7(a)). For increasing coupling, $\gamma \neq 0$, these revivals are more and more suppressed until a monotonous decay of the purity is observed (see the case $\gamma = 0.5$, Fig. 3.7(a)). In the case where the additional bath leads to phase damping in the reservoir qubit, the substructure in the time evolution of the qubit's purity remains rather pronounced even for strong coupling (Fig. 3.8(a)). As expected, an increase in the coupling strength results in a decrease of the quantumness of the respective channel (Figs. 3.7(b) and 3.8(b)). Still, however, the Birkhoff defect stays well above zero for a considerable number of channels. This behaviour can be observed for both processes. For γ large enough, the quantumness is zero for almost all times. That means that the respective channels may then, in principle, be decomposed

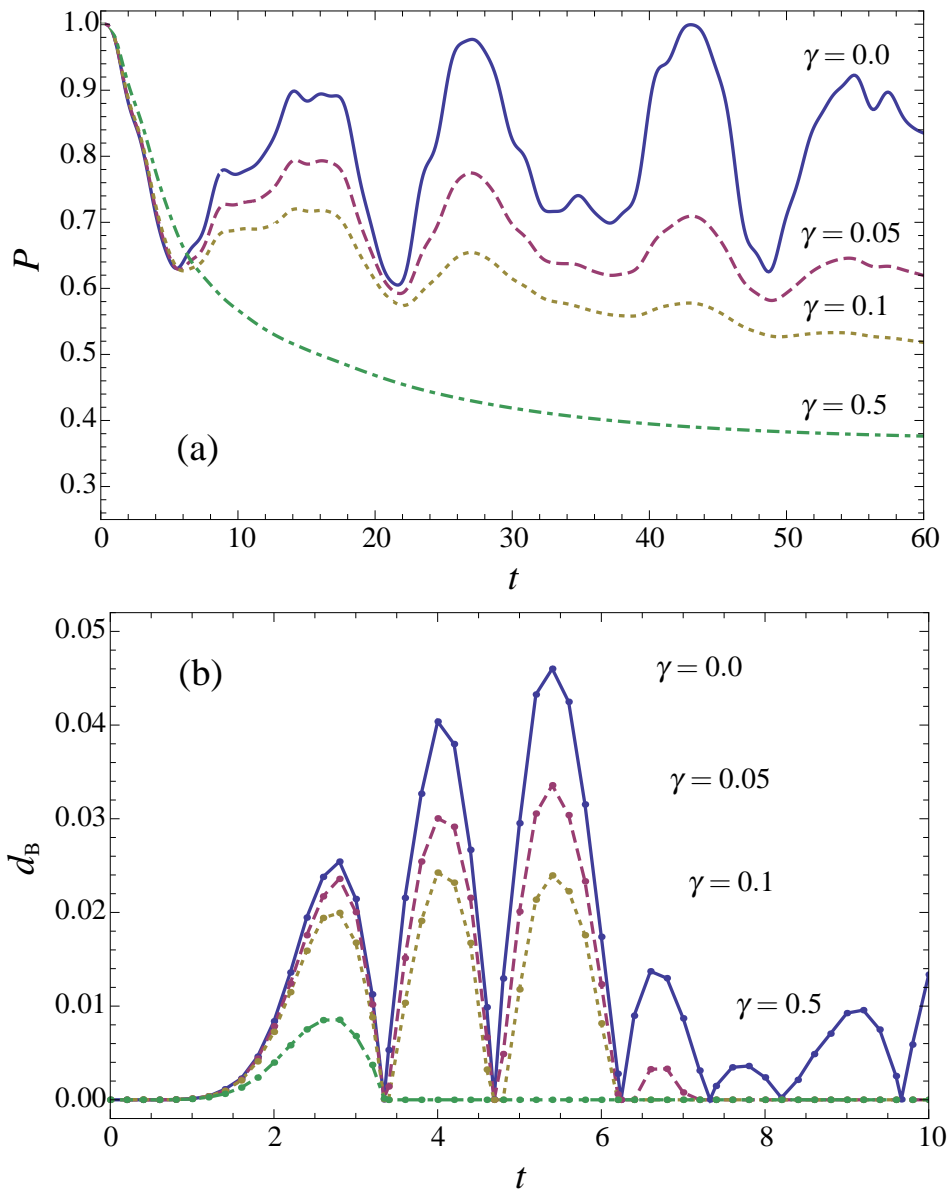


Figure 3.7: (a) Purity and (b) Birkhoff defect for the toy model coupled to an additional bath of zero temperature. The blue, solid lines represent the original, reversible toy model ($\gamma = 0$), the coupling parameters for non-zero couplings are given in the plots. For growing coupling strength γ , the Birkhoff defect of an average channel decreases until, for γ large enough, it is zero at almost any time.

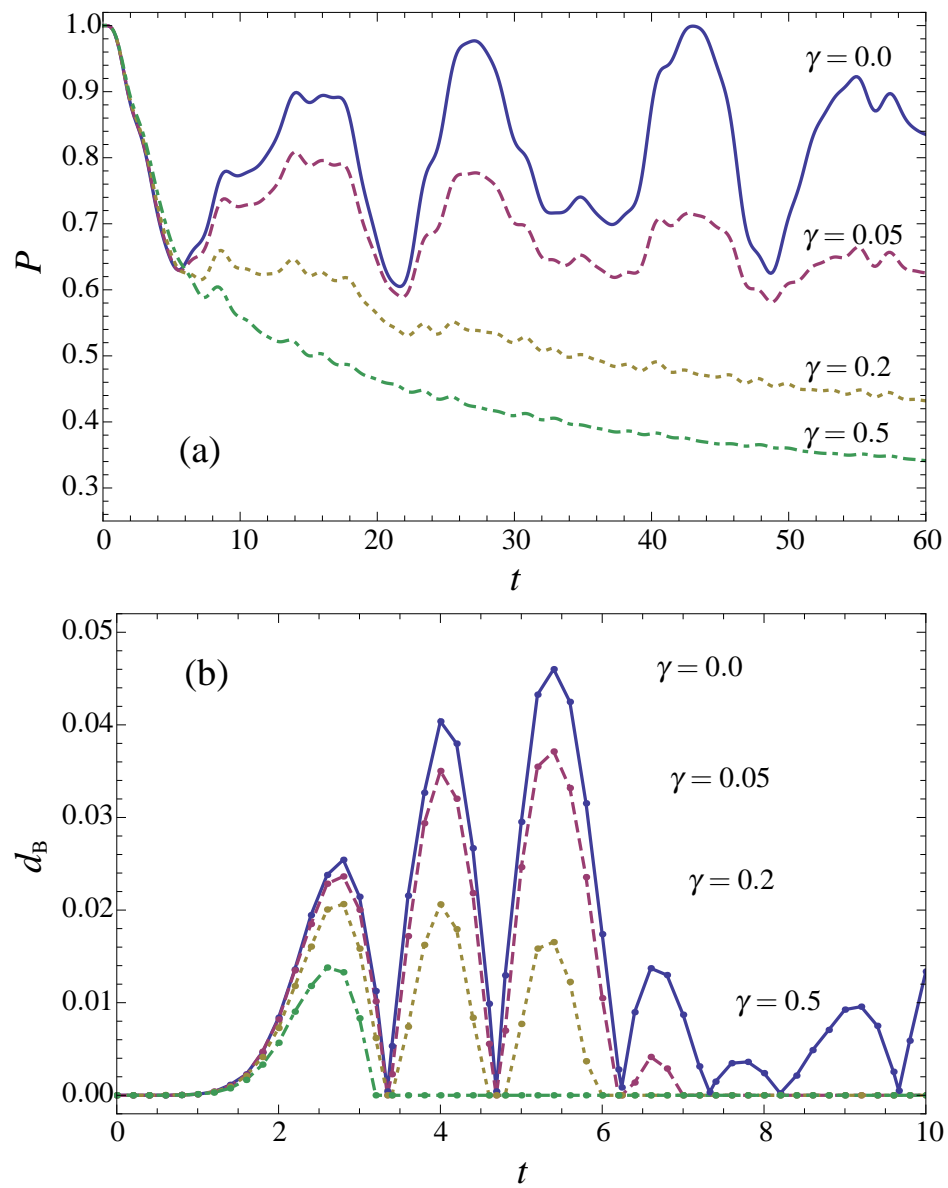


Figure 3.8: (a) Purity and (b) Birkhoff defect for the toy model coupled to an additional bath via phase damping. As in the case of relaxation, we observe a decrease of quantumness for growing coupling γ . Here, however, the substructure in the purity stays pronounced even for higher γ .

3.4 *Adding Irreversibility*

into a RU decomposition. We thus observe the quantumness to be of rather fragile nature. If the disturbance by the additional environment becomes intense enough, it is lost for almost all times.

4 A Geometric Measure of Quantumness

In Chapter 3 the Birkhoff defect was introduced, measuring the norm distance of a given decoherence channel to the convex set of RU channels. With it, a quantitative analysis of the quantum decoherence channels obtained from the toy model, Sec. 3.2, was possible. It was also used to identify quantum decoherence in cases where the extremality criterion was of no avail. A major drawback of this measure of quantumness, however, is its computational complexity: On average, the time effort for the optimization to yield a result is about 40 minutes per channel¹ for a two-qubit system.

In the present chapter, we present a surprisingly simple and intuitive way around this difficulty. Based on the interpretation of a channel in terms of the Bloch representation (cf. App. A.3), we give a new, geometrically motivated measure of the quantumness of dynamics. The intuitive character of this geometric measure allows for remarkable ways to characterize the set of decoherence channels with respect to their quantumness. This is illustrated for the case of two-qubit phase damping. Here, we are able to identify the channel of *maximum quantumness*, i.e., the dynamics with maximum distance to the set of RU channels. We also find a one-parameter class of channels, maximizing the quantumness for a given purity of the dynamics.

In order to test the validity of our findings, we discuss yet another approach to such a measure based on the entanglement of assistance of a channel's Jamiołkowski state. Despite some qualitative variations with respect to the previously introduced measures, it is equally suitable to distinguish classical from true quantum decoherence in the model Hamiltonian of Chap. 3. Due to its greatly reduced complexity, this measure enables a rigorous comparison with the geometric measure. The insights gained on the basis of the geometric measure are in outstanding agreement with results based on the entanglement measure.

¹Using the built-in numerical minimization routine *NMinimize* in Mathematica version 7.0.1.0 on a usual workstation CPU with 2.66 GHz.

4.1 Bloch Volume as a Measure of Quantumness

The Bloch vectors corresponding to the dynamical vectors of a phase-damping channel already play an important role in the identification of quantum decoherence (see Sec. 3.2). In the toy model describing the phase damping of a system of two qubits coupled to a single environmental qubit, we saw that extremality of the channel was given as soon as the Bloch vectors satisfy

$$\begin{vmatrix} 1 & 1 & 1 & 1 \\ \vec{b}_1 & \vec{b}_2 & \vec{b}_3 & \vec{b}_4 \end{vmatrix} \neq 0. \quad (4.1)$$

Once extremality is assured, the channel represents an instance of quantum decoherence, which may not be described in terms of RU dynamics. Some elementary matrix algebra shows that the determinant in Eq. (4.1) is actually equivalent—up to a factor—to the 3-dimensional volume spanned by the Bloch vectors (see App. A.6). We may thus define the *Bloch volume* of the phase-damping channel D via

$$V_B := \text{Vol}(\vec{b}_1, \dots, \vec{b}_4) = \frac{1}{6} \begin{vmatrix} 1 & 1 & 1 & 1 \\ \vec{b}_1 & \vec{b}_2 & \vec{b}_3 & \vec{b}_4 \end{vmatrix}. \quad (4.2)$$

The nature of the dynamics is therefore directly linked to a geometric object: the dynamics may be written in terms of a RU channel if and only if the respective Bloch vectors point to the same hyperplane². If, however, they span a non-zero volume, the related dynamics is of true quantum nature (cf. Fig. 4.1). Moreover, the size of the volume seems to give a meaningful measure of the distance to the set of RU channels. Figure 4.2 allows to compare the Bloch volume V_B with the Birkhoff defect d_B , which measures the norm distance of a given channel to the set of RU channels in terms of the cb-norm (see Sec. 3.3). Here, we use the same set of parameters entering the Hamiltonian of the toy model, Eq. (3.7), as before. Also, the initial environmental state corresponds to $\vec{b}_0 = (0, 0, 1)$. The two approaches show a remarkable agreement. We would like to stress the significance of the implication: rather than having to perform a prolonged optimization procedure, the volume involves the evaluation of the determinant of a 4×4 -matrix.

²Strictly speaking, only the “only if”-part has been shown so far. In order to see the “if”-part, first note that for a channel with $\vec{b}_1, \dots, \vec{b}_4$ pointing to a plane parallel to the x - y -plane RU nature follows immediately, for we can write the corresponding relative states in the form $|\psi_n\rangle = \left(\sqrt{1-p} e^{i\phi_1^{(n)}}, \sqrt{p} e^{i\phi_2^{(n)}} \right)$ with the same p for all $n = 1, \dots, 4$. This results in a Kraus form $\rho' = (1-p)U_1\rho U_1^\dagger + pU_2\rho U_2^\dagger$ with $U_i = \text{diagonal}(e^{i\phi_i^{(1)}}, \dots, e^{i\phi_i^{(4)}})$. For arbitrary coplanar Bloch vectors a suitable rotation of both the initial state $|\psi_0\rangle$ and the relative Hamiltonians $\tilde{H}_{\mathcal{R}}^{(n)}$ leaves the phase-damping channel unaltered, whereas the plane spanned by the new Bloch vectors is again parallel to the x - y -plane.

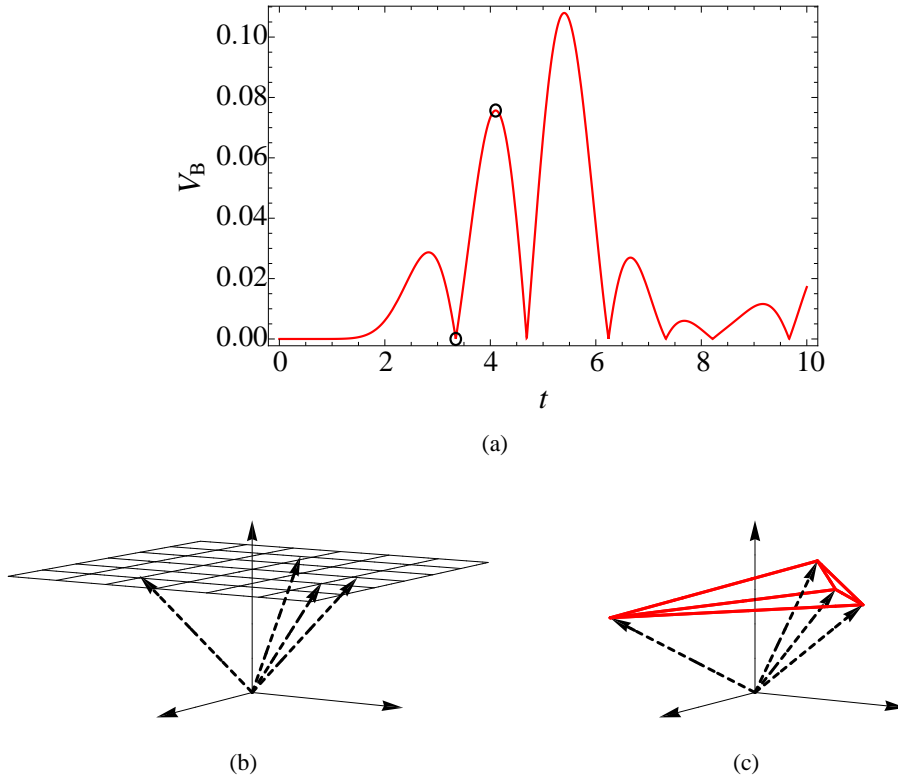


Figure 4.1: The Bloch volume: Phase-damping channels representing true quantum decoherence may be characterized in terms of the volume spanned by the corresponding Bloch vectors. For values of $V_B = 0$, (left circle and (b), exemplary) the corresponding Bloch vectors are coplanar, and the phase-damping channel is RU. For $V_B > 0$, (right circle and (c), exemplary) the dynamical vectors $|\psi_n\rangle$ form a FSOV, so that the corresponding Bloch vectors are not coplanar. In this case, the model gives a true quantum decoherence channel.

Recall that we have seen in Sec. 3.1 that extremality is possible for $r^2 \leq N$ only (remember that r denotes the rank, N is the dimension of the channel). From this we know that $r = 2$ is mandatory for two-qubit phase-damping dynamics ($N = 4$) to be extremal. Hence, the extremal channels in this case are in one-to-one correspondence to vectors in Bloch sphere spanning a tetrahedron with non-zero volume. Within the set consisting of quadruples of vectors in \mathbb{R}^3 , the set of coplanar vectors is a null set. We can thus conclude that extremality is generic for channels with dimension 4 and rank 2.

4.1.1 Direct Calculation of the Bloch Volume

Of course, in order to be able to calculate the Bloch volume of a phase-damping channel, the corresponding Bloch vectors have to be assessed first. To begin with, given an arbitrary

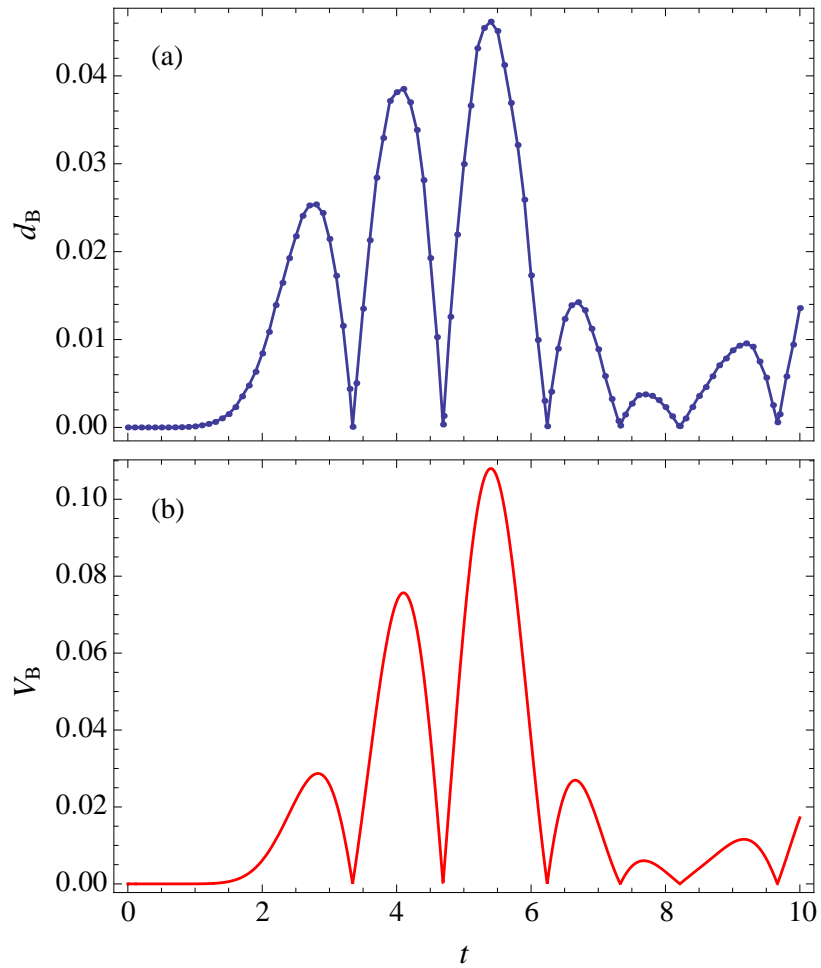


Figure 4.2: The quantumness of the phase-damping channels resulting from the toy model in Sec. 3.2 for the set of parameters $[\kappa_A = 0.4; \kappa_B = 1.2; \vec{\Gamma} = (0.4, 0, 1.0)]$. The agreement between (b) Bloch volume V_B and (a) Birkhoff defect d_B is quite remarkable.

4.1 Bloch Volume as a Measure of Quantumness

phase-damping channel D one has to extract the dynamical vectors $|a_n\rangle$, using, e.g., the Cholesky factorization (App. A.2). Next, these dynamical vectors have to be translated into Bloch vectors (see App. A.3). Arising from the matrix representation of the channel, there are thus two intermediate steps to be completed before the Bloch volume may be obtained.

There is, however, a direct and much more elegant way to evaluate the Bloch volume. It is based on the so-called *Caley-Menger determinant* (see App. B). We find that

$$V_B^2 = \frac{1}{288} \begin{vmatrix} 0 & 1 & 1 & 1 & 1 \\ 1 & & & & \\ 1 & 4 & (\text{id} - D \star D^*) & & \\ 1 & & & & \\ 1 & & & & \end{vmatrix}. \quad (4.3)$$

Recall that \star denotes the Hadamard product, i.e., the entry-wise product of matrices. As a consequence, the matrix representation of the identity, id , is a matrix with *all* entries equal to 1.

Generalization to Arbitrary Dimension

How can the above result, Eq. (4.3), be generalized to higher dimension? Again, recall that $r^2 \leq N$ is necessary for a channel to be extremal (with r being the rank and N the dimension of the channel, respectively). Extremal channels with $r^2 < N$ are, furthermore, directly connected to the cases $r^2 = \tilde{N}$ with $\tilde{N} < N$ (see Sec. 3.2). In order to find interesting instances of extremality, we therefore have to examine dynamics in dimension $N = r^2$, that is $N = 4, 9, 16$ and so on. For simplicity we may thus assume that $N = r^2$. In this case, the calculation of the volume may again be carried out using the Caley-Menger determinant (for details see App. B). The relation is given by

$$V_B^2 = \frac{(-1)^N}{2^{N-1}((N-1)!)^2} \begin{vmatrix} 0 & 1 & \dots & 1 \\ 1 & & & \\ \vdots & 4(\text{id} - D \star D^*) & & \\ 1 & & & \end{vmatrix}. \quad (4.4)$$

In case the square of the rank is smaller than the channel's dimension, $r^2 < N$, the direct calculation of the Caley-Menger determinant will yield a zero volume at all times. Rather, one has to check the corresponding determinant for all r^2 -dimensional sub-matrices of D obtained by discarding $N - r^2$ rows and columns of the same indices.

4.1.2 The Channel with Maximum Bloch Volume

The Bloch volume seems to give an exceptionally effortless way of determining a channel's quantumness. Furthermore, its geometric character offers a very intuitive approach to the issue of RU vs. non-RU dynamics. How can we exploit this fact in order to gain insights into the geometry of the set of true quantum decoherence? Let us first limit the discussion to the case of two-qubit dynamics, where the relevant object of interest is a volume in \mathbb{R}^3 . From geometric considerations it is rather straightforward to arrive at the phase-damping channel with maximum Bloch volume. It corresponds to the case where the Bloch vectors span a regular tetrahedron inside the Bloch sphere, having an edge length of $\sqrt{\frac{8}{3}}$ and volume $\frac{8}{9\sqrt{3}}$. A possible choice of Bloch vectors leading to this object is given by the following four vectors:

$$\vec{b}_1 = \begin{pmatrix} 0 \\ 0 \\ 1 \end{pmatrix}, \quad \vec{b}_2 = \begin{pmatrix} \sin \alpha \\ 0 \\ \cos \alpha \end{pmatrix}, \quad \vec{b}_3 = \begin{pmatrix} \sin \alpha \cos \frac{2\pi}{3} \\ \sin \alpha \sin \frac{2\pi}{3} \\ \cos \alpha \end{pmatrix}, \quad \vec{b}_4 = \begin{pmatrix} \sin \alpha \cos \frac{2\pi}{3} \\ -\sin \alpha \sin \frac{2\pi}{3} \\ \cos \alpha \end{pmatrix}, \quad (4.5)$$

where $\alpha = \arccos(-\frac{1}{3})$ is the so-called tetrahedral angle. With $x := \sqrt{\frac{1+\cos \alpha}{2}} = \sqrt{\frac{1}{3}} \approx 0.57735$ the corresponding phase-damping channel has the matrix representation

$$D_\Delta = \begin{pmatrix} 1 & x & x & x \\ x & 1 & ix & -ix \\ x & -ix & 1 & ix \\ x & ix & -ix & 1 \end{pmatrix}. \quad (4.6)$$

In terms of the Bloch volume V_B , there exists no channel with greater quantumness.

4.1.3 SIC-POVMs and Quantum Decoherence

What about channels of maximum quantumness in higher dimension? In dimension N , the maximum Bloch volume is achieved for vectors spanning a regular $(N-1)$ -simplex. Note that we have encountered this situation before: the projectors $|\psi_n\rangle\langle\psi_n|$ of the dynamical vectors compatible with this situation form a SIC-POVM (see Sec. 2.6.2). If we conjecture the Bloch volume to be a suitable measure of quantumness, we can claim the channel corresponding to a SIC-POVM to be the dynamics which is maximally quantum in any dimension. Remember that the N dynamical vectors forming a SIC-POVM are distinguished

by the relation³

$$|\langle \psi_m | \psi_n \rangle|^2 = \frac{1}{\sqrt{N+1}}, \quad m \neq n. \quad (4.7)$$

The Bloch volume of such a phase-damping channel may be evaluated using the Caley-Menger determinant (see App. B.3). It is given by

$$V_B = \frac{\sqrt{N} \left(2 \frac{\sqrt{N}}{\sqrt{N+1}} \right)^{\frac{N-1}{2}}}{(N-1)!}. \quad (4.8)$$

Note, however, that we now face the same difficulty mentioned in Sec. 2.6.2: it is hitherto unknown whether such an object exists in any dimension.

The construction of both analytical and numerical examples of SIC-POVMs in dimension N relies on the identification of a *fiducial state* $|\psi\rangle$, which is mapped onto the final set by a group of unitary operators. For $N = 2$, for example, one fiducial state is identified as the Bloch vector $(1, 1, 1)/\sqrt{3}$. The additional states are obtained after simple rotations by π about the x , y , and z axis, respectively [82]. Note that this situation is very similar to our toy model (see Sec. 3.2). Here, too, the environment starts out in a single pure state $|\psi_0\rangle$, which is subsequently mapped onto the relative states of the environment via some unitary transformation \tilde{U}_n . It is thus interesting to note that there are instances where the relative environmental Hamiltonians of our model of quantum decoherence succeed in spanning a SIC-POVM. This is the case if, for example, we choose the parameters to be $[\kappa_A = 1.688; \kappa_B = 0.918; \vec{\Gamma} = (1, 0, 0)]$, the Bloch vector of the initial state points in x -direction, that is, $\vec{b}_0 = (1, 0, 0)$. The Bloch volume achieves the maximum possible value for $t \approx 1.35$; then, the Bloch vectors of the relative states of the environment span a regular tetrahedron inside the Bloch sphere (see Fig. 4.3).

Another interesting idea relating to SIC-POVMs is discussed in several papers by Chris Fuchs and co-workers [88, 89, 90]. His idea is to look at implementations of quantum cryptography protocols. Usually, the security of such schemes relies on the fact that any eavesdropper reveals himself by disturbing the quantum information he reads. The amount of disturbance, however, delicately depends on the set of states in which the information is encoded. Just consider the example given in [90]: “given a state $|\psi\rangle$, the measurement which projects onto $|\psi\rangle$ and its orthogonal complement causes no disturbance to the state”. For the purpose of securely transmitting quantum information, one thus needs an ensemble of states that enables the legitimate user to detect an intruder. The idea is formally cast into a measure

³Note that the definition of N here is different from the one in Sec. 2.6.2.

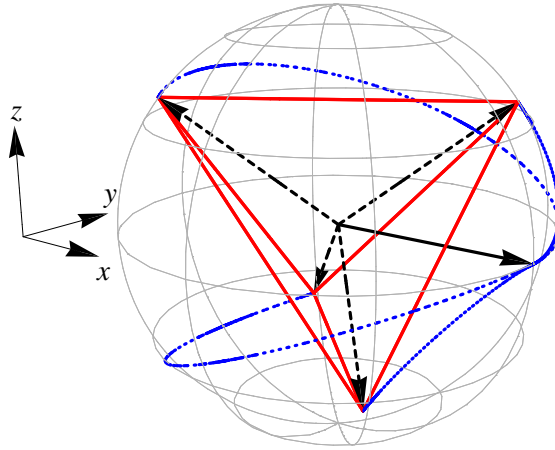


Figure 4.3: If the parameters in the model Hamiltonian are chosen appropriately, the relative states of the environment form a SIC-POVM. Here, we chose the initial state to point in x -direction (straight, black vector). Starting from this point, the relative states (dashed vectors) evolve along the blue, dotted arcs until they span a regular tetrahedron, indicated in red.

called “the quantumness of a set of quantum states”, giving an evaluation of how difficult it is for an eavesdropper to remain unnoticed. It turns out that an optimal choice for encoding the information is given by a SIC-POVM [89].

4.2 Characterization of Two-Qubit Phase Damping

How can the geometric character of the Bloch volume be used to gain further insight into the set of quantum decoherence channels? We study this question in the present section with the help of the example of two-qubit phase-damping dynamics. In the following section, the purity plays a central role in the characterization of channels. Recall that the purity P of a quantum state is simply defined as the trace of the state’s density matrix squared:

$$P(\rho) := \text{tr} [\rho^2]. \quad (4.9)$$

It is a very helpful way to categorize quantum states with respect to their “mixedness”, giving an estimation of how close the state is to being pure. A pure state is distinguished by its idempotence: $\rho^2 = \rho$. Its purity is thus equal to 1. The completely mixed state, on the other

hand, is the most remote to the set of pure states. It is an incoherent superposition of all basis states with equal weights. Its purity evaluates to $1/N$, depending on the dimension N of the quantum system scrutinized.

4.2.1 Purity of a Phase-Damping Channel

How can the purity help in the characterization of phase-damping channels? It is important to note that purity remains unchanged under unitary (Hamiltonian) dynamics. A change of a quantum system's purity is thus a definite indicator that the underlying dynamics is non-unitary. A damping of the coherences will always result in a purity loss. Looking at the diminution a channel causes may therefore reveal how strong the state is affected by the decoherence process. But how exactly can the loss of purity, due to a certain phase-damping channel D , be measured? Let us consider the situation where the channel is applied to the initial state ρ with $\rho_{mn} = 1/N$ for all $m, n = 1, \dots, N$. Certainly, this initial state is pure, that is, $P(\rho) = 1$. The final state, however, has a purity given by

$$\begin{aligned} P(D \star \rho) &= \text{tr}[(D \star \rho)^2] \\ &= \left(\sum_{n=1}^N \rho_{nn}^2 + \sum_{m,n=1; m \neq n}^N |d_{mn}|^2 |\rho_{mn}|^2 \right) \\ &= \frac{1}{N} + \frac{1}{N^2} \sum_{m,n=1; m \neq n}^N |d_{mn}|^2. \end{aligned} \quad (4.10)$$

Note that this is trivially equal to the purity of the Jamiolkowski state of the phase-damping channel D ,

$$\begin{aligned} P(\rho^D) &= P\left(\frac{D}{N}\right) \\ &= \frac{1}{N} + \frac{1}{N^2} \sum_{m,n=1; m \neq n}^N |d_{mn}|^2. \end{aligned} \quad (4.11)$$

We will refer to $P(\rho^D)$ simply as the *purity of the channel D* . Since all matrix elements of D are equally weighted in this sum, it may be seen as a way to evaluate a channel's effect on the purity of a state *on average*.

Since the Kraus rank of the channel is equal to the rank of the corresponding Jamiolkowski state [77], we know that the (unital) channel represents unitary dynamics if and only if $P(\rho^D) = 1$. In this case, the dynamics of course cannot change any state's purity. On the other hand, we see in Eq. (4.11) that $P(\rho^D) = 1/N$ is only possible if $d_{mn} = 0$ for all $m, n = 1, \dots, N$ with $m \neq n$. Then, however, *any* initial state is mapped onto a state with

4 A Geometric Measure of Quantumness

diagonal density matrix. We may call this channel the *completely decohering channel*, D_{cd} . Based on these considerations, a channel's purity may thus be used as an indication of the effect of the channel on any arbitrary initial state. In other words, it measures the *decoherence potential* of the dynamics. If it is close to 1, the channel cannot change a state's purity to a great extent. If it approaches a value of $1/N$, however, its impact, in terms of purity, will perhaps be large.

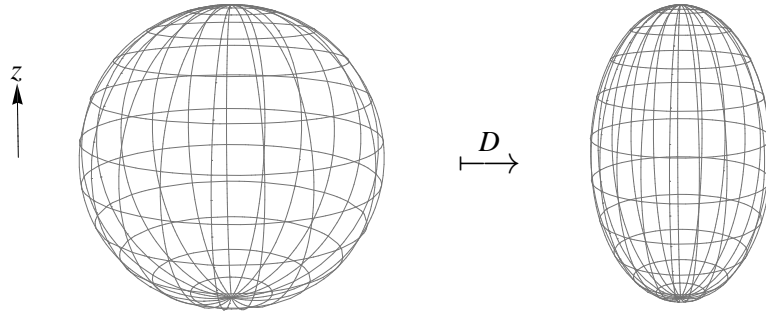


Figure 4.4: The single-qubit phase-damping channel D simply contracts the Bloch sphere towards the z -axis. Here, a parameter of $|c| = 0.6$ is used. The dynamics leads to a deformation of the sphere into an ellipsoid, causing a decrease of the volume by a factor of $|c|^2$.

The underlying idea is easily understood at the example of single-qubit dynamics. Here, a phase-damping channel is fully characterized by a single, complex parameter c . In order to estimate the average effect of the dynamics, we consider its influence on the manifold of all pure qubit states, represented by the Bloch sphere (a sphere in \mathbb{R}^3 of radius 1, see App. A.3). In effect, the channel simply contracts the sphere by the factor $|c|$ towards the z -axis, leaving intact only the eigenstates of σ_z , $|0\rangle$ and $|1\rangle$ (Fig. 4.4, see also App. A.7). The phase-damping dynamics thus leads to a deformation of the Bloch sphere, causing a reduction of the volume. To estimate the overall effect of the channel, it is instructive to look at the relative change in volume which is easily obtained to be (see App. A.7)

$$\frac{V'}{V} = |c|^2. \quad (4.12)$$

(Here, V and V' denote the volume before and after the phase damping, respectively.) The

purity of the channel, on the other hand, is simply given by

$$P(\rho^D) = \frac{1}{2}(1 + |c|^2). \quad (4.13)$$

The connection between the channel's purity and the volume reduction is thus obvious. Although this clear-cut geometric interpretation is no longer valid in higher dimensions, the general idea about the purity measuring the decoherence potential should be clear.

4.2.2 Mixed Channels of Maximum Quantumness (MCMQ)

We may now use the purity together with the Bloch volume in order to gain some more insights into the geometry of the set of phase-damping channels. In the preceding sections, we have been acquainted with several extremal examples. First, we have successfully identified the channel of maximum Bloch volume and, hence, arguably of maximum quantumness. Note that it has a purity of

$$\begin{aligned} P(\rho^{D_\Delta}) &= \frac{1}{4} + \frac{12}{16} |x|^2 \\ &= \frac{1}{2} \end{aligned} \quad (4.14)$$

On the other hand we saw that the pure (unital) channels correspond to unitary transformations, thus trivially belonging to the set of RU channels. What can be said about channels with intermediate values of $1/2 < P(\rho^D) < 1$? Certainly, at any given amount of purity, there must exist channels maximizing the Bloch volume. In order to find these channels, we have to maximize the volume for a given value of purity. The purity P of an arbitrary phase-damping channel of rank 2 may be expressed in terms of the corresponding Bloch vectors $\vec{b}_n \in \mathbb{R}^3$. In fact, it is straightforward to arrive at the following form:

$$P(\rho^D) = \frac{1}{2}(1 + |\vec{b}_S|^2), \quad (4.15)$$

where \vec{b}_S denotes the barycentre of the Bloch vectors, that is, $\vec{b}_S = (\vec{b}_1 + \dots + \vec{b}_4)/4$.

We are thus interested in finding the tetrahedron spanning the maximum volume, while the distance from its corners' barycenter to the origin has a fixed value. We find this maximum numerically: it is achieved for the cases depicted in Fig. 4.5. The Bloch vectors may be defined as in Eq. (4.5), yet with $\alpha \in [0, \arccos(-1/3)]$. For $\alpha = 0$ the volume is zero, the purity equals one and the corresponding channel is unitary. For $\alpha = \arccos(-1/3)$ we have the case of the channel with maximum volume. The values in between give the *mixed channels with maximum quantumness* (MCMQ). The picture that comes to mind is the act of

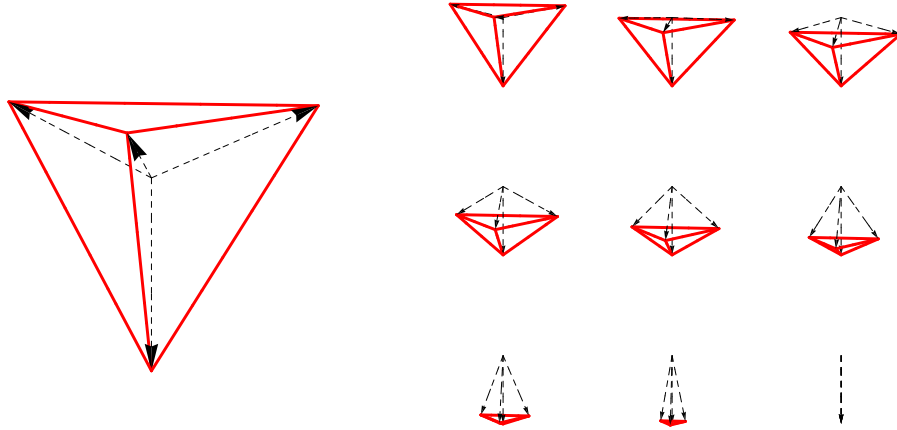


Figure 4.5: Schematic Plot of the Bloch vectors (black, dashed arrows) corresponding to the channel with maximum volume (big) and to a selection of MCMQ (small) spanning tetrahedra (red lines) of decreasing volume.

closing an umbrella: while one of the Bloch vectors (the central rod) remains fixed, the three remaining ones move towards the first just like the metal frame carrying the fabric.

4.3 Quantumness of Assistance

In this section we discuss yet another option for a quantumness measure, enabling us to rigorously test the validity of all results found so far. Its major advantage as compared to the Birkhoff defect is that the calculations involved require much less effort. The main reason is that less optimization procedures are involved. The basic idea, which relies on the Jamiolkowski isomorphism, was first presented in [21]. Recalling the definition from Sec. 2.4, the Jamiolkowski state $\rho^{\mathcal{E}}$ of the channel \mathcal{E} is defined via

$$\rho^{\mathcal{E}} = \frac{1}{N} \sum_{m,n} \mathcal{E}(|m\rangle\langle n|) \otimes |m\rangle\langle n|. \quad (4.16)$$

That is, the channel is applied to one “half” of the maximally entangled pure state $\sum_n |nn\rangle / \sqrt{N}$.

For a RU channel it is rather obvious that the corresponding Jamiolkowski state is a convex mixture of maximally entangled states, since entanglement is unaffected by local unitary transformations [30]. Conversely, the Jamiolkowski state being a convex mixture of maxi-

mally entangled states also implies the channel is RU. This is true since maximum entanglement may be attained by pure states only. The pure states forming the Jamiolkowski state thus have to be connected to the initial, maximally entangled state via some unitary transformation. The identification of a RU channel may now be achieved using the entanglement of assistance. Remember that the entanglement of assistance involves a maximization of the entanglement over all pure-state decompositions of a mixed state:

$$E_A(\rho) := \max_{\{p_i, |\psi_i\rangle\}} \left\{ \sum_i p_i E(|\psi_i\rangle) : \sum_i p_i |\psi_i\rangle\langle\psi_i| = \rho \right\}. \quad (4.17)$$

Therefore, a quantum channel \mathcal{E} is RU if and only if its Jamiolkowski state has maximum entanglement of assistance [21].

In order to arrive at a measure of quantumness, we choose to make some minor yet helpful modifications. First, the entanglement of assistance gets renormalized, such that it is bound from above and below by 1 and 0, respectively. In the second step we invert this renormalized quantity simply by subtracting it from 1. The quantumness, as measured in terms of the entanglement of assistance, is thus given by

$$Q_A(\mathcal{E}) = 1 - \frac{E_A(\rho^{\mathcal{E}})}{\log_2 N}, \quad (4.18)$$

$\log_2 N$ giving the maximum value for the entanglement of assistance. We now have $0 \leq Q_A \leq 1$ with $Q_A = 0$ if and only if the corresponding channel is RU.

Quantumness of Assistance: First Results

For the calculation of the entanglement of assistance E_A we use the method described in [91] and [92] (see also App. A.1), which was originally formulated in the context of entanglement of formation. For channels of rank 2, the evaluation involves optimization with respect to a unitary 4×4 matrix $U \in \mathcal{M}_4$. Thus, a total number of 15 parameters is involved—much less than was the case for the Birkhoff defect d_B . This results in a great reduction of computational cost: here, the average computation time is about 2 minutes, making the calculation 20 times as fast. In a first step, we compare the results of this new measure with the Birkhoff defect and the Bloch volume. The comparison is again based on the toy model of Chap. 3. The results are shown in Figs. 4.6 and 4.7. We observe that the quantumness of assistance is equally able to identify RU dynamics. That is, we find $Q_A = 0$ whenever the other measures are zero as well. Qualitatively, the agreement of Birkhoff defect and Bloch volume appears best. A direct comparison reveals that some of the local maxima are shifted

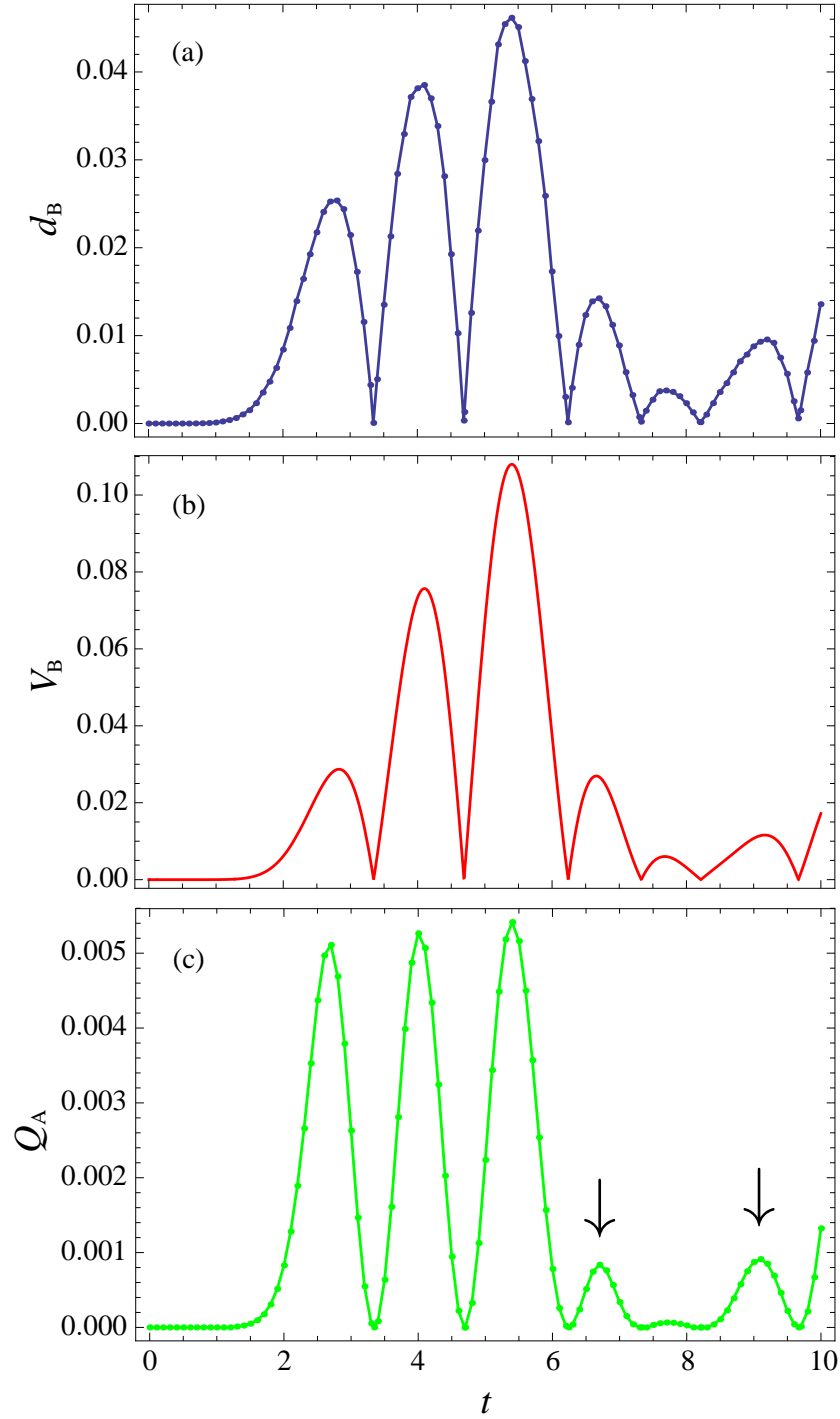


Figure 4.6: Comparison of (a) Birkhoff defect d_B , (b) Bloch volume V_B , and (c) the quantumness of assistance Q_A for channels arising from the model Hamiltonian of Sec. 3.2. Here, the same parameters as in Fig. 4.2 are used [$\kappa_A = 0.4$; $\kappa_B = 1.2$; $\vec{\Gamma} = (0.4, 0, 1.0)$]. While the quantumness of assistance is clearly able to identify RU dynamics, it shows some qualitative aberrations compared to the previously defined measures. It may be observed, for example, that the hierarchy of certain maxima is reversed (indicated with arrows).

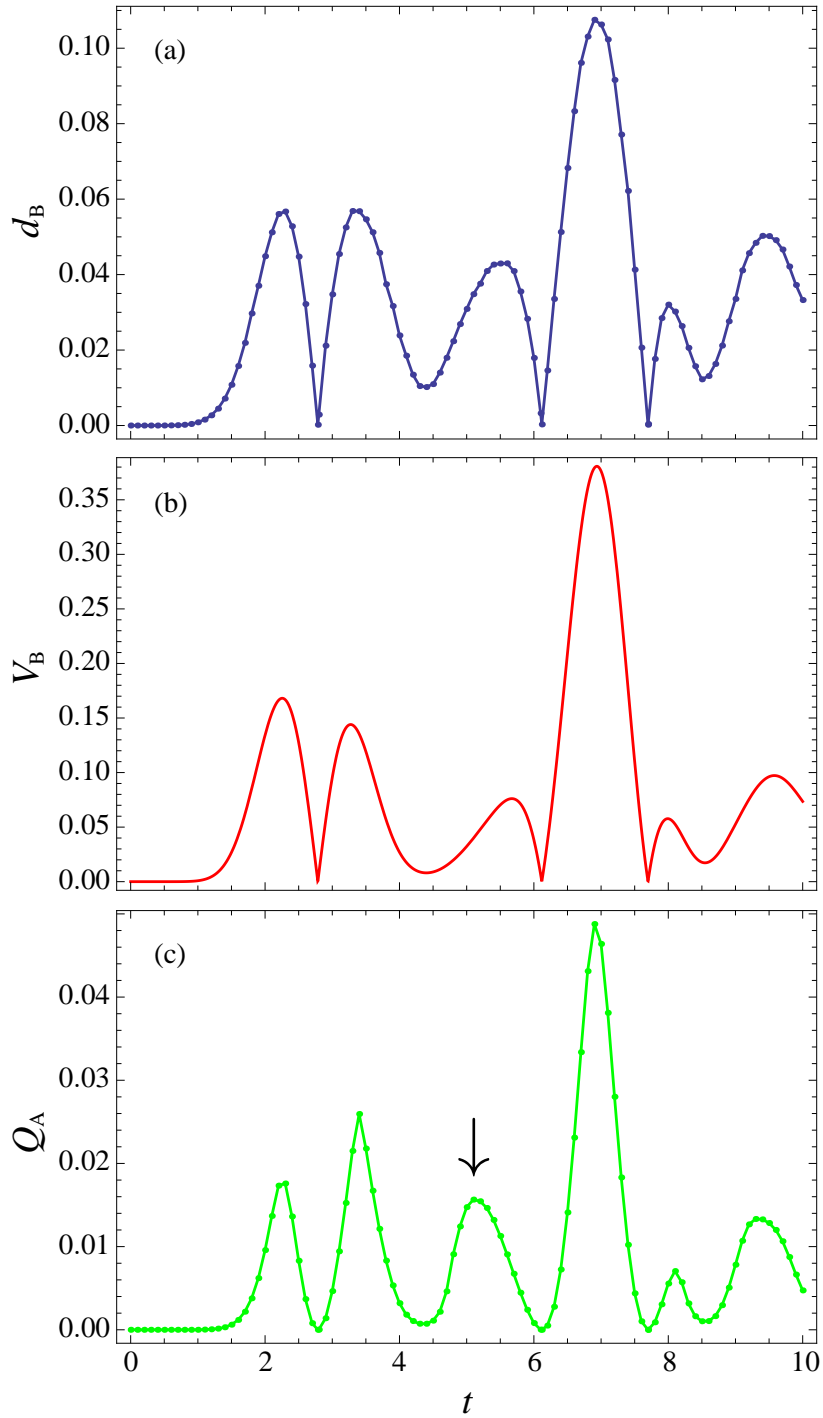


Figure 4.7: Comparison of (a) Birkhoff defect d_B , (b) Bloch volume V_B , and (c) the quantumness of assistance Q_A for a different set of parameters [$\kappa_A = 0.32$; $\kappa_B = 1.35$; $\vec{\Gamma} = (0.55, 1.14, 0.9)$]. In addition to a change in the hierarchy of local maxima, one may observe an obvious shift in the location of the third local maximum (indicated with an arrow).

quite significantly towards different values of time t (see the third maximum in Fig. 4.7 (b) between $t = 5$ and $t = 6$, for example).

4.4 Comparison of Bloch Volume and Quantumness of Assistance

The measures introduced in the present chapter shall now be studied as to their mutual relation. We start by looking at random samples of two-qubit phase-damping channels. They are generated according to the property $D_{mn} = \langle a_n | a_m \rangle$, where the $|a_n\rangle \in \mathbb{C}^r$ are normalized vectors, r giving the rank of the resulting channel. That is, we define D as the *Gram matrix* of the complex $|a_n\rangle$. We use vectors equally distributed on the unit sphere in \mathbb{C}^r . First, only channels of rank 2 are studied. For each channel we calculate Bloch volume V_B and quantumness Q_A as well as the purity P . The result is shown in Fig. 4.8.

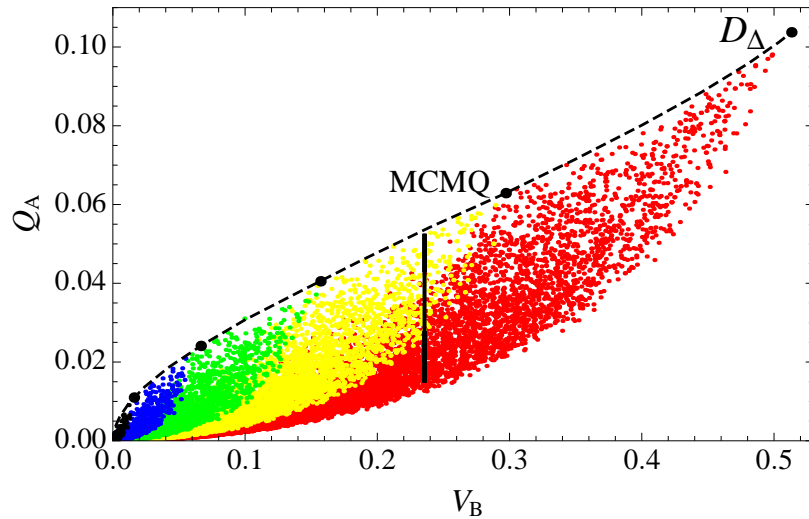


Figure 4.8: Quantumness vs. Bloch volume of a set of randomly generated phase-damping channels of rank 2. The color coding indicates the purity of the channel in the following way: red ($0.5 \leq P < 0.6$), yellow ($0.6 \leq P < 0.7$), green ($0.7 \leq P < 0.8$), blue ($0.8 \leq P < 0.9$), black ($0.9 \leq P < 1$). The dashed line corresponds to the one-parameter set of MCMQ. The channel with maximum Bloch volume D_Δ (and purity 0.5) is indicated with a black dot, as are the MCMQ with purity 0.6, 0.7, 0.8, and 0.9 (from right to left). The agreement of the upper bound of the quantumness for fixed V_B with the analytically obtained set of MCMQ is quite remarkable. The vertical black line represents the one-parameter class of channels D_ϕ with constant Bloch volume of $V_B \approx 0.2357$.

One can clearly see that, depending on the purity of the channel, there exist certain bounds to the quantumness as well as to the Bloch volume: the lower the purity, the higher the

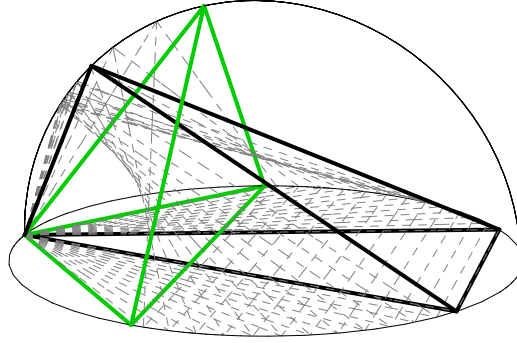


Figure 4.9: Schematic Plot of the tetrahedra spanned by the one-parameter class of phase-damping channels with constant Bloch volume. The black and green tetrahedra correspond to values of $\phi = -0.5$ and $\phi = 0.25$, respectively. The values in between are indicated with gray, dashed lines.

accessible quantumness and volume. In Fig. 4.8 this is highlighted using a color scheme to single out specific purity intervals. Certainly, there is no one-to-one correspondence between the two measures; yet, the correlation is evident. Towards the channels of maximum volume within a given purity interval both measures seem to converge. Note that this would strongly support the validity of the MCMQ in terms of the quantumness of assistance Q_A . Also shown in the figure is the set of MCMQ (black, dashed line). They form an upper bound on Q_A for a fixed Bloch volume. The Black dots on this line represent the MCMQ of purity $0.5, 0.6, \dots, 0.9$ (from right to left).

4.4.1 Quantum Channels With Constant Bloch Volume

The comparison of Bloch volume and quantumness reveals a clear correlation which, however, obviously depends on additional parameters. The accessory dependence on the purity of the channel is clearly visible in Fig. 4.8. How can the connection between Bloch volume V_B and quantumness Q_A in relation to the purity be studied more closely? For this, we define a one-parameter class of phase-damping channels of constant Bloch volume yet parameter dependent quantumness and purity. We let

$$\vec{b}_1 = \begin{pmatrix} \cos \phi \\ -\sin \phi \\ 0 \end{pmatrix}, \quad \vec{b}_2 = \begin{pmatrix} -\cos \phi \\ -\sin \phi \\ 0 \end{pmatrix}, \quad \vec{b}_3 = \begin{pmatrix} 0 \\ -1 \\ 0 \end{pmatrix}, \quad \vec{b}_4 = \begin{pmatrix} 0 \\ -\sin \theta \\ \cos \theta \end{pmatrix}. \quad (4.19)$$

The volume V_B spanned by these 4 vectors is easily obtained to be

4 A Geometric Measure of Quantumness

$$V_B = \frac{1}{3} \cos \theta \cos \phi (1 - \sin \phi), \quad (4.20)$$

a value conditional on the two independent angles θ and ϕ . In order to fix the volume to a certain value we can simply let

$$\theta = \arccos \left(\frac{3V_B}{\cos \phi (1 - \sin \phi)} \right). \quad (4.21)$$

In order to proceed we set the Bloch volume to an arbitrary fixed value $V_B = \sqrt{2}/6 \approx 0.2357$.

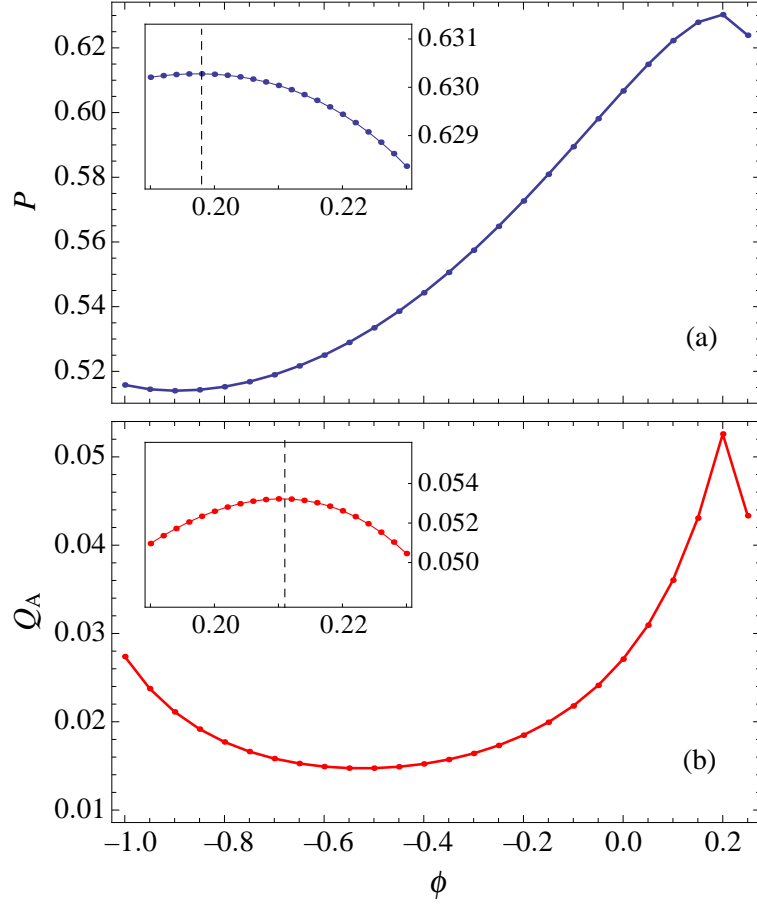


Figure 4.10: Purity P (a) and quantumness of assistance Q_A (b) against ϕ for the one-parameter class of phase-damping channels of constant Bloch volume. It is clearly visible that there is no monotonic relation. As the insets reveal, the maxima of the two curves (indicated with dashed lines) are at different angles, too.

Translating the Bloch vectors into quantum states, $\vec{b}_n \mapsto |\psi_n\rangle$, we can define (via $D_{mn}^\phi = \langle \psi_n | \psi_m \rangle$) the phase-damping channels D^ϕ . This way we are able to present a one-parameter

set of phase-damping channels D^ϕ , all having the same Bloch volume (see Fig. 4.9). Note that the angle θ is defined for values of ϕ approximately hedged by $-0.5 \leq \phi \leq 0.25$.

For the related class of phase-damping channels we analyze both purity and quantumness Q_A . The quantumness covers a range of roughly 0.015 to 0.05. In Fig. 4.8 this interval is depicted as a thick, black line. It covers almost the whole span of available values at the specified Bloch volume. In Fig. 4.10 it is clearly noticeable that there is no monotonic correlation between quantumness and purity. Both the minimum and the maximum of the respective quantity do not appear at the same value of ϕ . Clearly, thus, the purity of a channel alone does not account for the ambiguity in the relation of Bloch volume and quantumness.

4.5 Characterization in the Quantumness-Purity-Plane

All results obtained so far are best visualized in the *Quantumness-Purity-Plane* (Fig. 4.11). It shows the relation between the dynamics's potential to decohere a quantum state (as measured by the purity) and the maximum possible quantumness. The maximally quantum channel, denoted with D_Δ , has a purity of 0.5. The channels corresponding to unitary dynamics, on the other hand, have $P = 1$. In the plot they are represented by D_U . In between D_Δ and D_U we have the MCMQ, which maximize the accessible quantumness for a given decoherence potential. They are depicted in Fig. 4.11 as a solid black line. In order to complete the picture, we further include the completely decohering channel, which has the matrix representation

$$D_{cd} = \begin{pmatrix} 1 & 0 & 0 & 0 \\ 0 & 1 & 0 & 0 \\ 0 & 0 & 1 & 0 \\ 0 & 0 & 0 & 1 \end{pmatrix}. \quad (4.22)$$

It simply annihilates all existing coherences in a quantum state and may be seen as the fiercest phase-damping process possible. It is easy to see that D_{cd} belongs to the set of RU channels: its RU decomposition is given by the diagonal matrices $(\mathbb{1} \otimes \mathbb{1})/4$, $(\sigma_z \otimes \mathbb{1})/4$, $(\mathbb{1} \otimes \sigma_z)/4$, and $(\sigma_z \otimes \sigma_z)/4$. The channel has a purity of $P(\rho^{D_{cd}}) = 0.25$.

In order to give an estimation of the validity of the MCMQ as an upper bound, we compare it with the quantities obtained for a randomly generated set of channels. This time, however, we draw channels of rank 2, 3, and 4. The resulting values can be observed in Fig. 4.11. Each random channel is shown by a single point, with the color indicating the respective rank. From Sec. 3.1 we know that channels of rank 2 with non-zero quantumness are extremal with respect to the set of quantum channels. With increasing rank, the average

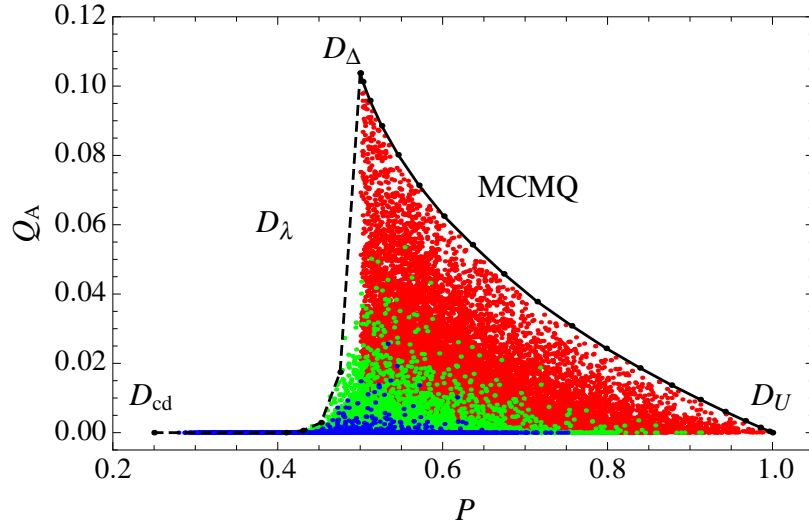


Figure 4.11: Quantumness in terms of Purity for a random set of phase-damping channels. The color coding indicates the rank of the respective channels: rank $r = 2$ (red), rank $r = 3$ (green), and rank $r = 4$ (blue). The solid line represents the MCMQ, yielding an upper bound to the accessible quantumness in terms of purity P . No single channel in violation of this bound is found. Also depicted are the channel of maximum quantumness, D_Δ , and the completely decohering channel D_{cd} . The D_λ are defined as convex mixture of these two, while D_U stands for channels representing unitary dynamics.

quantumness is thus expected to decline, as may be observed in the plot. For a total number of 70000 randomly generated channels no single violation of the upper bound introduced by the MCMQ is observed. We take this as a strong sign that the MCMQ also maximize the quantumness Q_A in terms of the purity. We deem it quite remarkable that the intuitive character of the Bloch volume is able to give such valuable insights into the geometry of quantum decoherence processes.

We further observe that below a purity of 0.5 there are only few channels with considerable quantumness. In order to understand this detail, we look at channels that are defined as convex mixture of the channel with maximum volume, D_Δ , and the completely decohering channel, D_{cd} :

$$D_\lambda = (1 - \lambda)D_\Delta + \lambda D_{cd}. \quad (4.23)$$

For this one-parameter class of channels we numerically estimate the quantumness. We find that the channels quantumness rapidly decays to zero for increasing λ (see the dashed line in Fig. 4.11). For a parameter of $\lambda > 0.2$, all channels already have zero quantumness and hence belong to the class of RU channels. Of course, we cannot claim this to be an upper

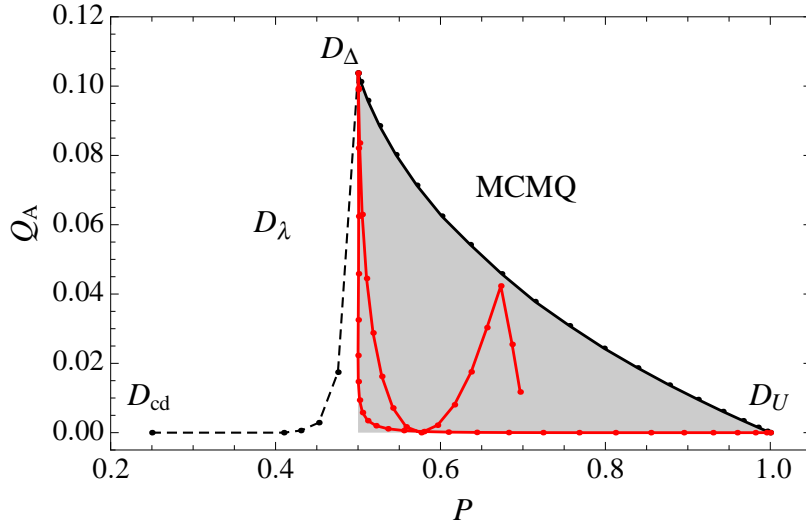


Figure 4.12: The trajectory of the model Hamiltonian of Sec. 3.2 in the Q_A - P -Plane. The accessible domain is indicated by a gray background. Here, the parameters are chosen such that the dynamics is of maximum quantumness at a certain instant of time.

bound for quantumness; yet, the consideration helps to better understand the small number of channels with considerable quantumness for purity below 0.5.

Toy model in the Quantumness-Purity-Plane

As a closure of the present chapter, we deem it instructive to depict the channels obtained from the model Hamiltonian of Sec. 3.2 in the Quantumness-Purity Plane (Fig. 4.12). Since the channels have rank $r \leq 2$ by construction, their purity may not drop below 0.5. Therefore, the accessible domain for channels based on the toy model is bound not only by the MCMQ, but also in purity. This accessible region is indicated with a gray shading. The example shown here is chosen so that there is a time at which the channel achieves the maximum possible quantumness (see Sec. 4.1.3). The corresponding parameters are $[\kappa_A = 1.688; \kappa_B = 0.918; \vec{\Gamma} = (1, 0, 0)]$. As an initial state we chose the Bloch vector pointing in x -direction, $\vec{b}_0 = (1, 0, 0)$. The quantumness reaches its maximum for $t \approx 1.35$. At this point, the Bloch vectors of the relative environmental states span a regular tetrahedron inside the Bloch sphere.

5 Quantum Decoherence via Entangled Local Reservoirs?

In Chapter 3 we saw that phase-damping dynamics of a single qubit is always of RU type. Clearly, thus, the dynamics of a system of qubits, which is subject to phase damping due to local reservoirs, is of RU type, too. Namely, the global dynamics is the sum of the individual RU terms. Such a situation is quite common in the context of *spin chains*. Here, the model Hamiltonian usually rests on next-neighbor coupling among the qubits, which additionally couple to their local environment [93, 94].

How does this situation change when we allow the local environments to be quantum correlated (i.e., entangled)? In the present section, we want to study this question in a realistic experimental context. We study a system of two qubits locally interacting with a bipartite environment sharing entanglement of some kind (see Fig. 5.1). The bipartite environment shall be represented by two electromagnetic field modes of a superconducting cavity. Each qubit interacts with its designated cavity mode, while any coupling to the other mode, as well as between the modes themselves, is suppressed. We consider different initial conditions of the two cavity modes. First, the entanglement manifests itself in an uncertainty of the location of a single photon shared by the two modes. In the second approach, the initial state is given by a squeezed, Gaussian state.

In order not to mislead the reader's expectations, we would like to anticipate that—most interestingly—the quest for true quantum decoherence via entangled reservoirs remains an open question. That is, despite the various initial conditions of the environment and despite the different models of interaction studied, all dynamics will be found to be of RU nature. To some extent, the identification of the dynamics' RU character is done numerically; however, for a large class of dynamics we are also able to definitely exclude the true quantum property analytically. Nonetheless, a general statement is yet to be found.

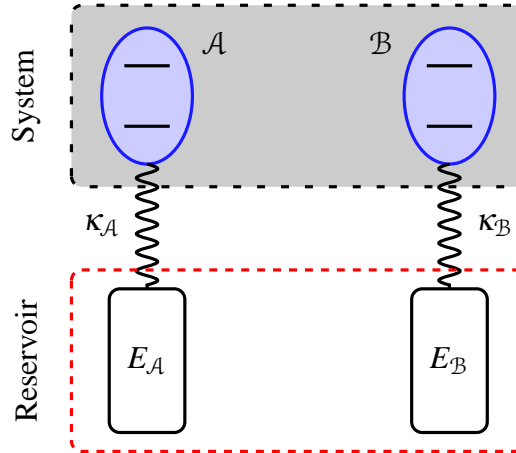


Figure 5.1: Can entanglement turn classical decoherence into quantum decoherence? The two qubits \mathcal{A} and \mathcal{B} are coupled to their local environments $E_{\mathcal{A}}$ and $E_{\mathcal{B}}$, respectively. A phase-damping channel is thus known to be RU as long as the two reservoirs are separable. Does entanglement between the local environments (here indicated by the red dashed line) change this?

5.1 Experimental Setup

Let us consider a possible experimental realization of the above mentioned scenario. Our discussion shall be based on actual experiments that have been realized at the “Laboratoire Kastler Brossel” at Ecole Normale Supérieure (ENS) in Paris. In the experiments, single circular Rydberg atoms are used to manipulate and probe the states of photons which are trapped in a superconducting cavity [95]. The atoms undergo the following procedure (cf. Fig. 5.2): A short maser pulse at stage B prepares single circular Rydberg states. The relevant atomic states are the Rydberg levels with quantum numbers 51 (excited state, $|e\rangle$) and 50 (ground state, $|g\rangle$), having a transition frequency of 51.1 GHz [96]. The atoms’ internal state may be manipulated using the microwave source S, allowing to initialize arbitrary superpositions of $|g\rangle$ and $|e\rangle$. During the time spent inside the cavity C, the atoms interact with the electromagnetic field. Using a second stage of microwave pulses allows the atomic state to be analyzed right before detection at the state-selective field-ionization detector D.

The cavity itself consists of two superconducting niobium mirrors facing each other. It resembles a resonator of ultrahigh finesse at frequency $\omega/2\pi = 51$ GHz. Its field energy damping time T_c is given by $T_c \approx 130$ ms, leading to a very long lifetime of the infused electromagnetic field. The corresponding quality factor is given by $Q = \omega T_c = 4.2 \times 10^{10}$. The mirrors exhibit a slightly asymmetric architecture: due to a toroidal surface with radii of curvature of 39.4 and 40.6 mm there is a frequency splitting of 1.2 MHz between the

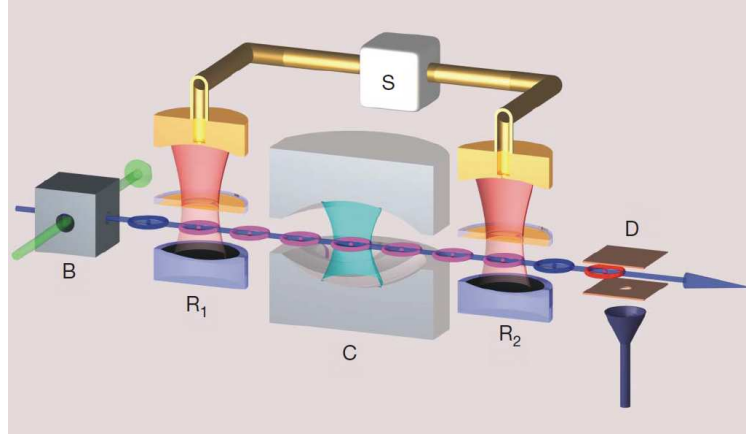


Figure 5.2: Experimental setup: Velocity-selected rubidium atoms first pass stage B, where single atoms are excited in circular Rydberg states. While passing cavity C, the atoms are able to interact with the cavity mode. Finally, the atoms are counted by the field-ionization detector D. At stages R_1 and R_2 , microwave fields are used to prepare and analyze the atoms before and after interaction with the resonator, respectively (Picture taken from [96]).

two TEM_{900} modes of orthogonal linear polarization near 51 GHz. This frequency splitting ensures that the atoms are effectively coupled to a single mode only. Tuning of the cavity is performed by four piezoelectric actuators translating one of the mirrors [95].

5.1.1 Resonant Coupling

For the case of resonant coupling, let us consider the situation where the atom enters the empty cavity in the excited state. The combined atom-cavity state is thus given as $|e, 0\rangle$ (for simplicity, only the relevant mode is included in the description). Tuning the cavity to resonance with the atomic transition then leads to Rabi oscillations of the atomic state: the probability of finding the atom in the excited state at time t is given by [40]

$$P_e(t) = \cos^2(\Omega_0 t), \quad (5.1)$$

where the vacuum Rabi frequency is found to be $\Omega_0/2\pi = 47$ kHz. Likewise, the combined atom-cavity state oscillates between $|e, 0\rangle$ and $|g, 1\rangle$. The velocity of the atoms is adjusted such that the full atom-cavity interaction time at resonance corresponds to a 2π Rabi pulse [97]. A shorter pulse length may be achieved by suddenly tuning the cavity out of resonance.

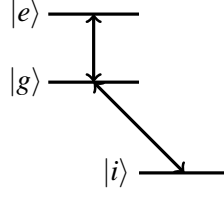


Figure 5.3: Atomic levels utilized in the realization of a QPG.

5.1.2 Conditional Quantum Phase Gate

The resonant interaction of atom and cavity may be used to design a conditional quantum phase gate (QPG), as has been shown in [98]. For a system of two qubits described by $|\mu\nu\rangle$ ($\mu, \nu = 0, 1$) a QPG is defined via

$$|\mu\nu\rangle \xrightarrow{\text{QPG}} e^{i\delta_{\mu 1}\delta_{\nu 1}\phi} |\mu\nu\rangle. \quad (5.2)$$

That is, it adds a phase ϕ to the state if both qubits are in state $|1\rangle$ or else leaves it unaltered. In order to realize the QPG, a third atomic level is utilized (cf. Fig 5.3). It is the Rydberg state with quantum number 49, denoted by $|i\rangle$. The relevant degrees of freedom for the two-qubit system are now described by the atomic qubit basis $\{|i\rangle, |g\rangle\}$ and the zero- and one-photon state of the cavity, $\{|0\rangle, |1\rangle\}$. An atom in state $|i\rangle$ passes the cavity without interaction; atom and cavity are thus fully decoupled. The same is true for the atom in state $|g\rangle$ with no photon in the cavity. The only interaction is thus taking place for the combined state $|g, 1\rangle$. With the cavity in resonance to the $|g\rangle - |e\rangle$ transition, the atom performs a full Rabi cycle, transforming [98]

$$|g, 1\rangle \mapsto -|g, 1\rangle = e^{i\phi} |g, 1\rangle, \text{ with } \phi = \pi. \quad (5.3)$$

Now, this is exactly what defines the action of a QPG. Note that the QPG is a universal two-qubit quantum gate in the sense that any unitary transformation on two qubits can be achieved using a sequence of this gate and additional rotations of the individual qubits [98, 99]. In the following sections we investigate the dynamics of two qubits \mathcal{A} and \mathcal{B} , which locally couple to their respective mode a and b of the cavity. The local character of the coupling may be achieved by letting the two qubits pass the cavity one at a time. During the interaction time, the cavity field is tuned such that each qubit may couple to its respective field mode. We study two different initial scenarios: First, the modes of the cavity share one single photon. Here, the entanglement of the state is due to the uncertainty in determining which mode the photon is in. In a second approach the cavity starts out in a squeezed entangled state,

requiring a formulation in continuous variables.

5.2 Two Modes Sharing a Single Photon

In the first situation there shall be only one photon inside the cavity, which is shared by the two modes a and b . Thus, clearly the modes may be treated as two-state systems in Fock space, where the basis states $|\mu\rangle$ denote the number of photons (here $\mu = 0, 1$) in the respective mode. As a generic Hamiltonian for our purposes, describing the joint time evolution of both Rydberg atoms and both modes, we may set

$$\begin{aligned} H &= \Omega_{\mathcal{A}}\sigma_z^{(\mathcal{A})} + g_{\mathcal{A}a}\sigma_z^{(\mathcal{A})}\sigma_z^{(a)} + \vec{\Gamma}^{(a)} \cdot \vec{\sigma}^{(a)} \\ &+ \Omega_{\mathcal{B}}\sigma_z^{(\mathcal{B})} + g_{\mathcal{B}b}\sigma_z^{(\mathcal{B})}\sigma_z^{(b)} + \vec{\Gamma}^{(b)} \cdot \vec{\sigma}^{(b)}. \end{aligned} \quad (5.4)$$

Here, the free evolution of the qubits and the modes is described via the parameters $\Omega_{\mathcal{A}}, \Omega_{\mathcal{B}}, \vec{\Gamma}^{(a)}$, and $\vec{\Gamma}^{(b)}$, respectively. (Note that due to the diagonal coupling the environmental modes stay within their initially assigned two-state subspace spanned by the Fock states $|0\rangle$ and $|1\rangle$). The free evolution of the environment may therefore be adequately characterized in terms of the Pauli matrices.) The (diagonal) coupling of qubit \mathcal{A} and \mathcal{B} to the corresponding mode a and b is described in terms of the parameters $g_{\mathcal{A}a}$ and $g_{\mathcal{B}b}$, respectively.

Rewriting the global Hamiltonian in terms of the two-qubit basis $\{|n\rangle\}_{n=1}^4$ gives the relative Hamiltonians $H_{\mathcal{R}}^{(n)}$ of the environment,

$$\begin{aligned} H &= \sum_{n=1}^4 |n\rangle\langle n| \otimes \tilde{H}_{\mathcal{R}}^{(n)} \\ &= \sum_{\mu, \nu=0}^1 |\mu\nu\rangle\langle\mu\nu| \otimes \left(\tilde{h}_a^{(\mu)} \otimes \tilde{h}_b^{(\nu)} \right). \end{aligned} \quad (5.5)$$

In the last step we use the standard definition of the computational basis for a two-qubit system, that is, $\{|1\rangle = |00\rangle, |2\rangle = |01\rangle, |3\rangle = |10\rangle, |4\rangle = |11\rangle\}$ ¹. We also define the abbreviations

$$\tilde{h}_{a/b}^{(0)} = +\Omega_{\mathcal{A}/\mathcal{B}} \mathbb{1} + \begin{pmatrix} \Gamma_x^{(a/b)} \\ \Gamma_y^{(a/b)} \\ \Gamma_z^{(a/b)} + g_{\mathcal{A}a/\mathcal{B}b} \end{pmatrix} \cdot \vec{\sigma}^{(a/b)} \quad (5.6)$$

¹Here and in the following we make use of both notations. In order to make clear which one is used, we will denote indices ranging from 1 to 4 with Latin symbols (m, n), whereas indices ranging from 0 to 1 will be written in Greek symbols (μ, ν).

5 Quantum Decoherence via Entangled Local Reservoirs?

and

$$\tilde{h}_{a/b}^{(1)} = -\Omega_{A/B} \mathbb{1} + \begin{pmatrix} \Gamma_x^{(a/b)} \\ \Gamma_y^{(a/b)} \\ \Gamma_z^{(a/b)} - g_{Aa'Bb} \end{pmatrix} \cdot \vec{\sigma}^{(a/b)}. \quad (5.7)$$

Again, we have that the phase-damping channel is determined by the overlap of the relative states of the environment

$$D_{mn} = \langle \psi_n | \psi_m \rangle = \langle \psi_0 | \tilde{U}_{mn} | \psi_0 \rangle \quad (5.8)$$

with $\tilde{U}_{mn} = e^{i\tilde{H}_{\mathcal{R}}^{(n)} t} e^{-i\tilde{H}_{\mathcal{R}}^{(m)} t}$. Due to the local coupling, the Hamiltonians relative to the phase-damping basis of the system are of the form $\tilde{H}_{\mathcal{R}}^{(n)} = \tilde{h}_a^{(\mu)} \otimes \tilde{h}_a^{(\nu)}$ (recall the identification of (n) with the double index (μ, ν) in Greek letters). The same is true of course for the unitary operators \tilde{U}_n . That means we can write $\tilde{U}_n = \tilde{u}_{\mu}^{(a)} \otimes \tilde{u}_{\nu}^{(b)}$ and, likewise,

$$\tilde{U}_{nn'} = \tilde{u}_{\mu\mu'}^{(a)} \otimes \tilde{u}_{\nu\nu'}^{(b)} \quad (5.9)$$

Now, if the environment's initial state is separable, that is $|\psi_0\rangle = |\phi_0^{(a)}\rangle \otimes |\theta_0^{(b)}\rangle$, the corresponding channel based on the Hamiltonian in Eq. (5.4) is certainly RU, for we may write

$$\begin{aligned} D_{nn'} &= \langle \psi_0 | \tilde{U}_{nn'} | \psi_0 \rangle \\ &= \langle \phi_0^{(a)} | \tilde{u}_{\mu\mu'}^{(a)} | \phi_0^{(a)} \rangle \cdot \langle \theta_0^{(b)} | \tilde{u}_{\nu\nu'}^{(b)} | \theta_0^{(b)} \rangle \\ &= D_{\mu\mu'}^{(a)} \cdot D_{\nu\nu'}^{(b)} \\ &= D_{\mu\nu, \mu'\nu'}. \end{aligned} \quad (5.10)$$

The channel may thus equally be written in tensor product form, that is,

$$D = D^{(a)} \otimes D^{(b)}. \quad (5.11)$$

The phase-damping channel is thus a product of two single-qubit phase-damping channels, which are known to be RU (see Chap. 3).

If the initial state $|\psi_0\rangle$ is entangled, however, the answer to the question of whether the resulting channel is of RU type is not as obvious. In our case, where the two modes share a single photon, a generic pure state is given as

$$|\psi\rangle = \alpha|01\rangle + \beta|10\rangle, \quad |\alpha|^2 + |\beta|^2 = 1, \quad (5.12)$$

Note that the state is entangled whenever $\alpha \neq 0$ or $\alpha \neq 1$. In the attempt to find a phase-damping channel representing a quantum decoherence process we take different parameters of Hamiltonian (5.4) and the initial state $|\psi_0\rangle$ of the environment, such that (i) $|\psi_0\rangle$ is entangled and (ii) the purity of the phase-damping channel covers the whole range between $P(\rho^D) = 0.25$ and $P(\rho^D) = 1$. This second criterion shall prevent the channels to reside in domains where little or no quantumness is to be expected (see Sec. 4.5). However, as already indicated in the introduction of the present chapter, the evaluation of the Birkhoff defect for these randomly chosen channels yields no single incident of quantum decoherence.

5.3 Two Modes in a Gaussian Entangled State

In the following attempt, we want to consider the situation where the two modes are initially prepared in an entangled Gaussian state. A standard example is the pure two-mode squeezed state (cf. Sec. 2.1.2) with a Wigner function given by

$$W(q_a, p_a, q_b, p_b) = \frac{4}{\pi^2} \exp \left\{ -e^{-2r} [(q_a + q_b)^2 + (p_a - p_b)^2] - e^{+2r} [(q_a - q_b)^2 + (p_a + p_b)^2] \right\}. \quad (5.13)$$

Recall that the state's entanglement depends on the squeezing parameter r only. With mode b traced out, e.g., it measures the uncertainties of both remaining quadratures q_a and p_a .

Remember that we want to consider the situation where the two qubits \mathcal{A} and \mathcal{B} couple locally to the two electromagnetic field modes a and b , respectively. We define our global Hamiltonian as

$$H = \Omega_{\mathcal{A}} \sigma_z^{(\mathcal{A})} + \sigma_z^{(\mathcal{A})} \otimes g_a \hat{q}_a + \omega_a \left(\frac{\hat{p}_a^2}{2} + \frac{\hat{q}_a^2}{2} \right) + \Omega_{\mathcal{B}} \sigma_z^{(\mathcal{B})} + \sigma_z^{(\mathcal{B})} \otimes g_b \hat{q}_b + \omega_b \left(\frac{\hat{p}_b^2}{2} + \frac{\hat{q}_b^2}{2} \right). \quad (5.14)$$

Note that this kind of coupling is very similar to the (non-dissipative) *Spin-Boson model*, which is a regularly employed tool to model decoherence in two-level systems [100]. Here, however, each qubit couples only to a single mode instead of an infinite continuum. As before, diagonalization with respect to the mutual basis $\{|n\rangle\}$ of qubits \mathcal{A} and \mathcal{B} yields the relative environmental Hamiltonians

$$\begin{aligned} \tilde{H}_{\mathcal{R}}^{(1)} &= (\Omega_{\mathcal{A}} + \Omega_{\mathcal{B}}) \mathbb{1} + \tilde{h}_a^{(+)} + \tilde{h}_b^{(+)} & \tilde{H}_{\mathcal{R}}^{(2)} &= (\Omega_{\mathcal{A}} - \Omega_{\mathcal{B}}) \mathbb{1} + \tilde{h}_a^{(+)} + \tilde{h}_b^{(-)} \\ \tilde{H}_{\mathcal{R}}^{(3)} &= (-\Omega_{\mathcal{A}} + \Omega_{\mathcal{B}}) \mathbb{1} + \tilde{h}_a^{(-)} + \tilde{h}_b^{(+)} & \tilde{H}_{\mathcal{R}}^{(4)} &= -(\Omega_{\mathcal{A}} + \Omega_{\mathcal{B}}) \mathbb{1} + \tilde{h}_a^{(-)} + \tilde{h}_b^{(-)}, \end{aligned} \quad (5.15)$$

5 Quantum Decoherence via Entangled Local Reservoirs?

where we define the relative Hamiltonians of mode a/b as

$$\begin{aligned}\tilde{h}_{a/b}^{(\pm)} &= \frac{\hat{p}_{a/b}^2}{2} + \frac{\hat{q}_{a/b}^2}{2} \pm g_{a/b} \hat{q}_{a/b} \\ &= \frac{\hat{P}_{a/b}^2}{2} + \frac{[\hat{q}_{a/b} \pm g_{a/b}]^2}{2} - \frac{g_{a/b}^2}{2}.\end{aligned}\quad (5.16)$$

In order to arrive at the matrix representation of the phase-damping channel D , we have to evaluate the following expressions:

$$\begin{aligned}D_{mn} &= \text{tr} \left[\hat{\rho} e^{i\tilde{H}_{\mathcal{R}}^{(n)} t} e^{-i\tilde{H}_{\mathcal{R}}^{(m)} t} \right] \\ &= \text{tr} \left[\hat{\rho} \tilde{U}_{mn}(t) \right] \\ &= \int dq_a \int dp_a \int dq_b \int dp_b W(q_a, p_a, q_b, p_b) \tilde{U}_{mn}^{(W)}(t).\end{aligned}\quad (5.17)$$

Here, we define the unitaries $\tilde{U}_{mn}(t) = e^{i\tilde{H}_{\mathcal{R}}^{(n)} t} e^{-i\tilde{H}_{\mathcal{R}}^{(m)} t}$ with corresponding Wigner representation

$$\begin{aligned}\tilde{U}_{mn}^{(W)} &= \int dq'_a \int dq'_b \langle q_a + \frac{q'_a}{2} | \otimes \langle q_b + \frac{q'_b}{2} | \tilde{U}_{mn}(t) | q_a - \frac{q'_a}{2} \rangle \otimes | q_b - \frac{q'_b}{2} \rangle \\ &\quad \times e^{-i(p_a q'_a + p_b q'_b)} \\ &= \exp \left\{ -4i \left(c_{q_a}^{mn} q_a + c_{p_a}^{mn} p_a + c_{q_b}^{mn} q_b + c_{p_b}^{mn} p_b \right) \right\}.\end{aligned}\quad (5.18)$$

The relevant calculations are carried out in the appendix (App. C.1). As a final result we arrive at the following form of the phase-damping channel

$$\begin{aligned}D_{mn} &= \exp \left\{ -e^{-2r} \left[\left(c_{q_a}^{mn} + c_{q_b}^{mn} \right)^2 + \left(c_{p_a}^{mn} - c_{p_b}^{mn} \right)^2 \right] \right. \\ &\quad \left. - e^{+2r} \left[\left(c_{q_a}^{mn} - c_{q_b}^{mn} \right)^2 + \left(c_{p_a}^{mn} + c_{p_b}^{mn} \right)^2 \right] \right\}.\end{aligned}\quad (5.19)$$

The respective coefficients are listed in Table 5.1.

5.3.1 Direct Assessment of the RU Character

The phase-damping channels arrived at in the previous section may actually directly be shown to be of RU type. For this we have to take a closer look at the unitary matrices $\tilde{U}_{mn}^{(W)}$ in Wigner representation, Eq. (5.18). They may be rewritten in the form

$$U_{mn}^{(W)}(t) = \exp \left\{ i4 \left(\Phi_m(\vec{r}) - \Phi_n(\vec{r}) \right) \right\}, \quad (5.20)$$

5.3 Two Modes in a Gaussian Entangled State

mn	$c_{q_a}^{mn}$	$c_{p_a}^{mn}$	$c_{q_b}^{mn}$	$c_{p_b}^{mn}$
12	0	0	$2g_b \sin(\omega_b t)$	$2g_b [1 - \cos(\omega_b t)]$
13	$2g_a \sin(\omega_a t)$	$2g_a [1 - \cos(\omega_a t)]$	0	0
14	$2g_a \sin(\omega_a t)$	$2g_a [1 - \cos(\omega_a t)]$	$2g_b \sin(\omega_b t)$	$2g_b [1 - \cos(\omega_b t)]$
23	$2g_a \sin(\omega_a t)$	$2g_a [1 - \cos(\omega_a t)]$	$-2g_b \sin(\omega_b t)$	$-2g_b [1 - \cos(\omega_b t)]$
24	$2g_a \sin(\omega_a t)$	$2g_a [1 - \cos(\omega_a t)]$	0	0
34	0	0	$2g_b \sin(\omega_b t)$	$2g_b [1 - \cos(\omega_b t)]$

Table 5.1: List of the coefficients appearing in the definition of the phase-damping channel D [Eq. (5.19)].

with $\vec{r} := (q_a, p_a, q_b, p_b)$. This may be done by letting

$$\Phi_n(\vec{r}) := \vec{\alpha}_n \cdot \vec{r}, \quad (5.21)$$

where the vectors $\vec{\alpha}_n$ are defined to be

$$\vec{\alpha}_1 = \begin{pmatrix} 2g_a \sin(\omega_a t) \\ 2g_a [1 - \cos(\omega_a t)] \\ 2g_b \sin(\omega_b t) \\ 2g_b [1 - \cos(\omega_b t)] \end{pmatrix}, \quad \vec{\alpha}_2 = \begin{pmatrix} 2g_a \sin(\omega_a t) \\ 2g_a [1 - \cos(\omega_a t)] \\ 0 \\ 0 \end{pmatrix}, \quad (5.22)$$

$$\vec{\alpha}_3 = \begin{pmatrix} 0 \\ 0 \\ 2g_b \sin(\omega_b t) \\ 2g_b [1 - \cos(\omega_b t)] \end{pmatrix}, \quad \vec{\alpha}_4 = \begin{pmatrix} 0 \\ 0 \\ 0 \\ 0 \end{pmatrix}.$$

When inserted into Eq. (5.17), which gives the matrix elements D_{mn} of the phase-damping channel, we find

$$D_{mn} = \int dq_a \int dp_a \int dq_b \int dp_b W(q_a, p_a, q_b, p_b) \exp \left\{ i4 (\Phi_m(\vec{r}) - \Phi_n(\vec{r})) \right\}. \quad (5.23)$$

Since the Wigner function $W(q_a, p_a, q_b, p_b)$ of a Gaussian state is positive (i.e., a probability distribution), we can immediately conclude that the corresponding channel is RU (see Sec. 2.2.4).

5.4 Entangled State With Negative Wigner Function

The positivity of the Wigner function in Eq. (5.23) is crucial in the identification of the channel's RU character. Clearly, thus, any positive and normalized distribution in the phase space of the two modes will lead to dynamics that may be interpreted in terms of a RU channel. But what about a Wigner function that is negative in some areas? If that is the case, we may not immediately decide the case. In order to find instances of such a situation, we choose to revisit the case where the two modes initially share a fixed number (n) of photons. The initial state of the modes may thus be described by the vector

$$|\psi\rangle = \alpha|0n\rangle + \beta|n0\rangle, \quad (5.24)$$

with $\alpha, \beta \in \mathbb{C}$ and $|\alpha|^2 + |\beta|^2 = 1$. The state's Wigner function may be derived directly from the characteristic function (see Sec. 2.1.2). With $L_n(x)$ denoting the *Laguerre polynomials* [101], it is given by (see App. C.2)

$$\begin{aligned} \chi^{(n)}(\eta_a, \eta_b) = & \left[|\alpha|^2 L_n(|\eta_b|^2) - \alpha\beta^* \frac{(\eta_a \eta_b^*)^n}{n!} \right. \\ & \left. - \beta\alpha^* \frac{(\eta_b \eta_a^*)^n}{n!} + |\beta|^2 L_n(|\eta_a|^2) \right] e^{-\frac{|\eta_a|^2}{2}} e^{-\frac{|\eta_b|^2}{2}}. \end{aligned} \quad (5.25)$$

In Fig. 5.4 we plot some of the resulting Wigner functions of the reduced states with mode b traced out. They are given by

$$W_{\text{red}}^{(1)}(q_a, p_a) = \frac{2}{\pi} (|\alpha|^2 - L_1(4(q_b^2 + p_b^2)) |\beta|^2) e^{-2(q_a^2 + p_a^2)}, \quad (5.26a)$$

$$W_{\text{red}}^{(2)}(q_a, p_a) = \frac{2}{\pi} (|\alpha|^2 + L_2(4(q_b^2 + p_b^2)) |\beta|^2) e^{-2(q_a^2 + p_a^2)}, \quad (5.26b)$$

and

$$W_{\text{red}}^{(3)}(q_a, p_a) = \frac{2}{\pi} (|\alpha|^2 - L_3(4(q_b^2 + p_b^2)) |\beta|^2) e^{-2(q_a^2 + p_a^2)}, \quad (5.26c)$$

respectively (see App. C.2). Clearly, the functions are not positive everywhere. The respective states are thus good examples of entangled states with a negative Wigner function. Having acquired the Wigner functions $W^{(n)}(q_a, p_a, q_b, p_b)$, the respective channels are obtained via Eq. (5.23). Now, the constructive proof of the channel's RU nature cannot be used anymore, since $W^{(n)}(q_a, p_a, q_b, p_b) < 0$ is possible. The corresponding channels are thus again numerically scrutinized for quantumness. Despite the negativity of the Wigner

5.4 Entangled State With Negative Wigner Function

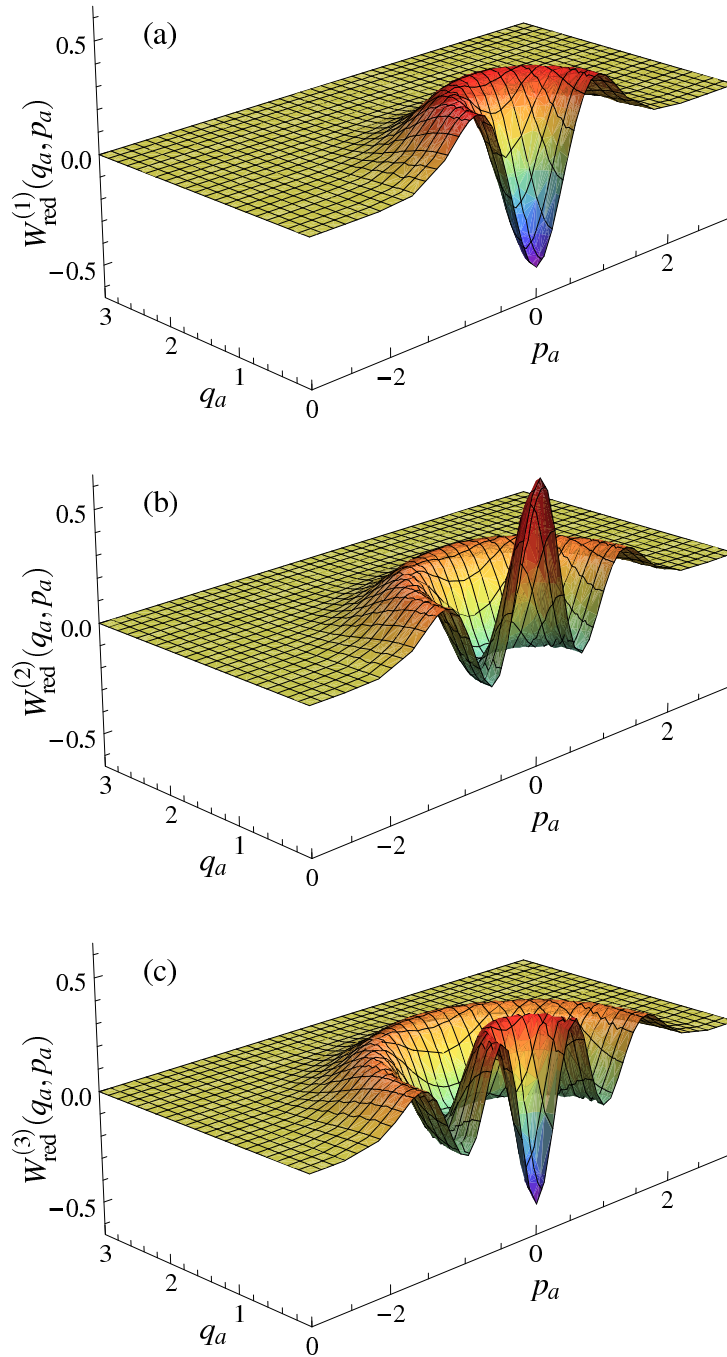


Figure 5.4: Wigner function $W_{\text{red}}^{(n)}(q_a, p_a)$ of the reduced state of mode a for the two modes sharing (a) one photon ($n = 1$), (b) two photons ($n = 2$), and (c) three photons ($n = 3$). In all cases we set $\alpha = \sqrt{0.1}$ and $\beta = \sqrt{0.9}$. All functions evidently take on negative values around the origin.

5 *Quantum Decoherence via Entangled Local Reservoirs?*

functions, we find no single instance where the dynamics is of non-RU type.

To summarize, in the present chapter we have studied a scenario where a system of two qubits couples to their respective, local environments. If the bipartite environment starts out in a separable state, the dynamics is trivially of RU nature. However, we consider different situations involving entanglement between the local reservoirs, where an RU affiliation may not be easily deduced. Despite this fact, we find no single instance of true quantum (i.e., non-RU) dynamics. In case of the (non-dissipative) Spin-Boson model with an environment described by a positive Wigner function, these findings are purely analytical. All other cases are studied numerically. Of course, it would be very satisfactory to have a definite explanation for the negative results of the present chapter. However, despite some mentionable effort, we have not succeeded yet in finding such an explanation. Thus, the subject provides an interesting field for further investigations.

6 Conclusion and Outlook

Decoherence is seen as the main obstacle preventing the realization of quantum information processors of relevant size. It leads to a complete loss of entanglement in quantum systems, thereby spoiling the main ingredient of many of the proposed algorithms which promise a significant speed-up over conventional, classical schemes. In the attempt to make use of quantum mechanical properties on larger and larger scales it is thus unquestionable that a thorough knowledge of all processes involved is needed.

A priori, there exist various mechanisms offering a possible explanation for the origin of decoherence. In perhaps the most prominent attempt, it is ascribed to growing correlations between the system of interest and its quantum environment. The constant “monitoring” of the system by its surroundings and the involved transfer of information are responsible for the state to finally become classical [5]. Often, however, decoherence may as well be attributed to stochastic fluctuations of classical fields. Due to local or temporal variations of the surrounding electromagnetic fields, the individual constituents of an ensemble may each accumulate a slightly varying phase during time evolution. As soon as an ensemble average is performed, the relative phases are washed out, causing the coherences to degenerate.

The purpose of the present thesis is to clarify what distinguishes *true quantum* from *classical* decoherence. This distinction is of genuine interest not only from an experimental perspective, where an identification of the processes leading to decoherence is needed in any effort to enhance accuracy. As in the case of the Spin Echo technique, a classical decoherence process might allow for a partial reversal of its effects without the need for additional measurements. Furthermore, we hope that our studies help to elucidate the true role of entanglement in open quantum system decoherence. Throughout the thesis, we concentrate on pure decoherence scenarios where no dissipation is involved, typically denoted with phase damping (or dephasing).

Based on a simple model we are able to give a generic example of a feasible two-qubit phase-damping channel, of which we show that it does not belong to the set of RU channels. It thus represents a case of true quantum decoherence which may not be understood in classical terms. While the actual example gives a channel acting on a four-dimensional Hilbert space, we give explicit instructions of how to generalize the results to arbitrary dimension.

6 Conclusion and Outlook

The resulting dynamics is studied with respect to the Birkhoff defect which introduces a measure of a channel's norm distance to the set of RU channels. For an extension of the model using an additional heat bath, thereby introducing veritable irreversibility, we still observe genuine quantum decoherence. For most of the channels, the quantumness remains non-zero as long as the coupling to the bath is small enough. For growing coupling strength, however, the quantum character of the dynamics becomes increasingly fragile. If the influence of the additional environment gets too large, the quantum character is lost for almost all channels.

Remarkably, we observe a strong correlation between the Birkhoff defect and the volume of the tetrahedron spanned by the Bloch vectors representing the relative states of the environmental qubit. This leads us to introduce a new, geometrically motivated measure of quantumness—the *Bloch volume*. Rather than demanding lengthy optimization routines as is the case for the calculation of the norm distance, the Bloch volume requires the evaluation of a single determinant. We exploit the intuitive character of the new geometric measure in order to arrive at a characterization of phase-damping dynamics. The purity of a channel is shown to give an estimation of its *decoherence potential*, i.e., the severity with which it possibly affects any given quantum state. For two qubits, we observe a strong correlation between a channel's achievable quantumness and its decoherence potential. Since the evaluation of a channel's purity is much less involved, this connection may be used to quickly estimate an upper bound to the quantumness potentially present. Furthermore, based on the geometric measure, we are able to identify the set of *mixed channels with maximum quantumness* (MCMQ), maximizing the distance to the set of RU channels for a given decoherence potential. In addition, it is demonstrated that the toy model introduced in Chapter 3 is capable of provoking dynamics which is maximally quantum, i.e., which has a maximum distance to the set of RU channels. The respective channel of maximum quantumness is intimately related to the concept SIC-POVMs, corresponding to a symmetrically-placed basis of Hilbert space operators.

In the last part of the thesis, we study the influence of entanglement between local reservoirs on the RU character of dynamics. The analysis is based on two qubits which couple locally to their respective environment. From the findings of Chapter 3, it is thus evident that the dynamics belongs to the RU class as long as the reservoirs are in a separable state. We examine various situations where the local environments are not separable but entangled. Despite the multitude of situations, we find no single instance of true quantum decoherence. In the case where the coupling is described by a (non-dissipative) Spin-Boson model, our findings are in part analytical. Here, we are able to confirm that local coupling leads to RU dynamics whenever the initial state of the environment is described by a positive Wigner function. Therefore, any attempt to construct a true quantum decoherence channel with the

environment in a Gaussian entangled state is doomed to fail. However, even in the case of a negative Wigner function, all channels studied are of RU type. Since no analytical results are found, we rely on a numerical examination of the resulting quantumness of the channels.

For future studies we see many interesting routes of continuation. Since the model of quantum decoherence is based on a physically feasible situation, it would be very interesting to actually try an experimental realization. As in our theoretical investigation, the corresponding channels may then also be studied with respect to the fragility of their true quantum nature. Secondly, we note that the Bloch volume suffers from being valid in the case of extremal channels only. Here, the great hope is to find a generalization of this measure of quantumness for the case of non-extremal channels.

In addition, we show that the toy model presented may lead to relative environmental states spanning a SIC-POVM (a symmetrically placed operator basis in Hilbert space). In this context, a rigorous study of the circumstances leading to a phase-damping channel with maximum Bloch volume might help in the construction of SIC-POVMs in higher dimension—a problem yet to be solved.

Not least, the results of Chapter 5 may indicate that entanglement between local reservoirs does not change a channel's RU nature (which trivially follows in the separable case). However, it remains an open question whether this is so in general. We deem it worthwhile to continue with the investigations for a definite criterion.

Appendix

A Technical Toolkit

A.1 Convex Roof Construction

Every pure-state decomposition of a density matrix ρ can be obtained via the following procedure [91]:

- (i) Via diagonalization of ρ , a complete set of orthogonal eigenvectors $|v_i\rangle$ corresponding to the nonzero eigenvalues λ_i is obtained. These vectors shall be subnormalized, such that $\langle v_i | v_i \rangle$ is equal to the i -th eigenvalue λ_i .
- (ii) Every decomposition $\{|w_i\rangle\}$ of ρ can then be obtained via

$$|w_i\rangle = \sum_{j=1}^r U_{ij}^* |v_j\rangle. \quad (\text{A.1})$$

where r denotes the rank of ρ . U is an $m \times m$ unitary matrix with $m \geq r$. The new states $|w_i\rangle$ are already subnormalized such that $\langle w_i | w_i \rangle$ is equal to the probability of $|w_i\rangle$ in the decomposition. In terms of the $|w_i\rangle$ the full state is thus given as $\rho = \sum_i |w_i\rangle \langle w_i|$.

The entanglement of formation is then obtained as the minimum of pure state entanglement (entanglement entropy) needed over all possible decompositions:

$$E_F(\rho) = \min_{\{|w_i\rangle\}} \left\{ \sum_i \langle w_i | w_i \rangle E \left(\frac{|w_i\rangle}{\sqrt{\langle w_i | w_i \rangle}} \right) \mid \rho = \sum_i |w_i\rangle \langle w_i| \right\}. \quad (\text{A.2})$$

In order to obtain the entanglement of assistance, the minimum has to be replaced by the maximum. For a density operator of rank r a maximum of r^2 pure states is needed for the minimum (maximum) to be achieved [92, 102].

A.2 The Cholesky Factorization

Given the non-negative matrix $D \in \mathcal{M}_N$, the Cholesky factorization gives

$$D = AA^\dagger, \quad (\text{A.3})$$

A Technical Toolkit

with $A \in \mathcal{M}_N$ a lower triangular matrix, where A is in general not unique. The n -th row of A may then be identified with a complex vector $|a_n\rangle \in \mathbb{C}^N$ such that $D_{nn} = \langle a_n | a_n \rangle$. If D is a positive semi-definite matrix of rank $r < N$, there exists a unique A with columns $r + 1$ through N identical to zero [103]. That is, the vectors $|a_n\rangle$ may be chosen as elements of \mathbb{C}^r . One possible algorithm for obtaining the Cholesky factorization is given by

$$\begin{aligned} m > n : \quad A_{mn} &= (D_{mn} - \sum_{k=1}^{n-1} A_{mk} A_{nk}^*) / A_{nn}, \\ m = n : \quad A_{mm} &= \sqrt{1 - \sum_{k=1}^{m-1} |A_{mk}|^2}. \end{aligned} \tag{A.4}$$

Starting from the upper left corner of the matrix, the algorithm proceeds to compute the matrix row by row. Note that if $A_{nn} = 0$ for $m > n$, one has to divide by 1.

A.3 Bloch Representation for N-level Systems

It is a well-known fact that any Hermitian matrix $\rho_H \in \mathcal{M}_N$ may be written in the form [30, 104]

$$\rho_H = \frac{1}{2} \left(\frac{2}{N} \mathbb{1}_N + \vec{b} \cdot \vec{\sigma} \right), \tag{A.5}$$

where $\vec{\sigma} = (\sigma_1, \dots, \sigma_{N^2-1})$ is the vector of traceless generators of the $SU(N)$ obeying

$$\sigma_i \sigma_j = \frac{2}{N} \delta_{ij} \mathbb{1}_N + f_{ijk} \sigma_k + i g_{ijk} \sigma_k. \tag{A.6}$$

The *structure constants* f_{ijk} (vanishing for $N = 2$) and g_{ijk} form a totally symmetric and a totally anti-symmetric tensor, respectively, \vec{b} is a real vector in \mathbb{R}^{N^2-1} . From a given matrix ρ_H , the vector elements b_i are obtained via

$$b_i = \text{tr}[\rho_H \sigma_i]. \tag{A.7}$$

A density matrix ρ is a Hermitian matrix with the additional properties

$$(i) \text{tr} \rho = 1 \quad \text{and} \quad (ii) \rho \geq 0. \tag{A.8}$$

In this case, the vector \vec{b} is usually called *Bloch vector*, and we denote the set of Bloch vectors with $\mathcal{B}(\mathbb{R}^{N^2-1})$. It is clear, that conditions (i) and (ii) impose additional constraints

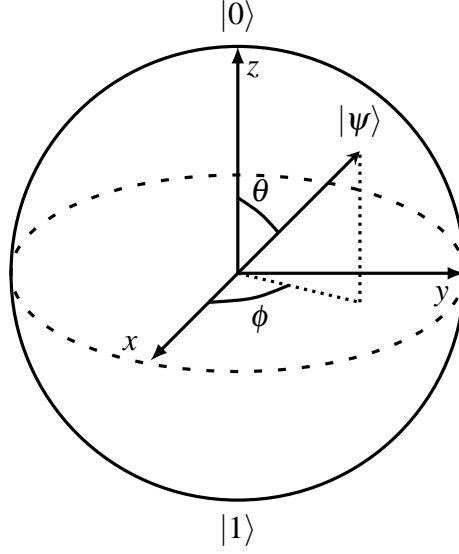


Figure A.1: Bloch representation of a two-level system. The north pole of the sphere is usually identified with the computational basis vector $|0\rangle$, its orthogonal counterpart $|1\rangle$ is found at the south-pole. The inside corresponds to the mixed state space.

on the vector \vec{b} . One can easily deduce that $\text{tr}\rho^2 \leq 1$, corresponding to

$$|\vec{b}| \leq \sqrt{\frac{2(N-1)}{N}} =: r_N. \quad (\text{A.9})$$

For $N = 2$, this concept leads to the well-known *Bloch sphere* (cf. Fig. A.1), a sphere in \mathbb{R}^3 of radius 1. Here, each vector on the surface represents a pure state, whereas the points inside correspond to the mixed states. Note, however, that in general not every vector with (A.9) represents an actual quantum state. Rather, it is known that for $N \geq 3$ the Bloch vector space $\mathcal{B}(\mathbb{R}^{N^2-1})$ is a proper subset of the ball $B_{r_N}(0)$ with radius r_N [104].

A.4 Identifying a FSOV Using the Bloch representation

In Sec. 3.1 we discuss the property of a set of complex vectors $\{|a_1\rangle, \dots, |a_N\rangle\} \subset \mathbb{C}^r$ called a “full set of vectors” (FSOV) [17], which is attained if, for a complex matrix $M \in \mathcal{M}_r$, $\langle a_n | M | a_n \rangle = 0 \forall n = 1, \dots, N$ implies $M = 0$.

How can this formal criterion be cast into a constructive one? For this we make use of the ideas leading to the Bloch representation. It is clear that any linear operator may be represented using a special operator basis and a complex vector. As operator basis we may choose the identity together with $\vec{\sigma} = (\sigma_1, \dots, \sigma_{r^2-1})$, the set of trace-less generators

A Technical Toolkit

of the $SU(r)$ already introduced in the definition of the Bloch representation, App. A.3. Rewriting both the projectors $P_n := |a_n\rangle\langle a_n|$ and operator M according to $P_n =: \vec{B}_n \cdot (\mathbf{1}_r, \vec{\sigma})$ and $M =: \vec{Q} \cdot (\mathbf{1}_r, \vec{\sigma})$, a simple calculation shows that

$$\begin{aligned} \text{tr}[MP_n] &= \text{tr}\left[\left(\vec{Q} \cdot (\mathbf{1}_r, \vec{\sigma})\right) \left(\vec{B}_n \cdot (\mathbf{1}_r, \vec{\sigma})\right)\right] \\ &= \vec{Q} \cdot \vec{B}_n. \end{aligned} \quad (\text{A.10})$$

Note that the \vec{B}_n representing the projectors P_n correspond to $\vec{B}_n = \frac{1}{2}\left(\frac{2}{r}, \vec{b}_n\right)$, where the \vec{b}_n are the Bloch vectors as defined in App. A.3.

The FSOV criterion is now satisfied if

$$\vec{Q} \cdot \vec{B}_n = 0 \quad \forall n = 1, \dots, N \quad \Rightarrow \quad \vec{Q} = 0. \quad (\text{A.11})$$

This is only possible if the vectors $\{\vec{B}_n\}_{n=1}^N$ span the \mathbb{R}^{r^2} , requiring $N \geq r^2$. For $N = r^2$ this may be checked using the determinant

$$\frac{1}{2^{r^2}} \begin{vmatrix} \vec{B}_1 & \vec{B}_2 & \dots & \vec{B}_{r^2} \end{vmatrix} = \begin{vmatrix} \frac{2}{r} & \frac{2}{r} & \dots & \frac{2}{r} \\ \vec{b}_1 & \vec{b}_2 & \dots & \vec{b}_{r^2} \end{vmatrix} \neq 0. \quad (\text{A.12})$$

In the case that $N > r^2$ all subsets of $\{\vec{B}_n\}$ containing r^2 elements have to be checked for linear independence.

A.5 Calculation of the cb-Norm

In this section we want to discuss a suitable method of calculating the cb-norm of a linear map. The method is presented and described in the article by Johnston, Kribs and Paulsen [105]. We here give a summary of the relevant steps needed in the numerical evaluation, introducing an important modification of the algorithm for our purposes discussing the case of diagonal maps. For further discussion and proofs please see the original article.

The calculation of the cb-norm of a linear map relies on the *generalized Kraus representation*: To a linear map $\Phi : \mathcal{M}_N \rightarrow \mathcal{M}_N$ there exist matrices $K_i \in \mathcal{M}_N$ and $L_i \in \mathcal{M}_N$,

$1 \leq i \leq m \leq N^2$, such that

$$\begin{aligned}\Phi(\rho) &= \sum_{i=1}^m K_i \rho L_i \\ &= \left(K_1, \dots, K_m \right) \begin{pmatrix} \rho & 0 & \cdots & 0 \\ 0 & \rho & \cdots & 0 \\ \vdots & \vdots & \ddots & \vdots \\ 0 & 0 & \cdots & \rho \end{pmatrix} \begin{pmatrix} L_1 \\ \vdots \\ L_m \end{pmatrix},\end{aligned}\quad (\text{A.13})$$

and such that the cb-norm of the map is given by $\|\Phi\|_{cb}^2 = \|\sum_i K_i K_i^\dagger\| \|\sum_i L_i^\dagger L_i\|$. Based on this representation the cb-norm is obtained in the following way:

Theorem 4. *The cb-norm of a linear map $\Phi : \mathcal{M}_N \rightarrow \mathcal{M}_N$ is given by*

$$\|\Phi\|_{cb} = \inf \left\{ \left\| \sum_i K_i K_i^\dagger \right\|^{1/2} \left\| \sum_i L_i^\dagger L_i \right\|^{1/2} \right\}, \quad (\text{A.14})$$

where the infimum is taken over all generalized Kraus representation of the map Φ .

The single steps in the calculation of the cb-norm are subsumed in the following algorithm

(I) Find a linearly independent generalized Kraus representation

- (I.1) Find a basis $\{X_1, \dots, X_l\}$ for the span of $\{K_1, \dots, K_m\}$ and express $K_i = \sum_j d_{ij} X_j$.
- (I.2) Insert into (A.13), obtaining

$$\begin{aligned}\Phi(\rho) &= \sum_{i=1}^m \left(\sum_{j=1}^l d_{ij} X_j \right) \rho L_i \\ &= \sum_{j=1}^l X_j \rho \left(\sum_{i=1}^m d_{ij} L_i \right) \\ &= \sum_{j=1}^l X_j \rho Y_j,\end{aligned}\quad (\text{A.15})$$

where $Y_j = \sum_i d_{i,j} L_i$.

- (I.3) Find a basis $\{\tilde{Y}_1, \dots, \tilde{Y}_k\}$ for the span of $\{Y_1, \dots, Y_l\}$. As in steps (1) and (2), express $Y_i = \sum_j \tilde{d}_{ij} \tilde{Y}_j$ and insert into (A.13), yielding

$$\Phi(\rho) = \sum_{i=1}^k \tilde{X}_i \rho \tilde{Y}_i. \quad (\text{A.16})$$

A Technical Toolkit

At this point, both sets $\{\tilde{X}_1, \dots, \tilde{X}_k\}$ and $\{\tilde{Y}_1, \dots, \tilde{Y}_k\}$ are linearly independent, completing the first part of the algorithm.

(II) Calculation of cb-Norm

Based on the linearly independent generalized Kraus representation obtained in part (I), the cb-norm is obtained with the help of a positive invertible matrix $S = (s_{ij}) \in \mathcal{M}_k$ with inverse $S^{-1} = (t_{ij})$. Based on this matrix we define $H_i = \sum_j s_{ij} \tilde{Y}_j$ and $G_i = \sum_j t_{ji} \tilde{X}_j$. Then

$$\|\Phi\|_{cb} = \inf_S \left\{ \left\| \sum_i G_i G_i^\dagger \right\|^{1/2} \left\| \sum_i H_i^\dagger H_i \right\|^{1/2} \right\}, \quad (\text{A.17})$$

where the infimum is taken over all invertible matrices S .

A.5.1 Specifics for Diagonal Maps of Full Rank

In the case of a diagonal map with full rank step (I) of the algorithm may be left out completely. With full rank we denote the case, where the diagonal map $D : \mathcal{M}_N \rightarrow \mathcal{M}_N$ has N nonzero eigenvalues, that is, the rows and columns of D are linearly independent. In this case we may introduce the linearly independent generalized Kraus representation with

$$G_i = \text{diagonal}(D_{1i}, \dots, D_{Ni}), \quad (\text{A.18})$$

$$H_i = \text{diagonal}(0, \dots, \underset{i}{\downarrow} 1, \dots, 0). \quad (\text{A.19})$$

We may thus circumvent step (I) without further ado.

A.6 Volume Spanned by a FSOV

We show the equivalence of the determinant of the FSOV criterion with the volume spanned by the Bloch vectors for arbitrary dimension. For simplicity we consider only the case $N = r^2$, the generalization is however straightforward. We thus have r^2 vectors $\vec{B}_n \in \mathbb{R}^{r^2}$ entering

the determinant. Based on the definitions in Sec. A.4 we get [72]

$$\begin{aligned}
\left(\frac{1}{2}\right)^{r^2} |\vec{B}_1 \cdots \vec{B}_{r^2}| &= \left| \begin{array}{ccc} \frac{2}{r} & \cdots & \frac{2}{r} \\ \vec{b}_1 & \cdots & \vec{b}_{r^2} \end{array} \right| \\
&= \left| \begin{array}{c} \left(\begin{array}{ccc} \frac{2}{r} & \cdots & \frac{2}{r} \end{array} \right) \left(\begin{array}{cccc} 1 & -1 & \cdots & -1 \\ & 1 & & \\ & & \ddots & \\ & & & 1 \end{array} \right) \\ \vec{b}_1 & \cdots & \vec{b}_{r^2} \end{array} \right| \\
&= \frac{2}{r} \left| \begin{array}{cccc} (\vec{b}_2 - \vec{b}_1) & (\vec{b}_3 - \vec{b}_1) & \cdots & (\vec{b}_{r^2} - \vec{b}_1) \end{array} \right| \\
&= \frac{2(r^2 - 1)!}{r} \text{Vol}(\vec{b}_1, \dots, \vec{b}_{r^2}) \\
&\neq 0,
\end{aligned} \tag{A.20}$$

where $\text{Vol}(\vec{b}_1, \dots, \vec{b}_{r^2})$ denotes the volume of the parallelepiped spanned by the real, $r^2 - 1$ dimensional vectors $\{\vec{b}_1, \dots, \vec{b}_{r^2}\}$.

A.7 Phase-Damping of a Single Qubit: Deformation of the Bloch Sphere

In order to estimate the effect of a phase-damping channel on the volume of the Bloch sphere, recall that a single qubit may be written as (cf. App. A.3)

$$\rho = \frac{1}{2}(\mathbb{1} + \vec{r} \cdot \vec{\sigma}) \tag{A.21}$$

$$= \frac{1}{2} \begin{pmatrix} 1 + r_z & r_x - ir_y \\ r_x + ir_y & 1 - r_z \end{pmatrix}, \tag{A.22}$$

where \vec{r} denotes the Bloch vector. In this representation, the effect of the phase-damping channel D on the Bloch vectors is straightforward. Applying the channel gives

$$D \star \rho = \begin{pmatrix} 1 & c \\ c^* & 1 \end{pmatrix} \star \frac{1}{2} \begin{pmatrix} 1 + r_z & r_x - ir_y \\ r_x + ir_y & 1 - r_z \end{pmatrix} \tag{A.23}$$

$$= \frac{1}{2} \begin{pmatrix} 1 + r_z & |c|e^{i\phi}(r_x - ir_y) \\ |c|e^{-i\phi}(r_x + ir_y) & 1 - r_z \end{pmatrix}, \tag{A.24}$$

where we made use of the polar decomposition $c = |c|e^{i\phi}$. It is now obvious that r_z is left unaltered, while the parts perpendicular to the z -axis suffer from a decrease by a factor of $|c|$

A Technical Toolkit

together with a rotation around z . Using the cylindrical symmetry properties, we assess the final volume via

$$V' = \int_0^{2\pi} d\varphi \int_{-1}^1 dz \int_0^{R(z)} dr r, \quad (\text{A.25})$$

where $R(z) = |c| \sqrt{1-z^2}$. As a result we find $V = \frac{4}{3}\pi|c|^2$, so that the relative change with respect to the initial Bloch sphere ($V = \frac{4}{3}\pi$) trivially equals

$$\frac{V'}{V} = |c|^2. \quad (\text{A.26})$$

B Calculation of the Bloch Volume

B.1 The Caley-Menger Determinant

The volume of a simplex spanned by real vectors in Euclidean space may be evaluated using the so-called *Caley-Menger* determinant. The following derivation may be found in [106]. Let us consider the volume of a $(N - 1)$ simplex, spanned by the vectors $\vec{x}_n = (x_n^{(1)}, x_n^{(2)}, \dots, x_n^{(N-1)}) \in \mathbb{R}^{N-1}, n = 1, \dots, N$. Using basic matrix algebra (cf. Sec. A.6), it is straightforward that the volume is given as

$$\text{Vol}_{N-1} = \frac{1}{(N-1)!} \begin{vmatrix} 1 & 1 & \cdots & 1 \\ x_1^{(1)} & x_2^{(1)} & \cdots & x_N^{(1)} \\ x_1^{(2)} & x_2^{(2)} & \cdots & x_N^{(2)} \\ \vdots & \vdots & & \vdots \\ x_1^{(N-1)} & x_2^{(N-1)} & \cdots & x_N^{(N-1)} \end{vmatrix}. \quad (\text{B.1})$$

In order to arrive at the Caley-Menger determinant, the matrix is augmented by a $(N + 1)$ th row and column, with all new elements zero except for the intersecting one which is equal to one. Note that the determinant is unaltered by this operation. Multiplying this new determinant with the one obtained from it by interchanging the first two rows and columns, followed by a transposition, leads to the equivalence

$$\text{Vol}_{N-1}^2 = \frac{-1}{((N-1)!)^2} \begin{vmatrix} 0 & 1 & 1 & \cdots & 1 \\ 1 & \vec{x}_1 \cdot \vec{x}_1 & \vec{x}_1 \cdot \vec{x}_2 & \cdots & \vec{x}_1 \cdot \vec{x}_N \\ 1 & \vec{x}_2 \cdot \vec{x}_1 & \vec{x}_2 \cdot \vec{x}_2 & \cdots & \vec{x}_2 \cdot \vec{x}_N \\ \vdots & \vdots & \vdots & & \vdots \\ 1 & \vec{x}_N \cdot \vec{x}_1 & \vec{x}_N \cdot \vec{x}_2 & \cdots & \vec{x}_N \cdot \vec{x}_N \end{vmatrix}. \quad (\text{B.2})$$

The distance $s_{mn} = \sqrt{(\vec{x}_m - \vec{x}_n) \cdot (\vec{x}_m - \vec{x}_n)}$ between the vertices m and n is related to the scalar product via

$$\vec{x}_m \cdot \vec{x}_n = \frac{1}{2} (\vec{x}_m \cdot \vec{x}_m + \vec{x}_n \cdot \vec{x}_n - s_{mn}^2). \quad (\text{B.3})$$

B Calculation of the Bloch Volume

After insertion into Eq. B.2, now subtracting from the n th row the product of the preceding row by $\frac{1}{2}(\vec{x}_{n-1} \cdot \vec{x}_{n-1})$, $n = 2, \dots, N$, one arrives after some additional reductions at

$$\text{Vol}_{N-1}^2 = \frac{(-1)^N}{2^{N-1}((N-1)!)^2} \det(A_N). \quad (\text{B.4})$$

Here, we have defined the Caley-Menger Determinant

$$\det(A_N) = \begin{vmatrix} 0 & 1 & 1 & \cdots & 1 \\ 1 & 0 & s_{1,2}^2 & \cdots & s_{1,N}^2 \\ 1 & s_{1,2}^2 & 0 & \ddots & \vdots \\ \vdots & \vdots & \ddots & \ddots & s_{N-1,N}^2 \\ 1 & s_{1,N}^2 & \cdots & s_{N-1,N}^2 & 0 \end{vmatrix}. \quad (\text{B.5})$$

B.2 Bloch Volume of a Phase-Damping Channel

The Caley-Menger determinant offers a very elegant way to directly calculate the volume spanned by the Bloch vectors corresponding to the dynamical vectors representing a phase-damping channel D . To see this, let D be a phase-damping channel of a quantum system of dimension N . As introduced in Sec. 2.2.4, its matrix elements may be obtained as overlap of N dynamical vectors

$$D_{mn} = \langle a_n | a_m \rangle, \quad m, n = 1, \dots, N, \quad (\text{B.6})$$

which may be identified as relative states of some quantum environment. For a channel of rank r , the dynamical vectors $|a_n\rangle$ may be chosen as vectors in \mathbb{C}^r (see App. A.2), allowing a representation in terms of $(r^2 - 1)$ -dimensional Bloch vectors \vec{b}_n . The mutual distance between any of these Bloch vectors equates to

$$\begin{aligned} s_{m,n}^2 &= |\vec{b}_m - \vec{b}_n|^2 = |\vec{b}_m|^2 - 2\vec{b}_m \cdot \vec{b}_n + |\vec{b}_n|^2 \\ &= 4 \left(1 - \frac{1}{r}\right) - 2\vec{b}_m \cdot \vec{b}_n, \end{aligned} \quad (\text{B.7})$$

B.2 Bloch Volume of a Phase-Damping Channel

where the Bloch vectors are defined according to Eq. (A.7). The matrix elements D_{mn} may be used to extract the distances in the following way.

$$\begin{aligned}
|D_{mn}|^2 &= |\langle a_n | a_m \rangle|^2 = \text{tr} [\rho_n \rho_m] \\
&= \text{tr} \left[\left(\frac{1}{r} \mathbb{1}_r + \frac{1}{2} \vec{b}_n \cdot \vec{\sigma} \right) \left(\frac{1}{r} \mathbb{1}_r + \frac{1}{2} \vec{b}_m \cdot \vec{\sigma} \right) \right] \\
&= \text{tr} \left[\frac{1}{r^2} \mathbb{1}_r + \frac{1}{2r} \vec{b}_n \cdot \vec{\sigma} + \frac{1}{2r} \vec{b}_m \cdot \vec{\sigma} + \frac{1}{4} (\vec{b}_n \cdot \vec{\sigma}) (\vec{b}_m \cdot \vec{\sigma}) \right] \\
&= \frac{1}{r} + \frac{1}{4} \text{tr} \left[\sum_{m,n} b_{j,m} b_{i,n} \left(\frac{2}{r} \delta_{mn} \mathbb{1}_r + (f_{ijk} + ig_{ijk}) \sigma_k \right) \right] \\
&= \frac{1}{r} + \frac{1}{2} \vec{b}_n \cdot \vec{b}_m.
\end{aligned} \tag{B.8}$$

Putting the last two results together we obtain

$$\begin{aligned}
s_{m,n}^2 &= 4 \left(1 - \frac{1}{r} \right) - 4 \left(|D_{mn}|^2 - \frac{1}{r} \right) \\
&= 4 \left(1 - |D_{mn}|^2 \right),
\end{aligned} \tag{B.9}$$

so that we arrive at the equivalence

$$\begin{pmatrix} 0 & s_{1,2}^2 & \cdots & s_{1,N}^2 \\ s_{1,2}^2 & 0 & \ddots & \vdots \\ \vdots & \ddots & \ddots & s_{N-1,N}^2 \\ s_{1,N}^2 & \cdots & s_{N-1,N}^2 & 0 \end{pmatrix} = 4 (\text{id} - D \star D^*). \tag{B.10}$$

Now, in case the Bloch vectors form a simplex, that is, we have N vectors $\vec{b}_n \in \mathbb{R}^{N-1}$, we can evaluate the volume via

$$\text{Vol}_{N-1}^2 = \frac{(-1)^N}{2^{N-1} ((N-1)!)^2} \det(A_N), \tag{B.11}$$

where the Caley-Menger determinant is now given as

$$\det(A_N) = \begin{vmatrix} 0 & 1 & \cdots & 1 \\ 1 & & & \\ \vdots & & 4(\text{id} - D \star D^*) & \\ 1 & & & \end{vmatrix}. \tag{B.12}$$

B.3 Bloch Volume of a SIC-POVM

As discussed in the preceding section the Caley-Menger determinant allows to evaluate the volume spanned by the dynamical vectors $\{|a_n\rangle\}_{n=1}^N$. Based on the matrix representation D , where $D_{mn} = \langle a_n | a_m \rangle$, the volume is given by

$$V_B^2 = \frac{(-1)^N}{2^{N-1}((N-1)!)^2} \begin{vmatrix} 0 & 1 & \cdots & 1 \\ 1 & & & \\ \vdots & & 4(\text{id} - D \star D^*) & \\ 1 & & & \end{vmatrix} \quad (\text{B.13})$$

In case the dynamical vectors form a SIC-POVM (see Sec. 2.6.2), we have

$$4(\text{id} - D \star D^*) = \begin{pmatrix} 0 & x & \cdots & x \\ x & 0 & \ddots & \vdots \\ \vdots & \ddots & \ddots & x \\ x & \cdots & x & 0 \end{pmatrix}, \quad (\text{B.14})$$

with $x = 4(1 - |\langle a_n | a_m \rangle|^2) = 4\left(\frac{\sqrt{N}}{\sqrt{N+1}}\right)$.

In order to calculate the Bloch volume we need the following

Lemma 1. *The determinant of*

$$A_N = \underbrace{\begin{pmatrix} 0 & 1 & 1 & \cdots & 1 \\ 1 & 0 & x & \cdots & x \\ 1 & x & 0 & \ddots & \vdots \\ \vdots & \vdots & \ddots & \ddots & x \\ 1 & x & \cdots & x & 0 \end{pmatrix}}_{N+1} \quad (\text{B.15})$$

is given by $|A_N| = N (-1)^N x^{N-1}$.

We give the proof by induction:

(I) Induction basis ($N = 2$):

$$|A_2| = \begin{vmatrix} 0 & 1 & 1 \\ 1 & 0 & x \\ 1 & x & 0 \end{vmatrix} = 2x = 2 (-1)^2 x^{2-1}, \quad (\text{B.16})$$

complying with the assumption.

(II) Induction step: Let $|A_N| = N(-1)^N x^{N-1}$

Through expansion along the first column with a successive rearrangement we find

$$\begin{aligned}
 |A_{N+1}| &= \begin{vmatrix} 0 & 1 & 1 & \cdots & 1 \\ 1 & 0 & x & \cdots & x \\ 1 & x & 0 & \ddots & \vdots \\ \vdots & \vdots & \ddots & \ddots & x \\ 1 & x & \cdots & x & 0 \end{vmatrix} \\
 &= (N+1)(-1)^{N+1} \begin{vmatrix} 1 & 1 & 1 & \cdots & 0 \\ 0 & x & x & \cdots & x \\ x & 0 & x & & x \\ \vdots & \ddots & \ddots & \ddots & \vdots \\ x & \cdots & x & 0 & x \end{vmatrix} \quad (\text{B.17})
 \end{aligned}$$

On the other hand we have

$$\begin{aligned}
 \begin{pmatrix} 1 & 0 & 0 & \cdots & 0 & 1 \\ 0 & 1 & 0 & \cdots & 0 & x \\ 0 & 0 & 1 & \ddots & \vdots & \vdots \\ \vdots & \vdots & \ddots & \ddots & 0 & x \\ 0 & 0 & \cdots & 0 & 1 & x \\ x & 0 & 0 & \cdots & 0 & 0 \end{pmatrix} \underbrace{\begin{pmatrix} 0 & 1 & 1 & \cdots & 1 & 0 \\ 1 & 0 & x & \cdots & x & 0 \\ 1 & x & 0 & \ddots & \vdots & \vdots \\ \vdots & \vdots & \ddots & \ddots & x & 0 \\ 1 & x & \cdots & x & 0 & 0 \\ 0 & 0 & \cdots & 0 & 0 & 1 \end{pmatrix}}_{\begin{pmatrix} & & & & 0 \\ & & & & \vdots \\ & A_N & & & 0 \\ 0 & \cdots & 0 & & 1 \end{pmatrix}} = \underbrace{\begin{pmatrix} 0 & 1 & 1 & \cdots & 1 & 1 \\ 1 & 0 & x & \cdots & x & x \\ 1 & x & 0 & \ddots & \vdots & \vdots \\ \vdots & \vdots & \ddots & \ddots & x & x \\ 1 & x & \cdots & x & 0 & x \\ \color{red}{0} & x & \cdots & x & x & 0 \end{pmatrix}}_{=:\tilde{A}_{N+1}} \quad (\text{B.18})
 \end{aligned}$$

Note that \tilde{A}_{N+1} is identical to A_{N+1} *except* for the lower left corner (highlighted in red—0 and 1, respectively). From expansion along the first column and comparison with (B.17) it is thus easy to see that the determinants of \tilde{A}_{N+1} and A_{N+1} are related

B Calculation of the Bloch Volume

by

$$\begin{aligned}
 |A_{N+1}| &= |\tilde{A}_{N+1}| + (-1)^{N+1} \begin{vmatrix} 1 & 1 & 1 & \cdots & 0 \\ 0 & x & x & \cdots & x \\ x & 0 & x & & x \\ \vdots & \ddots & \ddots & \ddots & \vdots \\ x & \cdots & x & 0 & x \end{vmatrix} \\
 &= |\tilde{A}_{N+1}| + (-1)^{N+1} \left[\frac{(-1)^{N+1}}{N+1} |A_{N+1}| \right] \\
 &= |\tilde{A}_{N+1}| + \frac{1}{N+1} |A_{N+1}|, \tag{B.19}
 \end{aligned}$$

leading to

$$|A_{N+1}| = \frac{N+1}{N} |\tilde{A}_{N+1}|. \tag{B.20}$$

In evaluating the determinant of the left-hand side in Eq. (B.18) we make use of the product formula $|AB| = |A||B|$. The determinant of the first matrix can easily be obtained via expansion along the last column, followed by some reshuffling, giving the value of $-x$. For the second matrix it is straightforward to see that its determinant is identical to $|A_N|$. Together with Eq. (B.20) this gives

$$\begin{aligned}
 |A_{N+1}| &= \frac{N+1}{N} |\tilde{A}_{N+1}| \\
 &= \frac{N+1}{N} (-x) |A_N| \\
 &= (N+1) (-1)^{N+1} x^N, \tag{B.21}
 \end{aligned}$$

thus completing the proof.

The volume itself finally equates to

$$V_B = \frac{\sqrt{N} \left(2 \frac{\sqrt{N}}{\sqrt{N+1}} \right)^{\frac{N-1}{2}}}{(N-1)!}. \tag{B.22}$$

C Calculations in the Wigner Representation

C.1 The Two-Mode Entangled Channel

In order to arrive at the full form of the phase-damping channel considered in Sec. 5, we have to evaluate all matrix elements defined as

$$D_{mn} = \int dq_a \int dp_a \int dq_b \int dp_b W(q_a, p_a, q_b, p_b) \tilde{U}_{mn}^{(W)}(t), \quad (\text{C.1})$$

with the Wigner representation of the two-mode squeezed entangled state

$$W(q_a, p_a, q_b, p_b) = \frac{4}{\pi^2} \exp \left\{ -e^{-2r} [(q_a + q_b)^2 + (p_a - p_b)^2] - e^{+2r} [(q_a - q_b)^2 + (p_a + p_b)^2] \right\}. \quad (\text{C.2})$$

and the unitary operators

$$\tilde{U}_{mn}^{(W)}(t) = \int dq'_a \int dq'_b \langle q_a + \frac{q'_a}{2} | \otimes \langle q_b + \frac{q'_b}{2} | \tilde{U}_{mn}(t) | q_a - \frac{q'_a}{2} \rangle \otimes | q_b - \frac{q'_b}{2} \rangle \times e^{-i(p_a q'_a + p_b q'_b)}. \quad (\text{C.3})$$

Remember that the unitaries are given as $\tilde{U}_{mn}(t) = e^{i\tilde{H}_R^{(n)}t} e^{-i\tilde{H}_R^{(m)}t}$. Using the expressions obtained in Eq. (5.15) for the relative Hamiltonians $\tilde{H}_R^{(n)}$, the unitary operators needed in order to calculate all matrix elements of the phase-damping channel are

$$\tilde{U}_{12}(t) = e^{-2\Omega_B t} e^{i\tilde{h}_b^{(-)}t} e^{-i\tilde{h}_b^{(+)}t} = \tilde{U}_{21}^*(t), \quad (\text{C.4a})$$

$$\tilde{U}_{13}(t) = e^{-2\Omega_A t} e^{i\tilde{h}_a^{(-)}t} e^{-i\tilde{h}_a^{(+)}t} = \tilde{U}_{31}^*(t), \quad (\text{C.4b})$$

$$\tilde{U}_{14}(t) = e^{-2(\Omega_A + \Omega_B)t} e^{i\tilde{h}_a^{(-)}t} e^{i\tilde{h}_b^{(-)}t} e^{-i\tilde{h}_a^{(+)}t} e^{-i\tilde{h}_b^{(+)}t} = \tilde{U}_{41}^*(t), \quad (\text{C.4c})$$

$$\tilde{U}_{23}(t) = e^{-2(\Omega_A - \Omega_B)t} e^{i\tilde{h}_a^{(-)}t} e^{i\tilde{h}_b^{(+)}t} e^{-i\tilde{h}_a^{(+)}t} e^{-i\tilde{h}_b^{(-)}t} = \tilde{U}_{32}^*(t), \quad (\text{C.4d})$$

$$\tilde{U}_{24}(t) = e^{-2\Omega_A t} e^{i\tilde{h}_a^{(-)}t} e^{-i\tilde{h}_a^{(+)}t} = \tilde{U}_{42}^*(t), \quad (\text{C.4e})$$

$$\tilde{U}_{34}(t) = e^{-2\Omega_B t} e^{i\tilde{h}_b^{(-)}t} e^{-i\tilde{h}_b^{(+)}t} = \tilde{U}_{43}^*(t). \quad (\text{C.4f})$$

C Calculations in the Wigner Representation

Exemplary we will carry out the evaluation of matrix element D_{12} . The Wigner representation of $\tilde{U}_{12}(t)$ is given by

$$\tilde{U}_{12}^{(W)}(t) = e^{-2i\Omega_B t} \int dq'_b \int dq \langle q_b + \frac{q'_b}{2} | e^{i\tilde{h}_b^{(-)}t} | q \rangle \langle q | e^{-i\tilde{h}_b^{(+)}t} | q_b - \frac{q'_b}{2} \rangle e^{-ip_b q'_b}. \quad (\text{C.5})$$

where an additional resolution of the identity, $\mathbb{1} = \int dq |q\rangle \langle q|$, has been inserted. The time-evolution amplitudes now appearing in the evaluation of the Wigner representation may be assessed with the help of the path integral formulation of quantum mechanics [107]. For our case the relevant results are given by

$$\begin{aligned} \langle q_b + \frac{q'_b}{2} | e^{i\tilde{h}_b^{(-)}t} | q \rangle &= e^{-ig_b^2/2t} \sqrt{\frac{1}{2\pi i \sin(\omega_b t)}} \exp \left\{ -\frac{i}{2} \frac{1}{\sin(\omega_b t)} \right. \\ &\quad \times \left(\left[(q - g_b)^2 + \left(q_b + \frac{q'_b}{2} - g_b \right)^2 \right] \cos(\omega_b t) \right. \\ &\quad \left. \left. - 2(q - g_b) \left(q_b + \frac{q'_b}{2} - g_b \right) \right) \right\} \end{aligned} \quad (\text{C.6})$$

and

$$\begin{aligned} \langle q | e^{-i\tilde{h}_b^{(+)}t} | q_b - \frac{q'_b}{2} \rangle &= e^{+ig_b^2/2t} \sqrt{\frac{1}{2\pi i \sin(\omega_b t)}} \exp \left\{ +\frac{i}{2} \frac{1}{\sin(\omega_b t)} \right. \\ &\quad \times \left(\left[(q + g_b)^2 + \left(q_b - \frac{q'_b}{2} + g_b \right)^2 \right] \cos(\omega_b t) \right. \\ &\quad \left. \left. - 2(q + g_b) \left(q_b - \frac{q'_b}{2} + g_b \right) \right) \right\}. \end{aligned} \quad (\text{C.7})$$

Multiplication of the two amplitudes yields

$$\begin{aligned} \langle q_b + \frac{q'_b}{2} | e^{i\tilde{h}_b^{(-)}t} | q \rangle \langle q | e^{-i\tilde{h}_b^{(+)}t} | q_b - \frac{q'_b}{2} \rangle &= \left| \frac{1}{2\pi \sin(\omega_b t)} \right| \exp \left\{ \frac{i}{2} \frac{1}{\sin(\omega_b t)} \right. \\ &\quad \times \left(\left[4q_b g_b - 4q_b \left(\frac{q'_b}{2} - g_b \right) \right] \cos(\omega_b t) + 2 \left(q q'_b - 2q g_b - 2q_b g_b \right) \right) \right\}. \end{aligned} \quad (\text{C.8})$$

We are now able to carry out the integration in Eq.(C.5). First, consider the integration with respect to q , leading to

$$\begin{aligned}
 I[q'_b] &:= \int dq \langle q_b + \frac{q'_b}{2} | e^{i\tilde{h}_b^{(-)}t} | q \rangle \langle q | e^{-i\tilde{h}_b^{(+)}t} | q_b - \frac{q'_b}{2} \rangle \\
 &= \left| \frac{1}{2\pi \sin(\omega_b t)} \right| \exp \left\{ -\frac{i}{2} \frac{1}{\sin(\omega_b t)} \left(4q_b \left(\frac{q'_b}{2} - g_b \right) \cos(\omega_b t) + 4q_b g_b \right) \right\} \\
 &\quad \times \int dq \exp \left\{ -i2\pi \left[\frac{1}{2\sin(\omega_b t)} \left(2g_b(\cos(\omega_b t) - 1) - q'_b \right) \right] q \right\} \\
 &= \exp \left\{ -\frac{i}{2} \frac{1}{\sin(\omega_b t)} \left(4q_b \left(\frac{q'_b}{2} - g_b \right) \cos(\omega_b t) + 4q_b g_b \right) \right\} \\
 &\quad \times \delta \left(q'_b + 2g_b[\cos(\omega_b t) - 1] \right). \tag{C.9}
 \end{aligned}$$

The second integration with respect to q'_b is then easily obtained, leading to the Wigner representation of the unitary operator $\tilde{U}_{12}(t)$:

$$\begin{aligned}
 \tilde{U}_{12}^{(W)}(t) &= \int dq'_b I[q'_b] e^{-ip_b q'_b} \\
 &= \exp \left\{ -iq_b g_b \sin(\omega_b t) - ip_b g_b [\cos(\omega_b t) - 1] \right\}. \tag{C.10}
 \end{aligned}$$

The result is obviously of the form $\exp\{-i(c_{q_b} q_b + c_{p_b} p_b)\}$ with $c_{q_b} = g_b \sin(\omega_b t)$ and $c_{p_b} = g_b [\cos(\omega_b t) - 1]$. In order to generalize the subsequent evaluation we may thus set

$$\tilde{U}_{mn}^{(W)}(t) = \exp \left\{ -i4 \left(c_{q_a}^{mn} q_a + c_{p_a}^{mn} p_a + c_{q_b}^{mn} q_b + c_{p_b}^{mn} p_b \right) \right\}. \tag{C.11}$$

We may now proceed with the calculation of the final result: the matrix elements D_{mn} . Based on the identity

$$\int dx \exp \{ -ax^2 - (b + ic)x \} = \sqrt{\frac{\pi}{a}} \exp \left\{ \frac{(b + ic)^2}{4a} \right\} \tag{C.12}$$

C Calculations in the Wigner Representation

mn	$c_{q_a}^{mn}$	$c_{p_a}^{mn}$	$c_{q_b}^{mn}$	$c_{p_b}^{mn}$
12	0	0	$2g_b \sin(\omega_b t)$	$2g_b [1 - \cos(\omega_b t)]$
13	$2g_a \sin(\omega_a t)$	$2g_a [1 - \cos(\omega_a t)]$	0	0
14	$2g_a \sin(\omega_a t)$	$2g_a [1 - \cos(\omega_a t)]$	$2g_b \sin(\omega_b t)$	$2g_b [1 - \cos(\omega_b t)]$
23	$2g_a \sin(\omega_a t)$	$2g_a [1 - \cos(\omega_a t)]$	$-2g_b \sin(\omega_b t)$	$-2g_b [1 - \cos(\omega_b t)]$
24	$2g_a \sin(\omega_a t)$	$2g_a [1 - \cos(\omega_a t)]$	0	0
34	0	0	$2g_b \sin(\omega_b t)$	$2g_b [1 - \cos(\omega_b t)]$

Table C.1: List of the coefficients in the final result, Eq. (C.13).

we arrive at

$$\begin{aligned}
D_{mn} &= \frac{4}{\pi^2} \int dq_a \int dp_a \int dq_b \int dp_b \exp \left\{ -e^{-2r} [(q_a + q_b)^2 + (p_a - p_b)^2] \right. \\
&\quad \left. -e^{+2r} [(q_a - q_b)^2 + (p_a + p_b)^2] - i4 \left(c_{q_a}^{mn} q_a + c_{p_a}^{mn} p_a + c_{q_b}^{mn} q_b + c_{p_b}^{mn} p_b \right) \right\} \\
&= \frac{4}{\pi^2} \int dq_a \int dq_b \exp \left\{ - \left(q_a^2 2 \cosh(2r) + q_a q_b 4 \sinh(2r) \right. \right. \\
&\quad \left. \left. + q_b^2 2 \cosh(2r) + i4 \left(c_{q_a}^{mn} q_a + c_{q_b}^{mn} q_b \right) \right) \right\} \\
&\quad \times \int dp_a \int dp_b \exp \left\{ - \left(p_a^2 2 \cosh(2r) - p_a p_b 4 \sinh(2r) \right. \right. \\
&\quad \left. \left. + p_b^2 2 \cosh(2r) + i4 \left(c_{p_a}^{mn} p_a + c_{p_b}^{mn} p_b \right) \right) \right\} \\
&= \exp \left\{ -e^{-2r} \left[\left(c_{q_a}^{mn} + c_{q_b}^{mn} \right)^2 + \left(c_{p_a}^{mn} - c_{p_b}^{mn} \right)^2 \right] \right. \\
&\quad \left. -e^{+2r} \left[\left(c_{q_a}^{mn} - c_{q_b}^{mn} \right)^2 + \left(c_{p_a}^{mn} + c_{p_b}^{mn} \right)^2 \right] \right\}. \tag{C.13}
\end{aligned}$$

The relevant results are listed in Table C.1.

C.2 Wigner Function of Two Modes Sharing 1,2, and 3 Photons

We consider a pure state of two modes containing n photons. The entanglement shall rest on the lack of knowledge which of the two modes is actually occupied. The initial state thus

C.2 Wigner Function of Two Modes Sharing 1, 2, and 3 Photons

reads

$$|\psi\rangle = \alpha|0n\rangle_{ab} + \beta|n0\rangle_{ab}, \quad (\text{C.14})$$

where $|\alpha|^2 + |\beta|^2 = 1$. The Wigner function may be obtained as Fourier transform of the characteristic function, which is defined as

$$\begin{aligned} \chi(\eta_a, \eta_b) &= \text{tr} \left[\hat{\rho} e^{\eta_a \hat{a}^\dagger - \eta_a^* \hat{a}} e^{\eta_b \hat{b}^\dagger - \eta_b^* \hat{b}} \right] \\ &= \langle \psi | \hat{D}_a(\eta_a) \hat{D}_b(\eta_b) | \psi \rangle. \end{aligned} \quad (\text{C.15})$$

Here we made use of the so-called *displacement operators* of the form $\hat{D}(\eta) = \exp\{\eta \hat{a}^\dagger - \eta^* \hat{a}\}$. These are unitary operators mapping the vacuum state onto a coherent state, that is,

$$\hat{D}(\eta)|0\rangle = |\eta\rangle = e^{-\frac{|\eta|^2}{2}} \sum_{n=0}^{\infty} \frac{\eta^n}{\sqrt{n!}} |n\rangle. \quad (\text{C.16})$$

If we now plug the initial state into Eq. (C.15) we get

$$\begin{aligned} \chi(\eta_a, \eta_b) &= |\alpha|^2 \langle 0 | \hat{D}_a(\eta_a) | 0 \rangle \langle n | \hat{D}_b(\eta_b) | n \rangle \\ &\quad + \alpha \beta^* \langle n | \hat{D}_a(\eta_a) | 0 \rangle \langle 0 | \hat{D}_b(\eta_b) | n \rangle \\ &\quad + \beta \alpha^* \langle 0 | \hat{D}_a(\eta_a) | n \rangle \langle n | \hat{D}_b(\eta_b) | 0 \rangle \\ &\quad + |\beta|^2 \langle n | \hat{D}_a(\eta_a) | n \rangle \langle 0 | \hat{D}_b(\eta_b) | 0 \rangle. \end{aligned} \quad (\text{C.17})$$

The individual factors in this sum are obtained to be

$$\langle 0 | \hat{D}(\eta) | n \rangle = \frac{(-\eta^*)^n}{\sqrt{n!}} e^{-\frac{|\eta|^2}{2}}, \quad \text{and} \quad \langle n | \hat{D}(\eta) | 0 \rangle = \frac{(\eta)^n}{\sqrt{n!}} e^{-\frac{|\eta|^2}{2}}. \quad (\text{C.18})$$

Furthermore, using the identity $\hat{D}(\eta) \hat{a}^\dagger = (\hat{a}^\dagger - \eta^*) \hat{D}(\eta)$, we arrive at

$$\begin{aligned} \langle 0 | \hat{D}(\eta) | 0 \rangle &= e^{-\frac{|\eta|^2}{2}} = L_0(|\eta|^2) e^{-\frac{|\eta|^2}{2}}, \\ \langle 1 | \hat{D}(\eta) | 1 \rangle &= [-|\eta|^2 + 1] e^{-\frac{|\eta|^2}{2}} = L_1(|\eta|^2) e^{-\frac{|\eta|^2}{2}}, \\ \langle 2 | \hat{D}(\eta) | 2 \rangle &= \frac{1}{2} [|\eta|^4 - 4|\eta|^2 + 2] e^{-\frac{|\eta|^2}{2}} = L_2(|\eta|^2) e^{-\frac{|\eta|^2}{2}}, \\ \langle 3 | \hat{D}(\eta) | 3 \rangle &= \frac{1}{6} [-|\eta|^6 + 9|\eta|^4 - 18|\eta|^2 + 6] e^{-\frac{|\eta|^2}{2}} = L_3(|\eta|^2) e^{-\frac{|\eta|^2}{2}}. \end{aligned} \quad (\text{C.19})$$

C Calculations in the Wigner Representation

Here, $L_n(x)$ denote the so-called *Laguerre Polynomials* [101]. Everything put together gives the characteristic function

$$\chi^{(n)}(\eta_a, \eta_b) = \left[|\alpha|^2 L_n(|\eta_b|^2) - \alpha \beta^* \frac{(\eta_a \eta_b^*)^n}{n!} - \beta \alpha^* \frac{(\eta_b \eta_a^*)^n}{n!} + |\beta|^2 L_n(|\eta_a|^2) \right] e^{-\frac{|\eta_a|^2}{2}} e^{-\frac{|\eta_b|^2}{2}}. \quad (\text{C.20})$$

The resulting Wigner functions read

$$W^{(1)}(q_a, p_a, q_b, p_b) = -\frac{4}{\pi^2} \left[|\alpha|^2 L_1 \left(4(q_b^2 + p_b^2) \right) - 4\alpha\beta^* (q_a + ip_a)(p_b - iq_b) - 4\beta\alpha^* (q_a - ip_a)(q_b + ip_b) + |\beta|^2 L_1 \left(4(q_a^2 + p_a^2) \right) \right] \times e^{-2(q_a^2 + p_a^2 + q_b^2 + p_b^2)} \quad (\text{C.21a})$$

for one photon ($n = 1$),

$$W^{(2)}(q_a, p_a, q_b, p_b) = +\frac{4}{\pi^2} \left[|\alpha|^2 L_2 \left(4(q_b^2 + p_b^2) \right) + 8\alpha\beta^* (q_a + ip_a)^2 (p_b - iq_b)^2 + 8\beta\alpha^* (q_a - ip_a)^2 (q_b + ip_b)^2 + |\beta|^2 L_2 \left(4(q_a^2 + p_a^2) \right) \right] \times e^{-2(q_a^2 + p_a^2 + q_b^2 + p_b^2)} \quad (\text{C.21b})$$

for two photons ($n = 2$), and finally

$$W^{(3)}(q_a, p_a, q_b, p_b) = -\frac{4}{\pi^2} \left[|\alpha|^2 L_3 \left(4(q_b^2 + p_b^2) \right) - \frac{64}{6} \alpha\beta^* (q_a + ip_a)^3 (p_b - iq_b)^3 - \frac{64}{6} \beta\alpha^* (q_a - ip_a)^3 (q_b + ip_b)^3 + |\beta|^2 L_3 \left(4(q_a^2 + p_a^2) \right) \right] \times e^{-2(q_a^2 + p_a^2 + q_b^2 + p_b^2)} \quad (\text{C.21c})$$

for three photons ($n = 3$).

The respective reduced states simply equate to (see also [40])

$$W_{\text{red}}^{(1)}(q_a, p_a) = \frac{2}{\pi} (|\alpha|^2 - L_1(4(q_b^2 + p_b^2)) |\beta|^2) e^{-2(q_a^2 + p_a^2)}, \quad (\text{C.22a})$$

$$W_{\text{red}}^{(2)}(q_a, p_a) = \frac{2}{\pi} (|\alpha|^2 + L_2(4(q_b^2 + p_b^2)) |\beta|^2) e^{-2(q_a^2 + p_a^2)}, \quad (\text{C.22b})$$

C.2 Wigner Function of Two Modes Sharing 1,2, and 3 Photons

and

$$W_{\text{red}}^{(3)}(q_a, p_a) = \frac{2}{\pi} (|\alpha|^2 - L_3(4(q_b^2 + p_b^2))) |\beta|^2 e^{-2(q_a^2 + p_a^2)}, \quad (\text{C.22c})$$

respectively.

Bibliography

- [1] A. Messiah: *Quantum Mechanics* (Dover Publications, New York, 1999).
- [2] A. Zeilinger, R. Gähler, C. G. Shull, W. Treimer, and W. Mampe: *Single-slit and double-slit diffraction of neutrons*, Rev. Mod. Phys. **60**, 1067 (1988).
- [3] S. Gerlich, S. Eibenberger, M. Tomandl, S. Nimmrichter, K. Hornberger, P. J. Fagan, J. Tuexen, M. Mayor, and M. Arndt: *Quantum interference of large organic molecules*, Nat. Commun. **2**, 263 (2011).
- [4] E. Joos, H. D. Zeh, C. Kiefer, D. Giulini, J. Kupsch, and I.-O. Stamatescu: *Decoherence and the Appearance of a Classical World in Quantum Theory* (Springer-Verlag, Berlin, 2002).
- [5] W. H. Zurek: *Decoherence, einselection, and the quantum origins of the classical*, Rev. Mod. Phys. **75**, 715 (2003).
- [6] M. Schlosshauer: *Decoherence and the Quantum-To-Classical Transition* (Springer-Verlag, Berlin, 2007).
- [7] D. Braun, F. Haake, and W. T. Strunz: *Universality of decoherence*, Phys. Rev. Lett. **86**, 2913 (2001).
- [8] M. A. Nielsen and I. L. Chuang: *Quantum Computation and Quantum Information* (Cambridge University Press, Cambridge, UK, 2002).
- [9] H. Weinfurter and A. Zeilinger: *Quantum Communication*, in G. Alber (editor), *Quantum Information*, volume 173 of *Springer Tracts in Modern Physics* (Springer-Verlag, Berlin, 2001).
- [10] J. Eisert and M. B. Plenio: *Quantum and classical correlations in quantum Brownian motion*, Phys. Rev. Lett. **89**, 137902 (2002).
- [11] C. J. Myatt, B. E. King, Q. A. Turchette, C. A. Sackett, D. Kielpinski, W. M. Itano, C. Monroe, and D. J. Wineland: *Decoherence of quantum superpositions through coupling to engineered reservoirs*, Nature **403**, 269 (2000).

Bibliography

- [12] T. Monz, K. Kim, A. S. Villar, P. Schindler, M. Chwalla, M. Riebe, C. F. Roos, H. Häffner, W. Hänsel, M. Hennrich, and R. Blatt: *Realization of universal ion-trap quantum computation with decoherence-free qubits*, Phys. Rev. Lett. **103**, 200503 (2009).
- [13] T. Monz, P. Schindler, J. T. Barreiro, M. Chwalla, D. Nigg, W. A. Coish, M. Harlander, W. Haensel, M. Hennrich, and R. Blatt: *14-qubit entanglement: creation and coherence*, Phys. Rev. Lett. **106**, 130506 (2010).
- [14] F. Mintert, A. R. Carvalho, M. Kus, and A. Buchleitner: *Measures and dynamics of entangled states*, Phys. Rep. **415**, 207 (2005).
- [15] T. Werlang, A. V. Dodonov, E. I. Duzzioni, and C. J. Villas-Boas: *Rabi model beyond the rotating-wave approximation: Generation of photons from vacuum through decoherence*, Phys. Rev. A **78**, 053805 (2008).
- [16] A. R. R. Carvalho, M. Busse, O. Brodier, C. Viviescas, and A. Buchleitner: *Optimal dynamical characterization of entanglement*, Phys. Rev. Lett. **98**, 190501 (2007).
- [17] L. J. Landau and R. F. Streater: *On Birkhoff's theorem for doubly stochastic completely positive maps of matrix algebras*, Linear Algebra Appl. **193**, 107 (1993).
- [18] F. Buscemi, G. Chiribella, and G. M. D'Ariano: *Inverting quantum decoherence by classical feedback from the environment*, Phys. Rev. Lett. **95**, 090501 (2005).
- [19] M. Gregoratti and R. F. Werner: *Quantum lost and found*, J. Mod. Opt. **50**, 915 (2003).
- [20] F. Buscemi: *On the minimum number of unitaries needed to describe a random-unitary channel*, Phys. Lett. A **360**, 256 (2006).
- [21] K. M. R. Audenaert and S. Scheel: *On random unitary channels*, New J. Phys. **10**, 023011 (2008).
- [22] J. Watrous: *Mixing doubly stochastic quantum channels with the completely depolarizing channel*, Quant. Info. Comp. **9**, 406 (2009).
- [23] C. B. Mendl and M. M. Wolf: *Unital quantum channels—convex structure and revivals of Birkhoff's theorem*, Commun. Math. Phys. **289**, 1057 (2009).
- [24] J. Novotny, G. Alber, and I. Jex: *Random unitary dynamics of quantum networks*, J. Phys. A **42**, 282003 (2009).

- [25] J. Novotny, G. Alber, and I. Jex: *Asymptotic evolution of random unitary operations*, Cent. Eur. J. Phys. **8**, 1001 (2010).
- [26] J. Novotny, G. Alber, and I. Jex: *Asymptotic dynamics of qubit networks under randomly applied controlled unitary transformations*, New J. Phys. **13**, 053052 (2011).
- [27] A. Jamiolkowski: *Linear transformations which preserve trace and positive semidefinite operators*, Rep. Mod. Phys. **3**, 275 (1972).
- [28] E. Schrödinger: *Die gegenwärtige Situation in der Quantenmechanik*, Die Naturwissenschaften **23**, 844 (1935).
- [29] J. Wheeler and W. Zurek: *Quantum Theory and Measurement* (Princeton University Press, Princeton, USA, 1983).
- [30] I. Bengtsson and K. Życzkowski: *Geometry of Quantum States* (Cambridge University Press, Cambridge, UK, 2006).
- [31] C. H. Bennett, D. P. DiVincenzo, J. A. Smolin, and W. K. Wootters: *Mixed-state entanglement and quantum error correction*, Phys. Rev. A **54**, 3824 (1996).
- [32] R. Horodecki, P. Horodecki, M. Horodecki, and K. Horodecki: *Quantum entanglement*, Rev. Mod. Phys. **81**, 865 (2009).
- [33] R. F. Werner: *Quantum states with Einstein-Podolsky-Rosen correlations admitting a hidden-variable model*, Phys. Rev. A **40**, 4277 (1989).
- [34] M. Horodecki, P. Horodecki, and R. Horodecki: *Mixed-State Entanglement and Quantum Communication*, in G. Alber (editor), *Quantum Information*, volume 173 of *Springer Tracts in Modern Physics* (Springer-Verlag, Berlin, 2001).
- [35] A. Peres: *Separability criterion for density matrices*, Phys. Rev. Lett. **77**, 1413 (1996).
- [36] O. Cohen: *Unlocking hidden entanglement with classical information*, Phys. Rev. Lett. **80**, 2493 (1998).
- [37] D. P. DiVincenzo, C. A. Fuchs, H. Mabuchi, J. A. Smolin, A. Thapliyal, and A. Uhlmann: *Entanglement of assistance*, in C. Williams (editor), *Quantum computing and quantum communication: First NASA International Conference*, volume 1509 of *Lecture Notes in Computer Science* (Springer-Verlag, Berlin, 1999).
- [38] J. Smolin, F. Verstraete, and A. Winter: *Entanglement of assistance and multipartite state distillation*, Phys. Rev. A **72**, 052317 (2005).

Bibliography

- [39] J. Eisert: *Discrete Quantum States versus Continuous Variables*, in D. Bruß and G. Leuchs (editors), *Lectures on Quantum Information* (Wiley-VCH, Weinheim, 2007).
- [40] D. Walls and G. J. Milburn: *Quantum Optics* (Springer-Verlag, Berlin, 1995).
- [41] W. Schleich: *Quantum Optics in Phase Space* (Wiley-VCH, Berlin, 2001).
- [42] L. M. Duan, G. Giedke, J. I. Cirac, and P. Zoller: *Inseparability criterion for continuous variable systems*, Phys. Rev. Lett. **84**, 2722 (2000).
- [43] P. van Loock: *Entanglement Theory with Continuous Variables*, in D. Bruß and G. Leuchs (editors), *Lectures on Quantum Information* (Wiley-VCH, Weinheim, 2007).
- [44] B. L. Schumaker and C. M. Caves: *New formalism for two-photon quantum optics. II. Mathematical foundation and compact notation*, Phys. Rev. A **31**, 3093 (1985).
- [45] T. Yu and J. H. Eberly: *Finite-time disentanglement via spontaneous emission*, Phys. Rev. Lett. **93**, 140404 (2004).
- [46] D. P. DiVincenzo: *Quantum Computation*, Science **270**, 255 (1995).
- [47] V. Giovannetti, S. Lloyd, and L. Maccone: *Quantum-enhanced measurements: Beating the standard quantum limit*, Science **306**, 1330 (2004).
- [48] A. L. Ekert: *Quantum cryptography based on Bell theorem*, Phys. Rev. Lett. **67**, 661 (1991).
- [49] C. H. Bennett, G. Brassard, C. Crépeau, R. Jozsa, A. Peres, and W. K. Wootters: *Teleporting an unknown quantum state via dual classical and Einstein-Podolsky-Rosen channels*, Phys. Rev. Lett. **70**, 1895 (1993).
- [50] D. Lidar and K. B. Whaley: *Decoherence-Free Subspaces and Subsystems*, in F. Benatti and R. Floreanini (editors), *Irreversible Quantum Dynamics*, volume 622 of *Lecture Notes in Physics* (Springer-Verlag, Berlin, 2002).
- [51] F. Verstraete, M. M. Wolf, and J. I. Cirac: *Quantum computation and quantum-state engineering driven by dissipation*, Nat. Phys. **5**, 633 (2009).
- [52] K. Hornberger: *Introduction to Decoherence Theory*, in A. Buchleitner, C. Viviescas, and M. Tiersch (editors), *Entanglement and Decoherence — Foundations and Modern Trends*, volume 768 of *Lecture Notes in Physics* (Springer-Verlag, Berlin, 2009).

- [53] W. T. Strunz: *Decoherence in Quantum Physics*, in A. Buchleitner and K. Hornberger (editors), *Coherent Evolution in Noisy Environments*, volume 611 of *Lecture Notes in Physics* (Springer-Verlag, Berlin, 2002).
- [54] A. Pernice and W. T. Strunz: *Decoherence and the Nature of System-Environment Correlations*, arXiv:1109.0147v3 [quant-ph] (2011).
- [55] G. Grawert: *Quantenmechanik* (Akademische Verlagsgesellschaft Wiesbaden, 1977).
- [56] R. Alicki and K. Lendi: *Quantum Dynamical Semigroups and Applications* (Springer-Verlag, Berlin, 1987).
- [57] H. Häffner, W. Hänsel, C. F. Roos, J. Benhelm, D. C. al kar, M. Chwalla, T. Körber, U. D. Rapol, M. Riebe, P. O. Schmidt, C. Becher, O. Gühne, W. Dür, and R. Blatt: *Scalable multiparticle entanglement of trapped ions*, *Nature* **438**, 643 (2005).
- [58] C. F. Roos, M. Riebe, H. Häffner, W. Hänsel, J. Benhelm, G. P. T. Lancaster, C. Becher, F. Schmidt-Kaler, and R. Blatt: *Control and measurement of three-qubit entangled states*, *Science* **304**, 1478 (2004).
- [59] F. Schmidt-Kaler, S. Gulde, M. Riebe, T. Deuschle, A. Kreuter, G. Lancaster, C. Becher, J. Eschner, H. Häffner, and R. Blatt: *The coherence of qubits based on single Ca⁺ ions*, *J. Phys. B* **36**, 623 (2003).
- [60] J. Honerkamp: *Statistical Physics* (Springer-Verlag, Berlin, 2002).
- [61] S. Rietzler: *Dekohärenz in Qubit-Speichern*, Master's thesis, Albert-Ludwigs-Universität Freiburg (2004).
- [62] E. L. Hahn: *Spin Echoes*, *Phys. Rev.* **80**, 580 (1950).
- [63] M. H. Levitt: *Spin Dynamics: Basics of Nuclear Magnetic Resonance* (John Wiley and Sons, LTD, Chichester, 2001).
- [64] M. Ziman and V. Bužek: *All (qubit) decoherences: Complete characterization and physical implementation*, *Phys. Rev. A* **72**, 022110 (2005).
- [65] K. Kraus: *States, Effects and Operations* (Springer-Verlag, New York, 1983).
- [66] P. Pechukas: *Reduced Dynamics Need Not Be Completely Positive*, *Phys. Rev. Lett.* **73**, 1060 (1994).

Bibliography

- [67] H. Ollivier and W. H. Zurek: *Quantum Discord: A measure of the quantumness of correlations*, Phys. Rev. Lett. **88**, 017901 (2001).
- [68] L. Henderson and V. Vedral: *Classical, quantum and total correlations*, J. Phys. A **34**, 6899 (2001).
- [69] A. Shabani and D. A. Lidar: *Vanishing Quantum Discord is Necessary and Sufficient for Completely Positive Maps*, Phys. Rev. Lett. **102**, 100402 (2009).
- [70] J. Helm and W. T. Strunz: *Decoherence and entanglement dynamics in fluctuating fields*, Phys. Rev. A **81**, 042314 (2010).
- [71] B. Trendelkamp-Schroer, J. Helm, and W. T. Strunz: *Environment-Assisted Error Correction of Single-Qubit Phase Damping*, arXiv:1110.4806v1 [quant-ph] (2011).
- [72] R. Horn and C. Johnson: *Matrix Analysis* (Cambridge University Press, Cambridge, UK, 2007).
- [73] R. Bhatia: *Positive Definite Matrices* (Princeton University Press, Princeton, USA, 2007).
- [74] V. Paulsen: *Completely Bounded Maps and Operator Algebras* (Cambridge University Press, Cambridge, UK, 2002).
- [75] P. Arrighi and C. Patricot: *On quantum operations as quantum states*, Ann. Phys.-New York **311**, 26 (2004).
- [76] T. Konrad, F. de Melo, M. Tiersch, C. Kasztelan, A. Aragão, and A. Buchleitner: *Evolution equation for quantum entanglement*, Nat. Phys. **4**, 99 (2007).
- [77] F. Buscemi: *On the minimum number of unitaries needed to describe a random-unitary channel*, Phys. Lett. A **360**, 256 (2006).
- [78] M. Gardner: *Mathematics - Magic squares cornered*, Nature **395**, 216 (1998).
- [79] G. Birkhoff: *Tres Observaciones sobre el algebra lineal*, Univ. Nac. Tucuman Revista A **5**, 147 (1946).
- [80] I. Bengtsson, A. Ericsson, M. Kus, W. Tadej, and K. Życzkowski: *Birkhoff's polytope and unistochastic matrices, $N=3$ and $N=4$* , Commun. Math. Phys. **259**, 307 (2005).
- [81] W. K. Wootters: *Quantum measurements and finite geometry*, Found. Phys. **36**, 112 (2006).

- [82] J. M. Renes, R. Blume-Kohout, A. J. Scott, and C. M. Caves: *Symmetric informationally complete quantum measurements*, J. Math. Phys. **45**, 2171 (2004).
- [83] R. Loewy: *Extreme points of a convex subset of the cone of positive semidefinite matrices*, Mathematische Annalen **253**, 227 (1980).
- [84] L. M. K. Vandersypen and I. L. Chuang: *NMR techniques for quantum control and computation*, Rev. Mod. Phys. **76**, 1037 (2004).
- [85] *see problem 30 of the list of open problems in quantum information theory on Prof. R. F. Werner's homepage* (<http://qig.itp.uni-hannover.de/qiproblems/30>).
- [86] K. Życzkowski and M. Kus: *Random unitary matrices*, J. Phys. A-Math. Gen. **27**, 4235 (1994).
- [87] H. Carmichael: *An Open Systems Approach to Quantum Optics* (Springer-Verlag, Berlin, 1993).
- [88] C. A. Fuchs and M. Sasaki: *Squeezing quantum information through a classical channel: Measuring the "quantumness" of a set of quantum states*, Quant. Info. Comp. **3**, 377 (2003).
- [89] C. A. Fuchs: *On the quantumness of a Hilbert space*, Quant. Info. Comp. **4**, 467 (2004).
- [90] K. M. R. Audenaert, C. A. Fuchs, C. King, and A. Winter: *Multiplicativity of accessible fidelity and quantumness for sets of quantum states*, Quant. Info. Comp. **4**, 1 (2004).
- [91] W. K. Wootters: *Entanglement of formation of an arbitrary state of two qubits*, Phys. Rev. Lett. **80**, 2245 (1998).
- [92] K. Życzkowski: *Volume of the set of separable states II*, Phys. Rev. A **60**, 3496 (1999).
- [93] S. Bose: *Quantum communication through an unmodulated spin chain*, Phys. Rev. Lett. **20**, 207901 (2003).
- [94] D. Burgarth, K. Maruyama, M. Murphy, S. Montengero, T. Calarco, F. Nori, and M. Plenio: *Scalable quantum computation via local control of only two qubits*, Phys. Rev. A **81**, 040303 (2010).

Bibliography

- [95] S. Kuhr, S. Gleyzes, C. Guerlin, J. Bernu, U. B. Hoff, S. Deleglise, S. Osnaghi, M. Brune, J.-M. Raimond, S. Haroche, E. Jacques, P. Bosland, and B. Visentin: *Ultra-high finesse Fabry-Perot superconducting resonator*, Appl. Phys. Lett. **90**, 164101 (2007).
- [96] S. Gleyzes, S. Kuhr, C. Guerlin, J. Bernu, S. Deleglise, U. B. Hoff, M. Brune, J.-M. Raimond, and S. Haroche: *Quantum jumps of light recording the birth and death of a photon in a cavity*, Nature **446**, 297 (2007).
- [97] A. Rauschenbeutel, G. Nogues, S. Osnaghi, P. Bertet, M. Brune, J.-M. Raimond, and S. Haroche: *Step-by-step engineered multiparticle entanglement*, Science **288**, 2024 (2000).
- [98] A. Rauschenbeutel, G. Nogues, S. Osnaghi, P. Bertet, M. Brune, J.-M. Raimond, and S. Haroche: *Coherent operation of a tunable quantum phase gate in cavity QED*, Phys. Rev. Lett. **83**, 5166 (1999).
- [99] S. Lloyd: *Almost any quantum logic gate is universal*, Phys. Rev. Lett. **75**, 346 (1995).
- [100] L. Viola and S. Lloyd: *Dynamical suppression of decoherence in two-state quantum systems*, Phys. Rev. A **58**, 2733 (1998).
- [101] M. Abramowitz and I. Stegun: *Handbook of Mathematical Functions with Formulas, Graphs, and Mathematical Tables* (Dover, New York, 1965), 1 edition.
- [102] M. Ziman: *private communications*.
- [103] J. E. Gentle: *Numerical Linear Algebra for Applications in Statistics* (Springer-Verlag, New York, 1998).
- [104] G. Kimura: *The Bloch vector for N-level systems*, Phys. Lett. A **314**, 339 (2003).
- [105] N. Johnston, D. W. Kribs, and V. I. Paulsen: *Computing stabilized norms for quantum operations via the theory of completely bounded maps*, Quant. Info. Comp. **9**, 16 (2009).
- [106] L. M. Blumenthal: *Theory and Applications of Distance Geometry* (Chelsea, Bronx NY, 1970).
- [107] H. Kleinert: *Path Integrals in Quantum Mechanics, Statistics, Polymer Physics, and Financial Markets* (World Scientific Publishing, Singapore, 2006).

List of Publications

- [1] J. Helm and W. T. Strunz, *Quantum decoherence of two qubits*, Phys. Rev. A **80**, 042108 (2009).
- [2] J. Helm and W. T. Strunz, *Decoherence and entanglement dynamics in fluctuating fields*, Phys. Rev. A **81**, 042314 (2010).
- [3] J. Helm, W. T. Strunz, S. Rietzler, and L. E. Würflinger, *Characterization of decoherence from an environmental perspective*, Phys. Rev. A **83**, 042103 (2011).
- [4] B. Trendelkamp-Schroer, J. Helm, and W. T. Strunz, *Environment-Assisted Error Correction of Single-Qubit Phase Damping*, arXiv:1110.4806v1 [quant-ph] (2011).

Danke!

...meinem Doktorvater Walter Strunz für sein leidenschaftliches Engagement bei der Betreuung dieser Arbeit. Seine Begeisterungsfähigkeit für alle wissenschaftlichen Fragen sowie die persönliche Wertschätzung werden mir immer in Erinnerung bleiben.

...meiner Freundin Anna für ihre unendliche Geduld und ihre großartige Unterstützung.

...meinem Sohn Anton für das überwältigende Abenteuer, Vater zu sein.

...meinen Eltern Magdalene und Walter sowie meinen Geschwistern Anne-Lotte und Andreas, immer als tolle Familie für mich da zu sein.

...der gesamten Arbeitsgruppe der Theoretischen Quantenoptik für die großartige Atmosphäre.

...meinem Büronachbarn Martin Schlesinger für Rat und Tat und die sehr angenehme gemeinsame Zeit.

...Sven Krönke für die unfreiwillige Erfindung des Bürostuhlduells.

...Elke Langdon, die durch ihre sympathische Art jedem Formular den Schrecken nahm.

...den Korrekturlesern Rosalind Perrin, Oliver Kaiser, Alexander Janke und Ansgar Pernice für ihre unermüdliche Arbeit.

...der Graduiertenschule *International Max Planck Research School* (IMPRS) des Max-Planck-Instituts für Physik komplexer Systeme in Dresden für die finanzielle Unterstützung.

...den tqo-Rechnern für all die freien Kerne.

Erklärung

Hiermit versichere ich, dass ich die vorliegende Arbeit ohne unzulässige Hilfe Dritter und ohne Benutzung anderer als der angegebenen Hilfsmittel angefertigt habe; die aus fremden Quellen direkt oder indirekt übernommenen Gedanken sind als solche kenntlich gemacht. Die Arbeit wurde bisher weder im Inland noch im Ausland in gleicher oder ähnlicher Form einer anderen Prüfungsbehörde vorgelegt.

Die Dissertation wurde am Institut für Theoretische Physik der Technischen Universität Dresden unter Betreuung von Herrn Prof. Dr. Walter Strunz angefertigt. Ich erkenne die Promotionsordnung der Fakultät Mathematik und Naturwissenschaften an der Technischen Universität Dresden vom 23. Februar 2011 an.

Dresden, den 25. Oktober 2011

.....

Julius Helm